Order Number 9020823

I. Hydrodynamic response of the water droplet to the laser irradiation. II. Electron relaxation in the parabolic quantum well

Yudanin, Boris, Ph.D.

City University of New York, 1990

U·M·I
300 N. Zeeb Rd.
Ann Arbor, MI 48106

A

I. Hydrodynamic Response of the Water Droplet to the Laser Irradiation.

II. Electron Relaxation in the Parabolic Quantum Well.

by

Boris Yudanin

A dissertation submitted to the Graduate Faculty in Physics in partial fulfillment of the requirements for the degree of Doctor of Philosophy, The City University of New York

1990

This manuscript has been read and accepted for the Graduate Faculty in Physics in satisfaction of the dissertation requirement for the degree of Doctor of Philosophy.

10/24/89
Date

Chairman of Examining Committee

10/24/89
Date

Executive Officer

Supervisory Committee

The City University of New York

Acknowledgements

I am greatly indebted to Professor Melvin Lax for his support and guidance during the years I spent in the City College. I am also grateful to all people with whom I have had the pleasure to work during the course of my education.

Table of Contents

Part II. Electron Transport Through Parabolic Quantum Wells

Part I.

Hydrodynamic Response of the Water Droplet to the Laser Irradiation.

General Discussion and Overview.

1. Introduction.

A wide variety of effects can influence the propagation of high-energy laser radiation in the atmosphere. The propagation of the beam is significantly affected by interactions with aerosols along the propagation path. For low and moderate beam irradiances scattering, aerosol heating, diffusive evaporation and conductive heating of the ambient atmosphere are the dominant aerosol-beam interactions[1]. At higher irradiance levels, convective processes become the dominant mechanism for removing the mass, momentum and energy from the aerosol. Strong shock waves are generated at the aerosol surface and propagate into the surrounding air, heating and compressing the ambient gas. A number of other processes, such as internal hydrodynamic effects, plasma formation and nonlinear optical effects may also occur[2-5]. Comprehensive discussions of a number of linear and nonlinear phenomena that impose limitations on beam propagation through the atmosphere have been published by Gebhardt[6] and Zuev[7].

In general, the problem of interaction of an electromagnetic wave with matter involves the solution of a coupled system of the Maxwell equations and the hydro

equations. As a first approximation in solving the problem, the coupling can be replaced by an external energy source proportional to the intensity of irradiation, for the hydrodynamical system and by a change in the index of refraction, due to the change in the matter density, for the electromagnetic part of the problem.

In our investigation we will concentrate on the hydrodynamical effects in the aerosol during the propagation of the laser beam of incident-flux levels in the range of $10^5 - 10^7$ W/cm^2. A typical droplet radius will not exceed $10\mu\, m$. As was pointed out by Armstrong[8], different mechanisms of interaction of the laser beam with the aerosol play a major role at different time intervals. The first two stages involve absorption of the laser energy and a hydrodynamic response to the heated, pressurized fluid. If the pulse length of the laser beam is short compared to the hydrodynamic response time (the droplet radius divided by the velocity of sound), these two steps occur separately: first, the energy is absorbed with essentially no motion; then there will be a hydrodynamic motion in response to the energy absorbed during the first stage of interaction. The effects of the energy absorption during the second stage can be neglected to a good approximation. Moreover, for pulses that are short compared to thermal relaxation times, the hydrodynamic response will be essentially complete before thermal effects become important. (The pulse repetition period is assumed to be long compared to all above times.)

From this we can conclude that there exists a time interval, perhaps $10^{-9} - 10^{-7}$sec., in which a purely hydrodynamic response of the water droplet (aerosol) is predominant. This is a response to the elevated temperature and pressure induced in the droplet relative to the surrounding air during the first stage of the laser - matter interaction. The solution of this short time hydrodynamic problem provides an

initial condition to the later events which are influenced by thermal processes. We will attack this problem, which arises when no energy is deposited, in the first part of our investigation. The following part will be devoted to the second stage, when the energy absorption is present and affects the expansion of the droplet.

In general, laser induced absorption in a spherical droplet will possess cylindrical symmetry (for circularly polarized input radiation) rather than spherical symmetry. Nevertheless, if the drop is small compared to the wave-length, the absorption will be approximately uniform. The evaluation of this hydrodynamic response for the case of uniform absorption is a problem of interest in its own right. It will also, later in this work, provide a test for a two-dimensional hydrocode. The latter, needed when the absorption is non-uniform, can be tested for accuracy in the uniform case.

To study the motion of a droplet in the presence of an energy source, a good hydro-code is needed. CAVEAT[9] (a code developed with many man-years of effort at Los Alamos) seems to be a good candidate for this purpose. This code is based on the Godunov algorithm[10], and it handles a set of hydrodynamical equations in two spatial dimensions and time.

The original Godunov scheme was designed for solving the one-dimensional gas-dynamical equations in the absence of external heat sources. According to Godunov's procedure, the space is divided into a number of cells. For each cell two kinds of values of the hydrodynamical variables are defined. They are the interfacial (cell boundary) values and the average over cell values. The initial cell averaged values are given first. Then each cell boundary can be treated as an infinite surface with uniform media on each side given by properties at the center of the adjacent cells. One can use the analytic solution of this one-dimensional "Riemann" problem of

shock creation and propagation into a perfect gas, due to the initial difference in pressure in two adjacent regions of the gas, to determine the time development of interfacial values at the boundaries of the cells. This is the Riemann part of the solution. Then one can calculate the average values at the cells (mid-points) for the next time step by solving the discretized hydro-equations using the Riemann information at the previous time. This is the Lagrangian* part of the solution. For the case when an energy source is present, modifications should be made to Godunov's procedure, which could affect both the Lagrangian part of the scheme and the Riemann solver. It seems to us that the numerical codes used for the hydro equations based on Godunov's idea tend to incorporate the influence of the energy source only in the Lagrangian part of the calculations. They retain the original one-dimensional solution of the Riemann problem without the heat source for those equations which relate the interfacial values to the cell ones. This will produce an error.

Another approximation was made by Dukovitz[11] for the solution of the Riemann problem without source. The original one-dimensional solution is constructed by using the shock conditions (Hugoniot) and the rarefaction wave conditions[12] for the perfect gas. The rarefaction wave conditions are difficult to employ when a realistic equation of state is used. For the CAVEAT code, Dukovitz[11] proposed to use a "double shock" approximation (rarefaction wave conditions are replaced by shock conditions). It shortens the calculations considerably for a general equation of state for the liquid involved.

If a heat source is present, the Hugoniot (shock) conditions are not changed unless the heat is supplied at the shock surface. On the other hand, the rarefaction

* This hydrodynamical iteration step can be Eulerian as well as Lagrangian.

wave conditions rely upon adiabaticity along the stream line. The adiabatic invariant, $p\,\rho^{-\gamma}$, will be changed by a factor of $\exp(\int_t^{t+\delta t} \frac{Q}{e} dt)$ in the presence of the external energy source. Here Q is the energy source per unit mass and e is the specific energy of the gas. It suggests that we must choose $\delta t < e/Q$ in order to maintain the desired accuracy in the calculations. As a result, for a sufficiently large energy source, the execution time for the code will increase tremendously.

There is another way of dealing with this problem. Instead of the no source Riemann solution one can use a solution that incorporates the source. However, such a solution is unknown at present. Or we can use the method of characteristics near those points where the solution exhibits a nonanalytic behavior and use a small number of mesh points and standard schemes in the other regions. The second proposal will be implemented in our thesis.

To check CAVEAT and get the solution for the hydrodynamical problem, we have to start first with the development of a numerical code which is not based on Godunov's method. This code should also be able to solve a system of hyperbolic equations, with the presence of discontinuities in the solution. In the Section III of the thesis we will design a numerical procedure to the required code. This procedure will be applied later to solve a spherical Riemann problem and a shock problem in the presence of the energy source. It can also be applied for a variety of problems with a "free boundary" such as crystal growth, flame propagation, etc.

In the main body of the thesis we will consider the numerical solution of a system of hydrodynamic equations. Such a system, due to its hyperbolical nature, can exhibit two principal types of discontinuities. The first is a cusp-type discontinuity,

where the derivatives of the solution experience a jump. This type of behavior is peculiar to a "rarefaction" wave. The other type a "perfect" discontinuity, where the functions themselves are discontinuous. That is the essential feature of a shock where all of the functions experience a jump, or a tangential (contact) discontinuity, where some of the functions are discontinuous (e.g., density, temperature), while the others (e.g., velocity, pressure) are continuous. In general, depending on the initial conditions of the problem, there can be any number of these specified discontinuities present in the solution. Discontinuities in higher derivatives can also be handled by the methods described here.

The existence of a shock-type behavior in the solution is fatal for numerical stability of most finite difference codes. Standard numerical methods, such as finite difference, when applied to hyperbolic equations, are susceptible to oscillations, especially in the regions of rapid change of the solution, or where the characteristics are crossing or overlapping (see, for example, Roache[13]). A shock front, being a point where characteristics cross, causes a failure of standard methods. On the other hand, an effort to overcome this difficulty by the introduction of small viscosity does not yield the most accurate results in the other regions of the solution. A good discussion of this point, as well as a review of different numerical methods, can be found in Turkel[14], Roache[13], Woodward and Colella[15], Sod[16] and Meyer[17].

In our numerical approach to the problem, we will design a method, that in some sense is a shock-tracking approach and differs somewhat from a large variety of shock-capturing or shock-tracking methods. The basics of the shock-capturing idea are described in Richtmyer and Morton[18]. Conventional shock-capturing codes require a separate procedure based on the method of characteristics for determination of the

moving grid for the discontinuity points for each time step. A different method was proposed by Boris and Book[19] which uses a low order numerically stable algorithm for tracking the shocks. Their method (Flux Corrected Transport) was used by Carls and Brock[20] for a test problem similar to ours.

The requirement of a separate stable method for capture the moving shock is avoided in our algorithm, which implements the Galerkin method. The use of the Galerkin algorithm transforms a system of partial differential equations into a system of ordinary differential equations (ODE's) in time, so that additional equations concerning positions of points of discontinuity (which usually are in the form of ordinary differential equation in time) simply supplement this system of ODE's, without significantly complicating it.

Shock and other special points in the solution are tracked in our code by means of additional differential equations, that analytically define these discontinuities. At the points where the shock is present jump conditions are used as an analytical equation for the shock; and at the cusp and tangential discontinuities the values of the corresponding solutions on both sides are matched. The instantaneous positions for each discontinuity are tracked by a special differential equation derived from the particular physical characteristics of each point of discontinuity. Our procedure is similar to that of Henshaw[21]. However, he uses a special purpose Riemann solver, while we adapt a well-established partial differential equation solver, POST, written by N. L. Schryer[22,23].

It is obvious that this procedure can be used only after the discontinuity was created. We can extend the method for the times when the discontinuity is not yet created. The same POST package (or any other partial differential equation solver)

may be used for the times when the solution is smooth and no shock (as well as other singularities) is present. When an instability arises at some point in space at some time, it will indicate a development of a discontinuity in the solution. From that time on the code must be switched to the one that incorporates the existing shock and which is described in the Section II.

2. Balloon Problem (Spherical Riemann Problem).

The prooftesting of any new (as well as some old) technique includes its application to problems with known solutions. Some of the examples include the one-dimensional shock tube problem, one-dimensional propagation of the simple wave, spherically symmetric point source explosion, etc. The problem we have chosen is a combination of the simple wave propagation and the shock tube problems with an extension to the spherically symmetric three dimensional hydro-dynamical equations. We also will explore the purely one-dimensional problem as well, to ascertain that the code that we will develop is working correctly. On the other hand, the spherical test problem will be a good check for the fully two-dimensional code - CAVEAT.

We define an idealized hydrodynamical problem (called sometimes a Riemann problem). A droplet is uniformly heated by a laser pulse, then a subsequent shock wave development is followed by solving the hydrodynamic equations of motion.

Heating the droplet at constant volume causes its pressure to increase. The high pressure then causes the droplet to expand violently against the surrounding gas. The strong dynamics generates shock waves and associated shock heating in the surrounding gas region, and adiabatic expansion, cooling and a rarefaction wave in the

droplet region. The investigation of the complete flowfield is the subject of the so-called spherical Riemann ("balloon") problem.

3. Initial Formulation of the Problem.

At the time $t = 0$, a droplet of radius R_0 starts in a state with temperature, pressure, density and velocity specified by:

$$T(x, 0) = T_w; \quad P(x, 0) = P_w; \quad \rho(x, 0) = \rho_w; \quad \upsilon(x, 0) = 0 \tag{I.1.1a}$$

The surrounding gas is in the initial state

$$T(x, 0) = T_a; \quad P(x, 0) = P_a; \quad \rho(x, 0) = \rho_a; \quad \upsilon(x, 0) = 0 \tag{I.1.1b}$$

where

$$T_w > T_a; \quad P_w \gg P_a; \quad \rho_w \gg \rho_a \tag{I.1.1c}$$

The subscripts "w" and "a" remind us of the original physical problem of a water droplet expansion into an air atmosphere.

At the initial instant the surface separating the aerosol from the surrounding gas is withdrawn, and the hydrodynamic interaction between the aerosol and the gas begins. The resulting evolution can be described by the usual set of hydrodynamical equations. The first equation is the mass conservation equation:

$$\frac{\partial \rho}{\partial t} + \rho \frac{\partial \upsilon}{\partial r} + \upsilon \frac{\partial \rho}{\partial r} + \frac{2\,\upsilon \rho}{r} = 0 \tag{I.1.2}$$

The second equation states the conservation of momentum (Euler equation):

$$\frac{\partial \upsilon}{\partial t} + \upsilon \frac{\partial \upsilon}{\partial r} + \frac{1}{\rho} \frac{\partial P}{\partial r} = 0 \qquad \text{(I.1.3)}$$

where the surface tension as well as the internal friction terms are disregarded for simplicity.

The third equation, the equation of conservation of internal energy in the absence of external heat sources and internal heat diffusion, can be cast into a quasiadiabatic form (see, for instance, Whitham[24]). To simplify the calculations we will use the perfect gas equation of state for both outside air and the inside water. We will choose $\gamma = 1.4$ for the outside gas and $\gamma = 3.0$ for the inside water. With these simplifications the energy conservation equation will become:

$$\frac{\partial (P\rho^{-\gamma_i})}{\partial t} + \upsilon \frac{\partial (P\rho^{-\gamma_i})}{\partial r} = 0 \qquad \text{(I.1.4)}$$

The methods of solution which we will use later in the thesis do not depend on the assumption of the perfect gas-like equation of state. It is worthwhile mentioning here that for the planar 1D case the term $(2 \upsilon \rho)/r$ is absent. An analytical solution for the system Eqs.(2-4) with initial conditions Eqs.(1a-1c) then exists. Therefore comparison between the numerical and analytical results is possible.

4. Self-Similar Solution for the Interface Velocity.

In this section we will provide a simple numerical solution for the spherically symmetric Riemann problem. It will give a flavor of the difficulties involved in the computations. It also can be used as a crude test for the numerical results, which we will

obtain later in a more reliable fashion.

The Riemann problem was formulated in the previous section. The full time-dependent solution to this problem in analytic form does not appear feasible. One major complexity arises because the boundary conditions on the surface of the droplet are unknown before the solution of the problem is found. It puts the problem into the class of "free boundary" problems[26]. As a result of an initial pressure difference inside and outside the droplet, the interface will gain velocity as soon as the interaction starts. This moving boundary will serve as a generator of waves in both water and air. On the other hand, boundary conditions at the surface couple changes in state of the water and air. If we neglect surface tension, then, at the interface, the pressure on both sides of the surface should be equal (the imaginary surface separating droplet from air does not have any mass; therefore even an infinitesimal excess force will result in the infinite acceleration). Furthermore, the hydrodynamical velocity of water and air should be the same and equal to the as yet unknown velocity of the surface $\dot{R}(t)$.

In other words, the boundary conditions for internal (droplet) and external (surrounding air) problems are:

$$V_{\text{water}}(r=R(t)) = V_{\text{air}}(r=R(t)) = \dot{R}(t) \tag{I.1.1}$$

$$P_{\text{water}}(r=R(t)) = P_{\text{air}}(r=R(t)) \tag{I.1.2}$$

where $\dot{R}(t)$ (rather $R(t)$) can be found from the mass conservation condition, provided the solution for the water droplet is known, e.g.

$$\int_0^{R(t)} \rho_{water}(r,t) r^2 dr = \int_0^{R_0} \rho_w r^2 dr \qquad (I.1.3)$$

where $R_0 = R(0)$.

We must deal with two sets of hydrodynamic equations that describe waves in water and air, respectively. For water, the simplified adiabatic equations are used because no additional energy source is present, and the wave does not produce any shocks. For the air this approximation generally is not valid because of the appearance and propagation of the shock wave. On the shock front there is production of the entropy. But the "nonadiabaticity" of the flow far from the shock is small and for the purposes of this chapter we still can use the "adiabatic" approximation for the air region as well. This reduces the number of the hydrodynamic equations to two everywhere:

$$\frac{2}{\gamma-1}\frac{\partial a}{\partial t} + a\frac{\partial V}{\partial r} + \frac{2}{\gamma-1}\frac{\partial a}{\partial r} + \frac{2Va}{r} = 0 \qquad (I.1.4)$$

$$\frac{\partial V}{\partial t} + V\frac{\partial V}{\partial r} + \frac{2}{\gamma-1}a\frac{\partial a}{\partial r} = 0 \qquad (I.1.5)$$

where $a(r,t) = \sqrt{(\partial P/\partial \rho)_s}$ - local sound velocity. The gas constant - γ was chosen 1.4 for air and 3.0 for water (see Appendix A for discussion). Additional condition (3), mass conservation, in integral form completes the set of equations. Here and in the following sections we will specialize, for illustrative purposes only, to the case where the water droplet has a gas-like equation of state.

Because of the unusual nature of the integral condition (3) we do not attempt to get a complete numerical solution for the stated problem in this section, but rather try to get the interface velocity using a crude approximation for the waves inside and

outside the droplet.

We are going to present a rough calculation of the interface velocity (assuming it to be constant in time). This velocity is a function of a given initial pressure difference in water and in air. At the same time we will present a very powerful method of solving a particular type of partial differential equations - the method of auto-model or self-similar solution described beautifully in the book by Sedov[26].

Let us first consider a wave that propagates in the air due to an expanding spherical surface near the origin. If the sphere expands with velocity greater than the sound velocity of the air, then a strong shock wave will develop[24]. In the case where the initial pressure of the water is greater than that of the air, the velocity of the interface will instantly become greater than the sound velocity of the air. This means that a shock will start immediately from the boundary and propagate into undisturbed air with some yet unknown velocity U_{shock} satisfying the relations $U_{shock} \gg \dot{R}(t) > a_{air}$. After a short time $t > R_0/a_0$ the shock in air will be at a distance R_{shock} much greater than the initial radius of the sphere R_0. Therefore, motion of the shock will not be affected by the expanding sphere any longer, and to a good approximation it can be considered self-similar. The solution of this problem was found by G.I.Taylor[27].

For a wave propagating in the drop the situation is more complicated. A rarefaction wave starting from the outwards - moving surface will propagate toward the center. Even before this wave reaches the center and reflects as a compression wave, interfering with the initial rarefaction wave and producing a very complicated "standing - type" wave, it cannot be considered a simple wave. This initial rarefaction wave has two points of weak discontinuity[28] separating regions in which different types of solution exist.

So the complete problem (drop and surrounding air) can be divided into 5 simpler ones in 5 different regions of radial variable r with matching conditions at the boundaries of these regions:

Region 1 ($0< r< r_1$) and Region 2 ($R_{shock} < r < \infty$), where no disturbance has yet arrived.

Region 3 ($r_1 < r < r_2$) in which the wave approximately possesses the "simple" wave relation, namely, one of the Riemann invariants (see Appendix A) is constant (in the one-dimensional case the approximation changes to equality)

$$V_{water} + \frac{2}{\gamma-1} a_{water} \approx \frac{2}{\gamma-1} a_w \qquad (I.1.6)$$

where a_w is the initial sound velocity of water.

Region 4 ($r_2 < r < R(t)$) and 5 ($R(t) < r < R_{shock}$). In these regions, to a good approximation, the wave can be considered of self-similar type.

The boundary points r_1, r_2 and R_{shock} are given via equations:

$$r_1 = R_0 - a_w\, t \qquad (I.1.7)$$

$$r_2 = (R_0 + Ut)(V_{water} - a_{water}) \,/\, U \qquad (I.1.8)$$

$$R_{shock} = U_{shock}\, t + R_0 \qquad (I.1.9)$$

where V_{water} and a_{water} are time-dependent.

In order to get a solution in regions 4 and 5 we introduce a self-similarity variable z and use rescaling of velocity and sound velocity (self-similar behavior of $V(r,t)$ and $a(r,t)$ was assumed)

$$z = \frac{r}{R(t)} = \frac{r}{R_0 + Ut} \qquad x = \frac{V(r,t)}{Uz} \qquad y = \frac{a^2(r,t)}{U^2 z^2} \tag{I.1.10}$$

where the surface velocity was assumed constant ($\dot{R}(t) = U$). Equations (4), (5) after the substitution (10) can be reduced to the set of 4 equations for water and air (subscripts w and a are suppressed):

$$\frac{dy}{dx} = 2\frac{y}{x}\frac{(1-x)(\gamma x - 1) + y}{3y - (1-x)^2} \tag{I.1.11}$$

$$\frac{dz}{dx} = \frac{z}{x}\frac{(x-1)^2 - y}{3y - (x-1)^2} \tag{I.1.12}$$

with boundary conditions

$$\begin{array}{ll} x_1 = 1 \quad z_1 = 1 \quad y_1 = ? & \\ x_2 = ? \quad z_2 = ? & \begin{cases} y_2 = (1 + 0.5(\gamma - 1)\, x_2)(1 - x_2) & (\gamma = 1.4) \\ y_2 = (1 - x_2)^2 & (\gamma = 3.0) \end{cases} \end{array} \tag{I.1.13}$$

Here we have used equations (6) and (8) at point r_2. At point R_{shock} - the shock front, we have used modified Hugoniot conditions (assuming a strong shock is developed), which in our dimensionless units are:

$$x_2 = \frac{2(P-1)}{(\gamma-1) + P(\gamma+1)}; \quad y_2 = 2\gamma P \frac{(\gamma+1) + p(\gamma-1)}{((\gamma-1) + P(\gamma+1))^2} \tag{I.1.13'}$$

and after elimination of P will transform to the condition in the Eq.(13).

In the outer gaseous region 2, all variables remain at their initial value. This value is used to initiate a solution of equations (4) and (5) into region 2 from R_{shock} to $R(t)$. Also, the undisturbed solution in region 1 is used to initiate a solution in region 3 which is approximately given by Eq.(6). These solutions provide one boundary condition at r_2 and another at $R(t)$. Thus, equations (10) and (11) in region 4 must be

solved for a two-point boundary condition which requires an iterative procedure. A numerical code for solving this system is based on the ODE package of the PORT library. Matching the solutions from the outer and inner sides at the boundary, we obtain the velocity of the surface of a droplet which agrees with the results of more complicated calculations presented in Section II.

POST Adaptation for a Numerical Solution of the Spherically-Symmetric Riemann Problem

1. General Description of the Method.

In this and following sections we will describe the code for testing the CAVEAT as well as for general use in the "free boundary" problems. As stated in the Introduction, our code implements POST for the problem of hyperbolic equations in one space variable and one time, where an initial discontinuity is present and a shock subsequently develops.

A detailed description of POST can be found in N. L. Schryer[22]. Here, we simply state the very general requirements of this package. POST is designed to handle a system of partial differential equations together with a set of ordinary differential equations. In the usual use of POST, the mesh points must be fixed. However, some of the points may have a multiplicity greater than one, thus allowing a piecewise-continuous solution.

A simple reformulation of the problem can let POST handle stepwise discontinuous functions with a constant discontinuity as a possible solution. But the ability to join the solution of a set of PDE's with a set of ordinary differential equations will let us handle variable jumps in the solutions and a moving mesh. Here we will discuss this particular modification.

Any discontinuity in the first (and, therefore, higher) derivatives of the continuous solution, to be fit by a spline function of degree $k - 1$, requires a mesh point with

multiplicity $k-1$. If the position X_0 of such point is known at time $t = t_0$, then its position at time t can be specified by an equation of the form:

$$\frac{dX}{dt} = f\left(X_0, \mathbf{u}, \frac{\partial \mathbf{u}}{\partial t}, \frac{\partial \mathbf{u}}{\partial x}, t, \ldots\right) \qquad \text{(I.2.1)}$$

where f is a function which reflects the specific physical property of the problem, the $\mathbf{u}(x,t)$ are unknown variables and ". . ." stands for higher derivatives. Similar equations can be used to make other special mesh points time dependent (e.g., boundaries).

A somewhat different situation arises when the solution u itself is discontinuous. It must be transformed into a smooth function for POST to succeed. There are two possible procedures for achieving this. The first is to define a new smooth function $\tilde{\mathbf{u}}$ such that:

$$\tilde{\mathbf{u}}(x,t) = \mathbf{u}(x,t) + \Delta\,\mathbf{u}(t)\cdot H(x - X(t)) \qquad \text{(I.2.2)}$$

where $H(x)$ is the Heaviside unit function. Eq.(2) adds an unknown jump $\Delta\,\mathbf{u}(t)$ to the solution $\mathbf{u}(x,t)$ at the point of discontinuity. An additional differential equation for $\Delta\,\mathbf{u}(t)$ is then required. As an example of such an equation, the jump in pressure for the spherical balloon problem at the surface of the balloon is equal to the surface tension ($\Delta p(t) \propto R^{-1}(t)$). The situation is not as simple for the jump in density across the boundary in the same balloon problem, which can not be described by any a priori equation. In addition, problems with an initial jump can be cast into a type of two point boundary value problem, where the boundary conditions for the unknown functions are prescribed at two different boundaries.

To overcome this difficulty we propose the following idea. Instead of transform-

ing dependent variables u to make them continuous via Eq.(2), we can transform independent variables, e.g., x. That will enable us to have two different functions in the place of each original one. To explain this, let us suppose that initially we had a discontinuity at point X_0. With time this point will move according to $X = X_0(t)$. Additionally, let the region of the space variable x be $X_l \leq x \leq X_r$. Then the transformation:

$$y = x \qquad \text{for } X_l \leq x \leq X_0 \tag{I.2.3a}$$

$$y = x\,\frac{X_l - X_0}{X_r - X_0} + X_0\,\frac{X_r - X_l}{X_r - X_0} \quad \text{for } X_0 \leq x \leq X_r \tag{I.2.3b}$$

will put the solution into the region $X_l \leq y \leq X_0(t)$ with $y = X_l$ at both $x = X_l$ and $x = X_r$. If in addition we introduce a set of new functions u_1 and u_2 such that:

$$u_1(x) = u(y) \quad \text{for } X_l \leq x \leq X_0 \tag{I.2.4a}$$

$$u_2(x) = u(y) \quad \text{for } X_0 \leq x \leq X_r \tag{I.2.4b}$$

then the initial problem for a set of discontinuous functions will be transformed into a new one for the "doubled" number of continuous functions in the "halved" space region. In addition, this "folding" procedure resolves "two point boundary conditions" difficulties, namely, it permits a single forward integration and does not require repeated integrations until a boundary condition at the far side is satisfied. The price paid, a doubling of the number of variables, is small compared to the computing time saved by avoiding the iterative procedure.

2. The "Folding" Transformation.

Employing the folding of Eqs.(3-4), we reduce the domain of our problem to the region of the spatial variable r between 0 and $R_b(t)$. This can be achieved by transforming the outer region into the inner region of the variable r via the transformation:

$$t' = t \quad y = R_b(t)\,\frac{r - R_s(t)}{R_b(t) - R_s(t)} \tag{I.2.9}$$

for $R_b(t) \le r \le R_s(t)$ and the identity transformation

$$t' = t \qquad y = r \tag{I.2.10}$$

for $0 \le r \le R_b(t)$. Here $R_s(t)$ is the position of the shock wave at time t and $R_b(t)$ is the position of the water-air boundary.

The region beyond the shock to infinity could be omitted from these calculations because the surrounding gas in that region retains its undisturbed values of velocity, pressure and density. Since these values are related to the ones behind the shock through the Hugoniot relations, they generate boundary conditions for the region behind the shock. After such a "folding", instead of three unknown functions υ, P, and ρ, we will get six new functions υ_1, υ_2, p_1, p_2, ρ_1, ρ_2, defined in the interval $0 \le y \le R_b(t)$, such that:

$$\upsilon(r,t) = \upsilon_1(r,t)\,H(R_b(t) - r) + \upsilon_2(r,t)\,H(r - R_b(t)) \tag{I.2.11}$$

$$P(r,t) = p_1(r,t)\,H(R_b(t) - r) + p_2(r,t)\,H(r - R_b(t)) \tag{I.2.12}$$

$$\rho(r,t) = \rho_1(r,t)\, H(R_b(t) - r) + \rho_2(r,t)\, H(r - R_b(t)) \tag{I.2.13}$$

here, again, $H(r)$ is the Heaviside unit function. As a result, we obtain a set of transformed equations in an expanding spatial region $0 < y < R_b(t)$:

$$\frac{\partial}{\partial y}(\upsilon_1 \rho_1) = -\frac{\partial \rho_1}{\partial t} - \frac{2\rho_1 \upsilon_1}{y} \tag{I.2.14}$$

$$\frac{\partial}{\partial y}(0.5\, \upsilon_1^2) = -\frac{1}{\gamma_w \rho_1}\frac{\partial p_1}{\partial y} - \frac{\partial \upsilon_1}{\partial t} \tag{I.2.15}$$

$$\frac{\partial}{\partial y}(p_1 \rho_1^{-\gamma_w}) = -\frac{1}{\upsilon_1}\frac{\partial}{\partial t}(p_1 \rho_1^{-\gamma_w}) \tag{I.2.16}$$

$$\frac{\partial}{\partial y}(\upsilon_2 \rho_2) = A\frac{\partial \rho_2}{\partial t} - (\dot{A}y - \dot{B})\frac{\partial \rho_2}{\partial y} + \frac{2\rho_2 \upsilon_2}{\frac{B}{A} - y} \tag{I.2.17}$$

$$\frac{\partial}{\partial y}(0.5\, \upsilon_2^2) = A\frac{\partial \upsilon_2}{\partial t} - (\dot{A}y - \dot{B})\frac{\partial \upsilon_2}{\partial y} - \frac{1}{\gamma_a \rho_2}\frac{\partial p_2}{\partial y} \tag{I.2.18}$$

$$\frac{\partial}{\partial y}(p_2 \rho_2^{-\gamma_a}) = \frac{1}{\upsilon_2}\left(A\frac{\partial}{\partial t}(p_2 \rho_2^{-\gamma_a}) - (\dot{A}y - \dot{B})\frac{\partial}{\partial y}(p_2 \rho_2^{-\gamma_a})\right) \tag{I.2.19}$$

where

$$A = A(t) \equiv \frac{R_s(t) - R_b(t)}{R_b(t)}\ ; \qquad B = B(t) \equiv R_s(t) - R_b(t) \tag{I.2.20}$$

All variables in the above equations are dimensionless. There are 5 independent dimensional parameters which define the initial state of the problem: initial radius of the droplet R_0, initial density of the air ρ_a, initial pressure of the air P_a, initial density of the water ρ_w and initial pressure of the water P_w. From these parameters we can construct dimensionless variables for distance, time, velocity, density and pressure as fol-

lows: distance - $\tilde{r} = r/R_0$, time - $\tilde{t} = t \cdot c_w/R_0$, velocity - $\tilde{\upsilon} = \upsilon/c_w$, pressure - $\tilde{p} = p/P_w$ and density - $\tilde{\rho} = \rho/\rho_w$. The variables with the " ~ " correspond to the dimensionless ones. In this and following sections the " ~ " is omitted. In the above formulas the sound velocity of the water c_w is related to the initial pressure and density of the water via relation: $c_w = \sqrt{\gamma_w P_w/\rho_w}$. All parameters here refer to the initial state of the water before motion has occurred. In the actual numerical calculations we have used the set of initial parameters:

$$R_0 = 10 \text{ microns} ; P_w = 1.1 \text{ atm.} ; \rho_w = 1 \text{ g/cm}^3 ; P_a = 1 \text{ atm.} ; \rho_a = 10^{-3}\text{g/cm}^3 ;$$

$$\gamma_a = 1.4 ; \gamma_w = 3.0 . \qquad \text{(I.2.21)}$$

However, different initial parameters consistent with the same dimensionless values are compatible with the same numerical results.

3. Boundary Conditions.

The above equations require a set of boundary and initial conditions. Because of the spherical symmetry of the problem, the velocity at the origin must remain zero at all times. Another boundary relation between the pressure and the density at the origin can be derived from the constancy of entropy if no shock is present. This is the case for the inside (water) part of the problem. Thus, at $y = 0$ we can require a boundary condition:

$$p_1(t,y=0)\, \rho_1^{-\gamma_w}(t,y=0) = P_w\, \rho_w^{-\gamma_w} \quad \text{— initial values} \qquad \text{(I.2.22a)}$$

$$v_1(t,y=0) = 0 \tag{I.2.22b}$$

or for the dimensionless variables

$$p_1(t,y=0)\ \rho_1^{-\gamma_w}(t,y=0) = 1 \tag{I.2.22c}$$

$$v_1(t,y=0) = 0 \tag{I.2.22d}$$

To obtain the velocity, pressure and density of the outside gas at the shock front (which has been transformed to the origin by Eqs.(9,10)) we use the Hugoniot conditions. In the strong shock approximation, relevant to our case because of the large pressure ratio ($\propto$100), these conditions are (see Ref.10):

$$\rho_2(t,y=0) = \rho_a \frac{\gamma_a + 1}{\gamma_a - 1} \tag{I.2.23a}$$

$$p_2(t,y=0) = \rho_a\ U^2_{shock}\ (t) \frac{2}{\gamma_a + 1} \tag{I.2.23b}$$

$$v_2 = \frac{2}{\gamma_a + 1} U_{shock} \tag{I.2.23c}$$

We should mention here that the Hugoniot conditions constitute a set of three equations for the jumps in density, velocity and pressure on the shock in terms of the as yet unknown shock velocity. We can eliminate the shock velocity from two of the Hugoniot relations and use them as boundary conditions. The remaining equation (in our case Eq.23c) will be used later as the differential equation for the shock itself (see Eq.(30)). In the dimensionless form the two relations (derived from the Eqs.23) are:

$$\rho_2(t,y=0) = \frac{\rho_a}{\rho_w} \frac{\gamma_a + 1}{\gamma_a - 1} \tag{I.2.23d}$$

$$p_2(t,y=0) = \gamma_w \frac{\rho_a}{\rho_w} v_2^2(t) \frac{\gamma_a + 1}{2} \qquad \text{(I.2.23e)}$$

Again, the subscripts "w" and "a" stand for water and air.

The remaining two boundary conditions can be derived from the continuity of velocity and pressure on the two sides of the droplet boundary. The latter follows because it is appropriate to neglect the surface tension in our applications.

$$v_1(t,y=R_b(t)) = v_2(t,y=R_b(t)) \qquad \text{(I.2.24)}$$

$$p_1(t,y=R_b(t)) = p_2(t,y=R_b(t)) \qquad \text{(I.2.25)}$$

The dimensionless form for these two conditions is the same.

4. Initial Conditions.

To conclude the formulation of the problem, we have to specify the initial conditions. The obvious ones, Eqs.(5a,5b), are difficult to employ, because of the jump at $r = R_0$ in pressure and density which at the next instant of time will result in a nonzero velocity distribution and jumps at the emerged shock. This suggests that we use as a set of initial conditions the pressure, density and velocity distributions shortly after the surface of the droplet was released (e.g., at time $t = 0 + \eta$).

To find the latter conditions, we note that for a sufficiently small time "η", the shock and the rarefaction waves will propagate the negligible distances from the droplet surface, $U_{shock}\eta$ and $-U_{sound}\eta$ respectively. Thus, the whole region where the solution is different from the initial constant values is of the order of η, much smaller

than the radius of the droplet $R_0 + U_b\eta$. Through the transformation into new variables τ and x such that

$$t = \eta\,\tau\,; \quad y = R_0 - \eta\,x \tag{I.2.26}$$

all the derivatives in the system of equations (13-18) will be multiplied by a factor $1/\eta$. Thus the only term which does not contain derivatives (e.g., the term which distinguishes the radially-symmetric case from the 1D planar case) to a first approximation in η will be of order unity and can be discarded. This proves that spherical geometry effects will not be important at such early times. In other words, we can use the exact analytical solution of a one-dimensional shock-tube (planar) problem to generate our initial conditions. Note that for the one-dimensional case, the shock and boundary velocities are time-independent. For consistency this 1D solution should also be transformed according to Eqs.(7,8) to employ our "folding" procedure.

4. Transformation to Quasi-Lagrangian Form.

In the above formulation the right boundary, which represents the surface of the gas droplet, is a moving one. To make a fixed mesh, this boundary should be transformed to a fixed point. POST allows us to have a system of partial differential equations accompanied by a system of ordinary differential equations in time. This will make possible the transformation of the original equations into a quasi-Lagrangian form and the splitting of the problem into several regions with fixed boundaries. In each of these regions the solution (for pressure, density, and velocity) is continuous and has a continuous first derivative. The transformations are not known a priori but

can be cast into a form of supplementary ordinary differential equations that involve the as yet unknown solution of the original set of the partial differential equations (similar to Eq.(1)). It is reasonable to expect that the continuity regions for the radially-symmetric problem are the same as for the planar 1D shock-tube problem at least for the initial time. Further propagation of these points of the discontinuity will be governed by a corresponding system of ODE's. The analytical solution of the 1D shock problem is presented in Fig.(I.1). It is easy to see that there are three regions in the gas inside the droplet where the solution is continuous: to the left of the point H, which corresponds to the region from the origin to the head of the wave (point H) which propagates towards the center; the region of the wave itself from the head (H) to the tail (T) where it exhibits a self-similar behavior (e.g., in this region the solution depends only on $\zeta = y/t$ and not on y and t separately). This self-similar wave is also called a "simple" wave or "fan". And the last region of continuity is from the tail of that "simple" wave (point T in Fig.(I.1)) to the material boundary (B). There is also one region in the outside gas, from the surface of the drop to the position of the shock (point S). Corresponding equations which describe positions of these points of discontinuity (in dimensionless units) are, respectively:

$$\dot{R}_h(t) = v_1(y=R_h,\ t) - \left[\frac{p_1}{\rho_1}\right]^{\frac{1}{2}}(y=R_h,\ t) \tag{I.2.27}$$

$$\dot{R}_t(t) = v_1(y=R_t,\ t) - \left[\frac{p_1}{\rho_1}\right]^{\frac{1}{2}}(y=R_t,\ t) \tag{I.2.28}$$

$$\dot{R}_b(t) = v_1(y=R_b,\ t) \tag{I.2.29}$$

$$\dot{R}_s(t) = \frac{\gamma_a + 1}{2}\, v_2(y=0,\, t) \qquad \text{(I.2.30)}$$

where the subscripts h, t, b, s correspond to the H, T, B, S points in Fig.(I.1). The first two equations above state that in the wave any weak discontinuity (e.g., at the head and tail of the simple wave) propagates with the instantaneous speed of sound relative to the particle motion. The propagation is in the direction away from the source of the disturbance. Eq.(29) represents the condition that the surface of the tangential discontinuity (which is the droplet surface boundary) moves together with the matter. Eq.(30) is a statement derived from the Hugoniot conditions for the shock velocity.

5. Results and Discussion.

In this section we present the results for the one-dimensional linear shock-tube problem and for the spherically-symmetric balloon problem. Our numerical results as well as analytical 1D solution are plotted in Figs.(I.1-I.5). Dimensionless variables in those figures are plotted versus dimensionless "unfolded" coordinate $\tilde{x}$. As can be seen from the graphs for the 1D case, the numerical and the analytical solutions are practically the same at all times (see Fig.(I.1) and Fig.(I.2)). The dots on those figures represent our numerical solution. The solid lines were obtained by plotting the analytical solution of the Riemann shock-tube problem with the initial and boundary conditions as stated in sections 6 and 7. The agreement of our numerical solution with the analytical one for the one-dimensional linear problem may indicate that in the spherical case the numerical results obtained by our procedure are reasonably correct as well. In Figs.(I.3-I.5) we plot the dimensionless solutions of the spherically-symmetric bal-

loon problem for different times. In this case we have used the analytical results of the Riemann problem as our initial conditions. Actually, the 1D solution at time t=0.0001 which is plotted on the Fig.(I.1) was used as the initial data for the numerical calculations of the spherical problem. As can be seen from the Figs.(I.3-I.5) (plots of the solution of the spherical balloon problem at times t=0.2, t=0.5, t=0.99) as the time progresses, the wave in the outer region (B - S) weakens. This is because of the spherical geometry, which induces $1/r$ effect. The other profound feature of the spherical problem is the emergence of a shock-like behavior at the tail of the rarefaction wave in the interior region (point T). But we did not find in our numerical calculations a real inward facing shock before the rarefaction wave reaches the center (see Fig.(I.5)).

As was mentioned previously a similar problem was solved by J. C. Carls and J. R. Brock[20]. Their solution is qualitatively similar to ours, but we have not made numerical comparison because they used a realistic equation of state for water in contrast to the ideal gas equation with $\gamma = 3$ for the liquid, used here.

Numerical Solution of the Riemann Problem in the Presence of an External Energy Source.

1. Overview.

To check the accuracy of CAVEAT and other codes derived from the original Godunov's method in the presence of a heat source, we have designed the following test problem.

A piston, located initially at the origin, moves with a constant speed in a one-dimensional tube filled with perfect gas. An external energy source pumps energy into the gas. The rate of energy absorption is proportional to the density of the gas. Mathematically this problem can be described by the following system of equations:

$$\frac{\partial \rho}{\partial t} + \frac{\partial \rho u}{\partial x} = 0 \tag{I.3.1}$$

$$\frac{\partial (\rho u)}{\partial t} + \frac{\partial (p + \rho u^2)}{\partial x} = 0 \tag{I.3.2}$$

$$\frac{\partial E}{\partial t} + \frac{\partial u(E+p)}{\partial x} = W \tag{I.3.3}$$

where ρ, p and u are density, pressure and velocity, respectively. Here $E = \rho(e + \frac{1}{2}u^2)$, $e = p/\rho(\gamma - 1)$ is the specific energy, and W is the energy source. If we set $\tilde{x} = x/x_o$, $\tilde{t} = t_o$, $\tilde{p} = p/p_o$, $\tilde{\rho} = \rho/\rho_o$, $\tilde{u} = u/c_o$, the equations retain their form (except that in Eq.2 above p is replaced by $\tilde{p}/\gamma$) and apply to the dimensionless variables $\tilde{p}$, $\tilde{\rho}$, $\tilde{u}$ and $\tilde{e}$. In the remaining part of the paper the "~" will be omitted. We have chosen as units

for the transformation to dimensionless form the following: for the distance - $x_o = 10\mu m$, for density and pressure - the initial ρ_o and p_o. For velocity we use $c_o = \sqrt{\gamma p_o/\rho_o}$, the sound velocity of the undisturbed gas. In this case, for time we can use $t_o = x_o/c_o$ and for the energy source - $Q_o = p_o/\rho_o t_o$.

Two cases are considered: source constant in space

$$W = Q\rho \tag{I.3.4}$$

and a source with Gaussian distribution located on the piston

$$W = Q\rho \exp\left[-\frac{(x - U_{piston}t)^2}{2\sigma^2}\right] \tag{I.3.5}$$

For our calculations, we choose the dimensionless width of the Gaussian to be $\sigma = 0.2$ and the source strength Q to be $10^{14}/1.29$ Watts/kg, which corresponds to a dimensionless $Q = 30.2$. The dimensionless piston velocity U_{piston} is 0.589.

We solve this problem for the piston which moves to the right into the gas, producing a compression shock and for the piston which moves to the left out of the gas. In the latter case a rarefaction wave develops and moves away from the piston into the gas.

2. POST Adaptation.

Now we will apply POST for solving the test problem discussed in the previous Section.

As we have stated above, our test problem considers both compressing and receding pistons. For both cases, the region of interest will be between the piston and the head of the wave - either shock or rarefaction. In front of those waves the gas would have been undisturbed if the energy source had not been added. For the source which is independent of the spatial coordinate, it is obvious that the velocity and the density in front of the waves, specified above, will retain their original values ($\upsilon = 0; \rho = \rho_o$), and only the pressure is changed. This change in the pressure can be calculated by integrating the equation:

$$\frac{\partial p}{\partial t} + \upsilon \frac{\partial p}{\partial x} = Q\rho(\gamma - 1) \qquad \text{(I.3.3')}$$

(which follows from Eq.2 and Eq.3). With $\upsilon = 0$ and constant ρ Eq.3' yields

$$p = (\gamma - 1)Q\rho t \,. \qquad \text{(I.3.6)}$$

The knowledge of the analytical solution (Eq.(6) as well as the constant velocity and density), allow us to omit the region in front of the shock and the rarefaction waves from our numerical calculations.

For the Gaussian source, the problem is more complicated because the region in front of the wave should also be taken into account. We have designed a method which permits POST to be applied to such problems. This method is based on "folding" the region in front of the wave onto the region behind it. A complete discussion of the "folding" method is given in the Section 2.

In order to track the singularities in the wave solution of the specified problems we will locate them and write a set of ordinary differential equations that describes the motion of the points at which singularities occur. The first point, for both cases, is the

position of a moving piston. At this point the velocity of the gas must be equal to the piston velocity. No other conditions for the variables (such as pressure and density) can be specified at this point.

For the compressing piston the second point of singularity is at the position of the shock. The hydrodynamical variables for the shock satisfy the Hugoniot jump conditions for a perfect gas:

$$U_{\text{shock}} = \frac{p_- - p_+}{v_-} \tag{I.3.7}$$

$$\rho_- = \frac{\gamma+1}{\gamma-1} - \frac{4\gamma}{\gamma-1}\,\frac{1}{p_-(\gamma-1)+p_+(\gamma+1)} \tag{I.3.8}$$

$$U^2_{\text{shock}} = \frac{1}{2\gamma}(p_-(\gamma+1)+p_+(\gamma-1)) \tag{I.3.9}$$

The above equations are the familiar Hugoniot conditions in dimensionless form, without assuming that the velocity ahead of the shock must vanish and the pressure ahead of the shock must be constant. On the contrary, the pressure ahead of the shock depends on the heat source.

For the receding piston, the equations for the velocities of the head and tail of the rarefaction wave (see Fig.(I.1)) can be obtained by using the fact that each point in the wave (including the head and the tail) propagates with the local sound velocity relative to the gas, e.g.:

$$U_{\text{head}} = v - \left[\frac{p}{\rho}\right]^{1/2} \quad \text{at} \quad x = X_{\text{head}} \tag{I.3.10}$$

$$U_{tail} = \upsilon - \left[\frac{p}{\rho}\right]^{1/2} \quad \text{at} \quad x = X_{tail} \tag{I.3.11}$$

The rest of the procedure follows closely that of Section II.

3. Godunov Algorithm.

As another check of the numerical results we use the first order Godunov method to solve the one-dimensional hydrodynamic equations in the Lagrangian coordinates,

$$\frac{\partial \rho^{-1}}{\partial t} - \frac{\partial \upsilon}{\partial \xi} = 0 \tag{I.3.12}$$

$$\frac{\partial \upsilon}{\partial t} + \frac{\partial p}{\partial \xi} = 0 \tag{I.3.13}$$

$$\frac{\partial E}{\partial t} + \frac{\partial \upsilon p}{\partial \xi} = \frac{W}{\rho} \tag{I.3.14}$$

with the "mass" coordinate, ξ, defined by:

$$d\xi = \rho dx\,, \tag{I.3.15}$$

the Eulerian velocity $\upsilon = \partial x/\partial t$, and W is defined in Eqs.(4,5).

In our numerical calculation, the energy term affects only the time step iteration process (as in CAVEAT). On the other hand, the energy source may demand a modified Riemann solver. But even at this point the CAVEAT code (and we follow it) still uses the same algorithm as that of Godunov to calculate the interfacial values as if

there were no source. This approximation could lead to inaccuracy. The source of this discrepancy lies in the adiabatic condition:

$$p(t)\rho^{-\gamma}(t) = p(t_o)\rho^{-\gamma}(t_o) \qquad \text{(I.3.16)}$$

which is no longer valid if energy is supplied to the system. The above condition is used in the Riemann solver of the original Godunov algorithm. The accuracy of this approximation will be tested by the following numerical comparison with POST.

4. Results and Discussion.

We have calculated the hydrodynamic motion of the one-dimensional shock-tube problem with an energy source by using both POST and the first order Godunov method. The results at t = 10ns for the two approaches, as given in Figs.(I.6-I.11).

Figs.(I.6-I.8) describe the results for the receding piston problem, which creates a rarefaction wave. A uniform (in space) energy source is distributed *everywhere* in the system. As can be seen from these figures, the results obtained by POST and by the Godunov method are in substantial agreement except for the pressure (Fig.(I.7)). The results due to Dukowicz's double shock wave approximation are very close to those of the original Godunov method.

In Figs.(I.9-I.11) we present the results for the problem where the piston pushes the air out of the tube to the right. Consequently a compressive shock wave is created. In this case a Gaussian source, localized relative to the piston, is considered. Spikes occur around the shock wave with the Godunov method because we have

used only the first order Godunov algorithm. These spikes can be reduced by using the second order Godunov approach as was pointed by Van Leer[29].

In conclusion we can say that the Godunov method produces quite good results for a source strength of the order of 10^{14} [W/kg]. Comparison with the POST method shows a discrepancy of about 1%. We are not yet prepared to claim that this discrepancy is real. The principal conclusion is that the Godunov algorithm seems to work even better than expected.

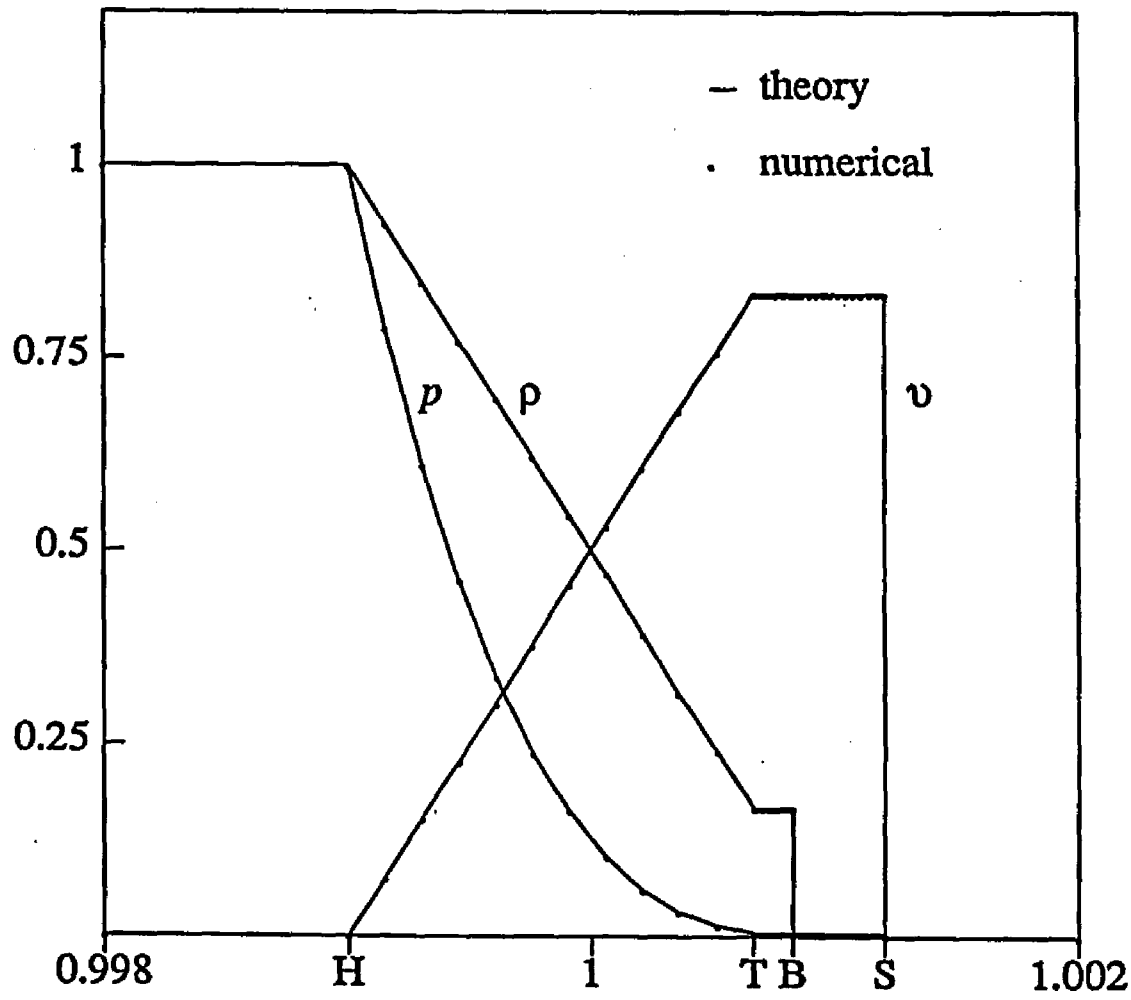

FIG. I.1. An analytical solution of the one-dimensional shock problem at time t=0.0001. The units for the dimensionless pressure, density and velocity are initial pressure, density and sound velocity of the undisturbed gas. The dimensionless coordinate is in the units of initial size of the system, and dimensionless time is in the units of the initial size of the system over the sound velocity of the undisturbed gas. The point "H" corresponds to the head of the wave which propagates into the "inside" gas with velocity equal to the sound velocity c_w. The point "S" represents the shock wave in the "outside" gas. The point "B" is the position of the interface surface. At this point a discontinuity in the density is present. The point "T" corresponds to the position of the tail of the "rarefaction wave" in the "inside" gas. This solution also serves as the initial condition for the spherical shock problem.

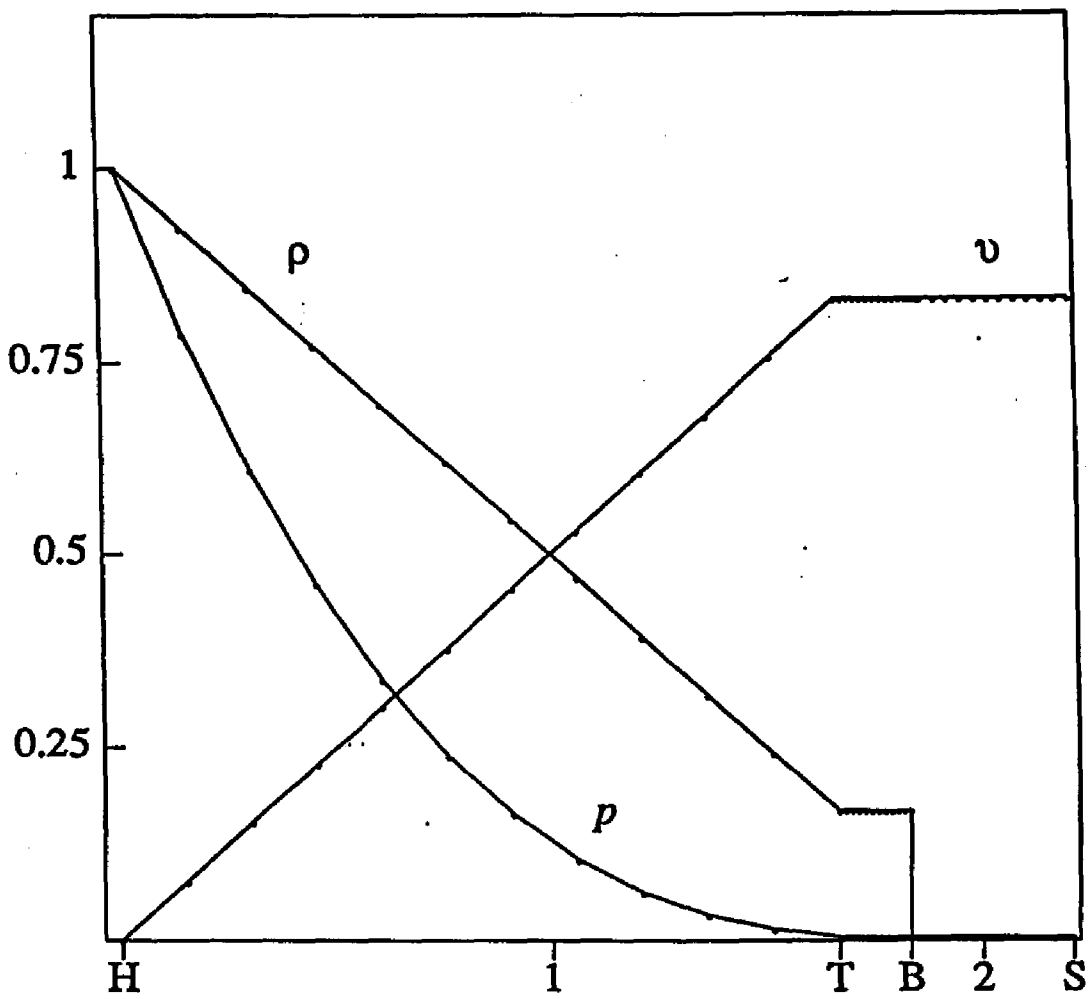

FIG. I.2. The numerical solution of the one-dimensional planar shock-tube problem for time t=1.0, when the "rarefaction" wave hits the left boundary of the "inside" gas. The results are practically the same as the analytical ones.

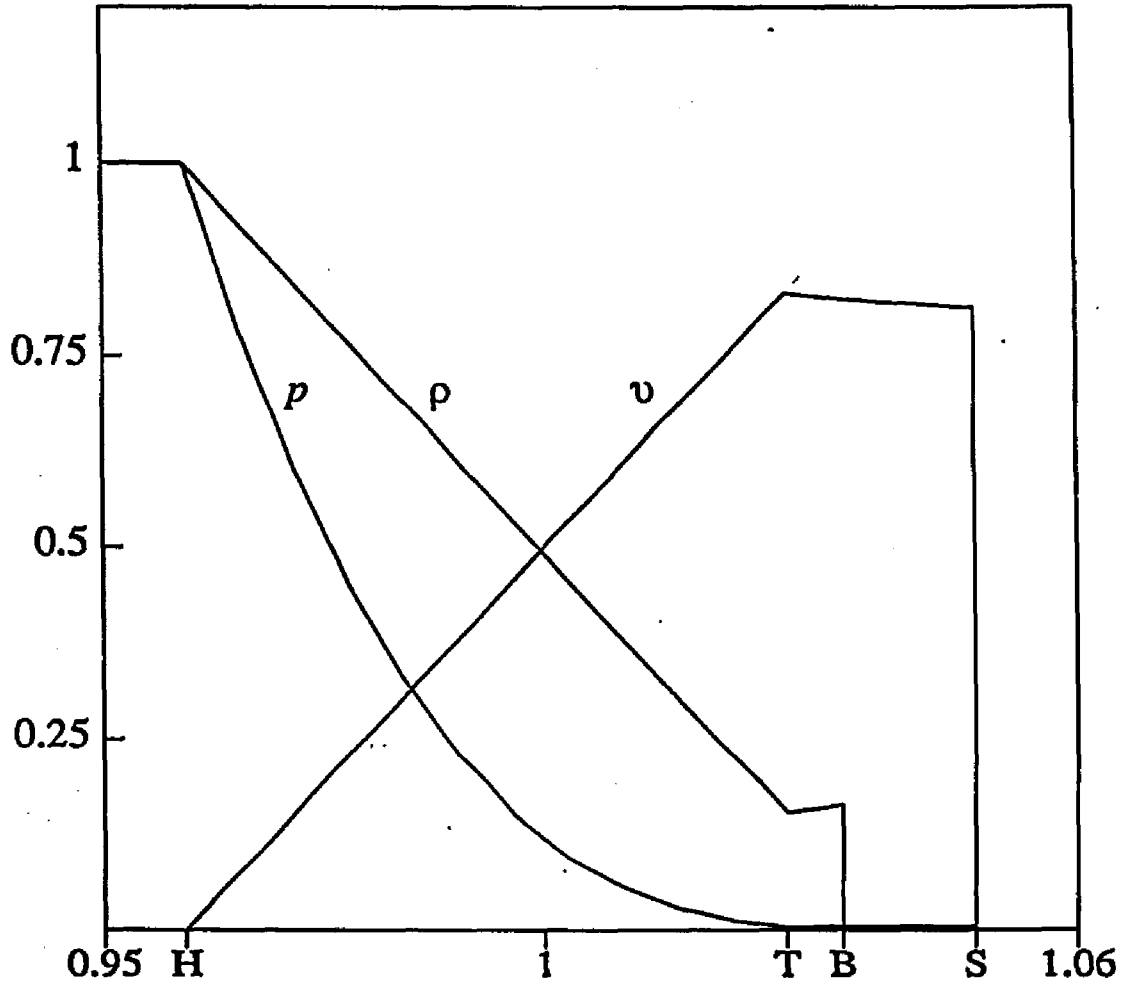

FIG. I.3. The numerical solution of the spherically-symmetric shock problem at time t=0.2. The general structure of the solution is similar to the one-dimensional one. In the "rarefaction" wave region there is a clear evidence of a backward facing shock-like formation at the point "T".

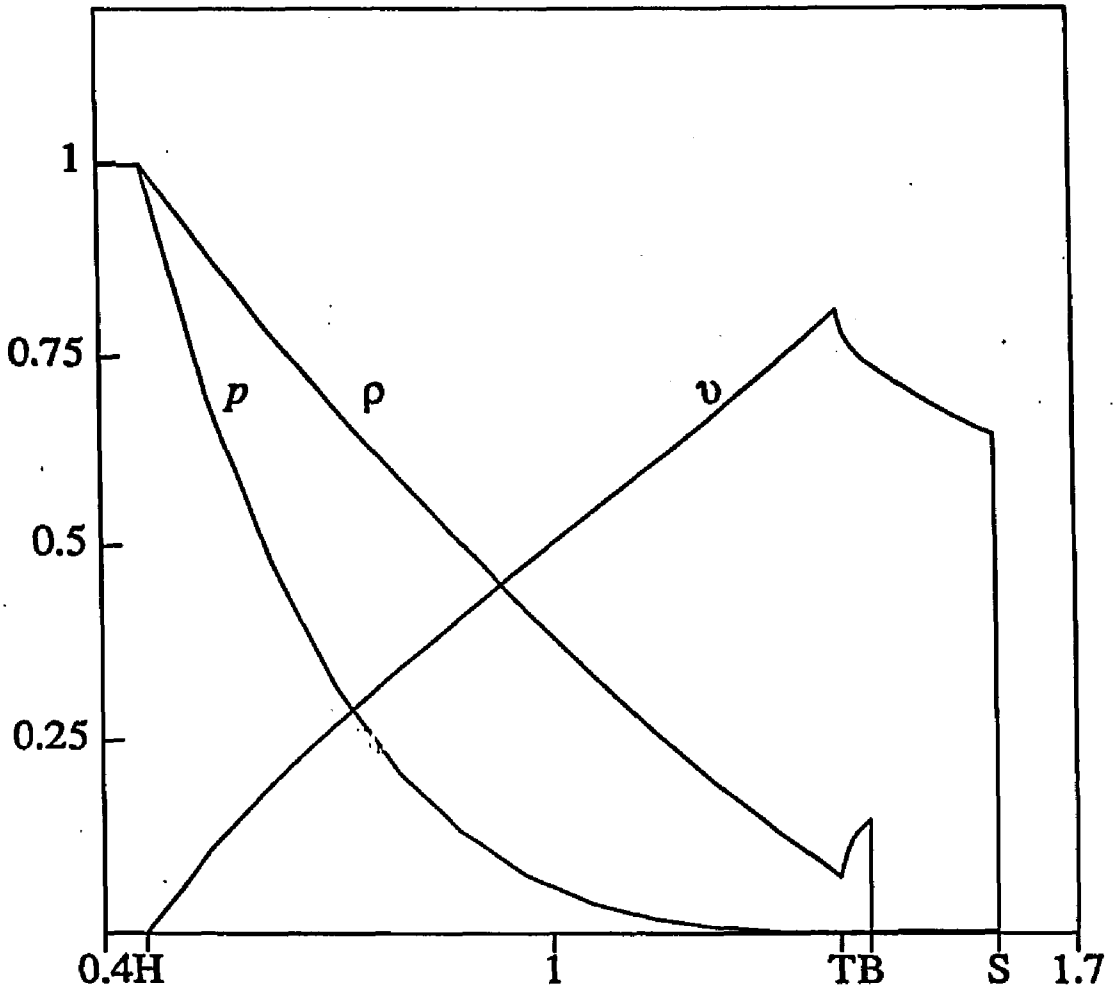

FIG. I.4. Solution of the spherical shock problem at time t=0.5. At the outside region the shock is clearly slowing down because of the spherical geometry effect.

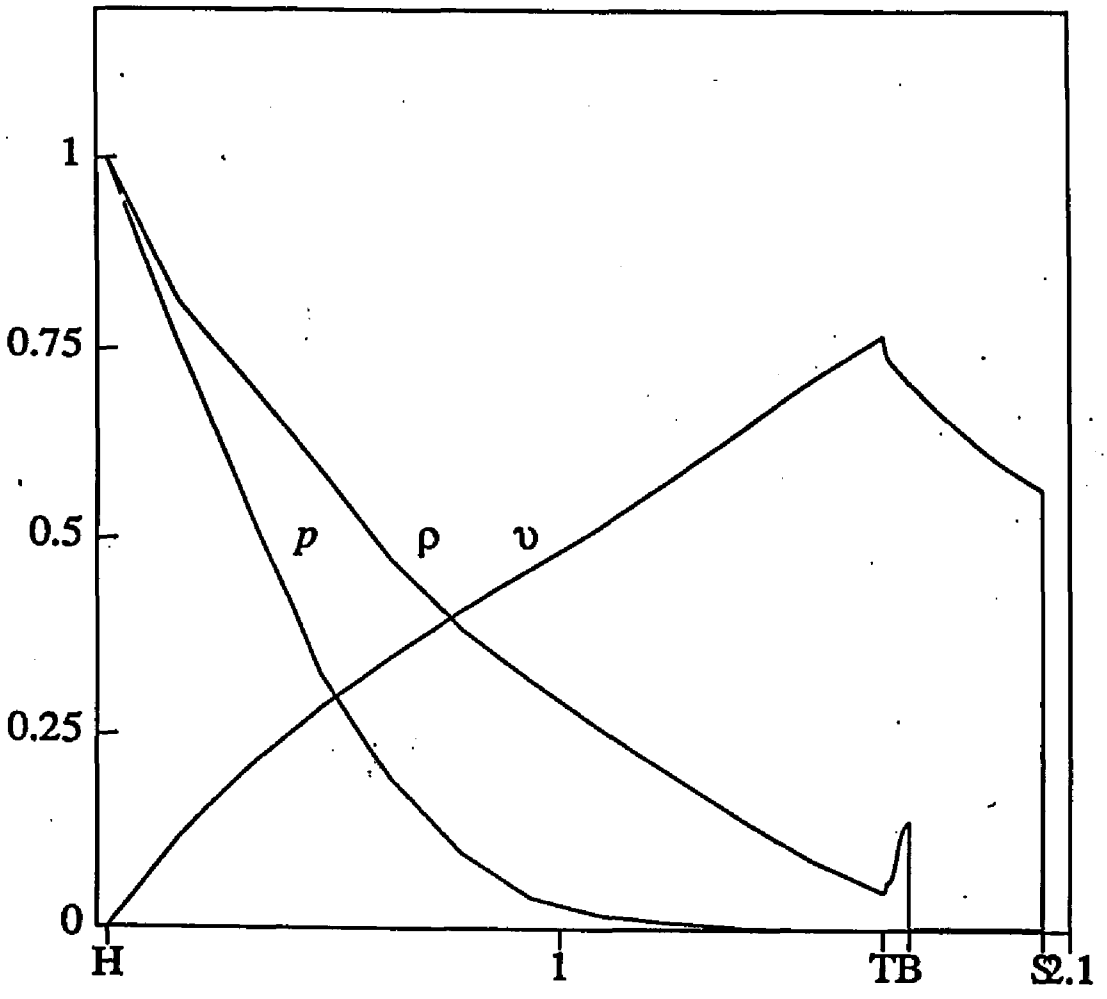

FIG. I.5. The numerical solution of the spherical shock problem for time t=0.99.

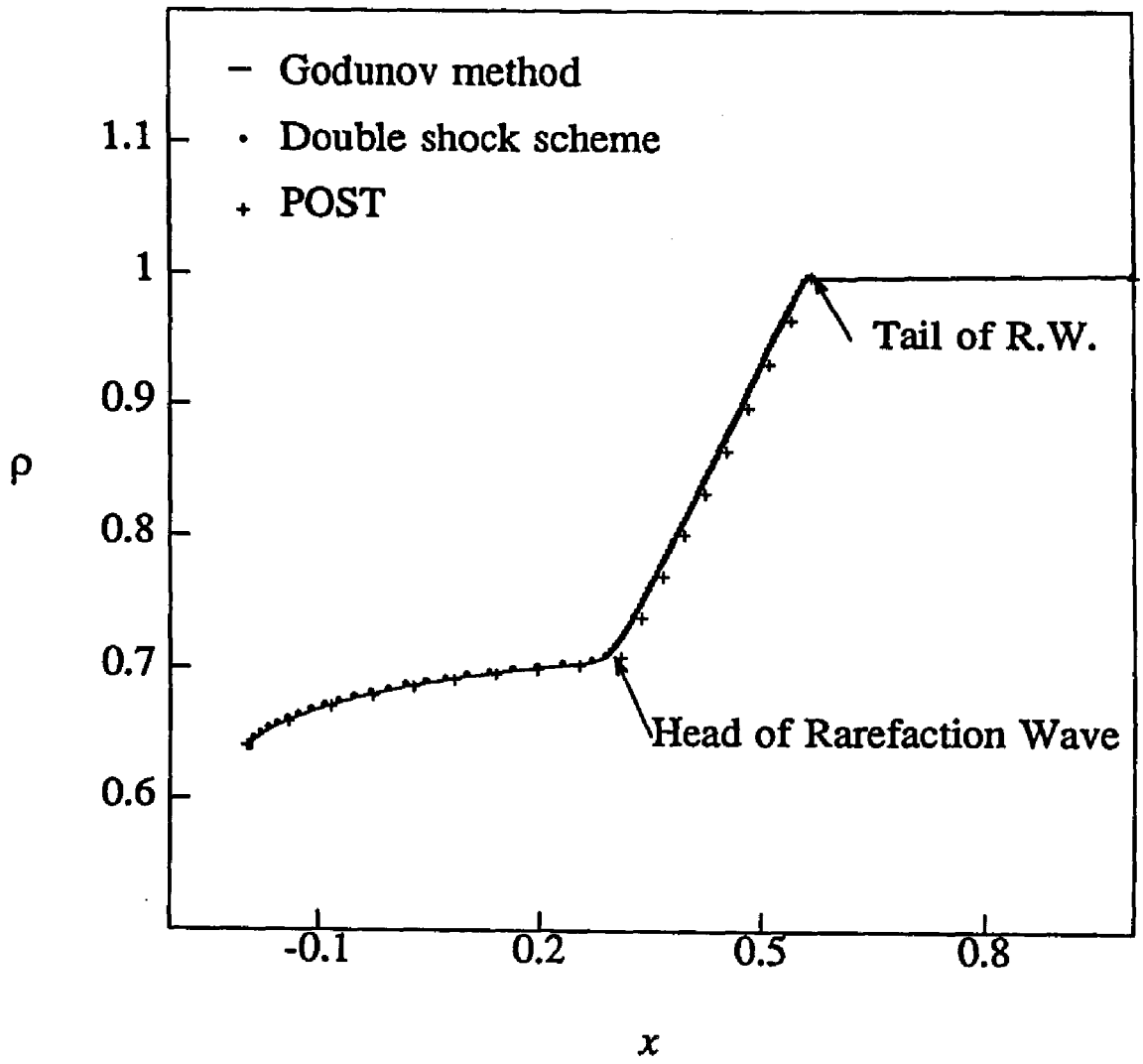

FIG. I.6. A numerical solution for density in the one-dimensional shock-tube problem at time t=10*n*sec. The units for the dimensionless density are the initial density of the undisturbed gas. The dimensionless coordinate is in units of 10μm. In this case we have used an energy source constant in the space and proportional to density of the gas. The piston, which was initially at point x=0, moves to the left with constant velocity $0.589c_o$. The piston recedes from the gas, creating a rarefaction wave, which propagates into the undisturbed gas to the right.

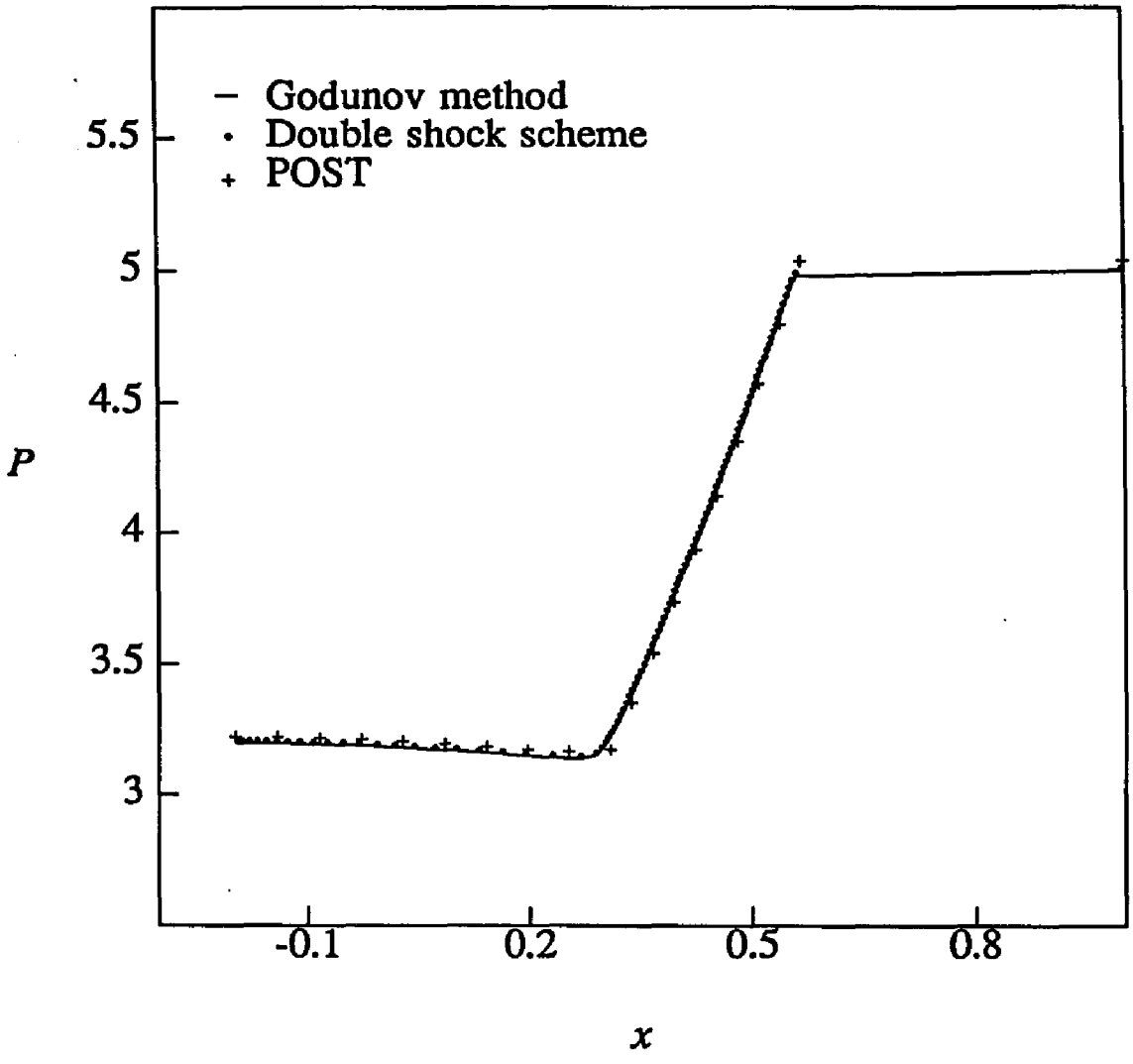

FIG. I.7. The numerical solution for pressure in the same problem as in Fig.(I.6). The results from Godunov schemes and from the POST are slightly different. The difference is more apparent than in density, because pressure is a "fast" responding hydrodynamical variable to the energy deposition. The inaccuracy in the rarefaction wave conditions used in Godunov's algorithm affects the position of the head and tail of the rarefaction wave.

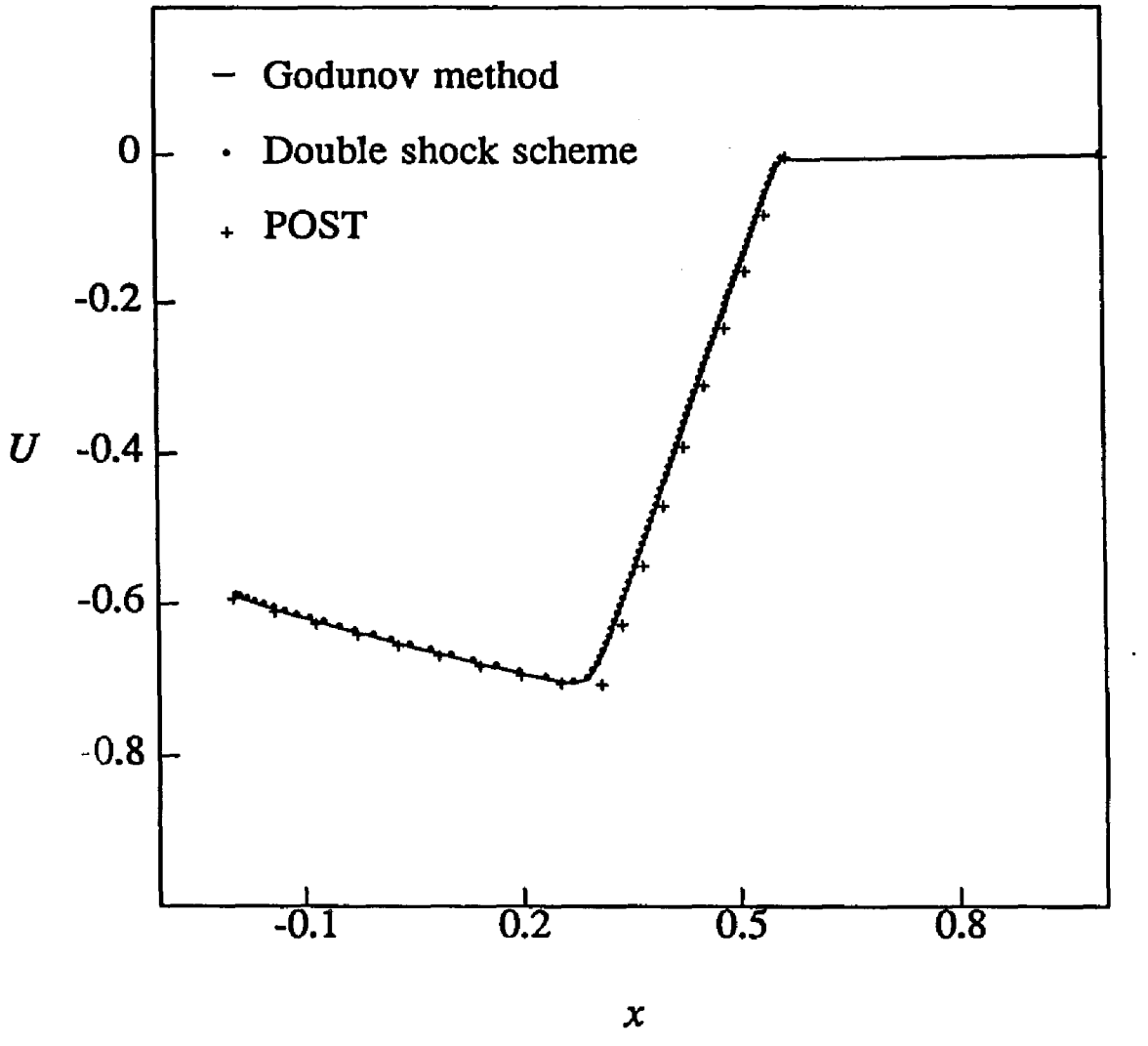

FIG. I.8. The numerical solution for velocity in the same problem as in Fig.(I.6).

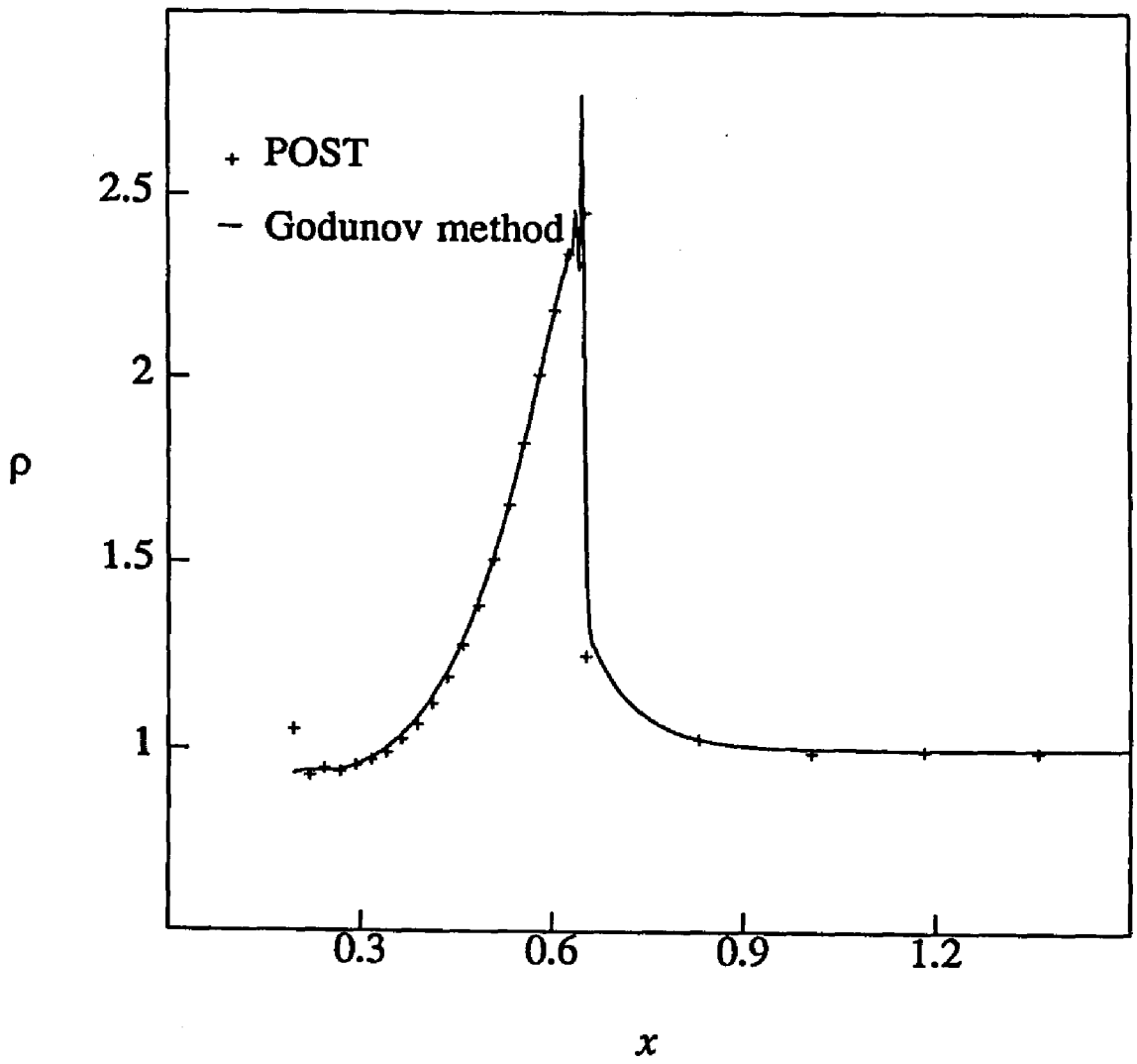

FIG. I.9. A numerical solution for density in the one-dimensional shock-tube problem at time t=10*n*sec. The units for the dimensionless density are the initial density of the undisturbed gas. The dimensionless coordinate is in the units of 10μ*m*. In this case we have used an energy source with Gaussian distribution located on the piston and proportional to the density of the gas. The piston, which was initially at point x=0, moves into the gas to the right with constant velocity $0.589c_o$. The piston compresses the gas on the right of it. This creates a strong shock wave, which propagates into the undisturbed gas to the right. The energy source raises pressure of the gas behind the shock much more, than in front of it, therefore the shock accelerates.

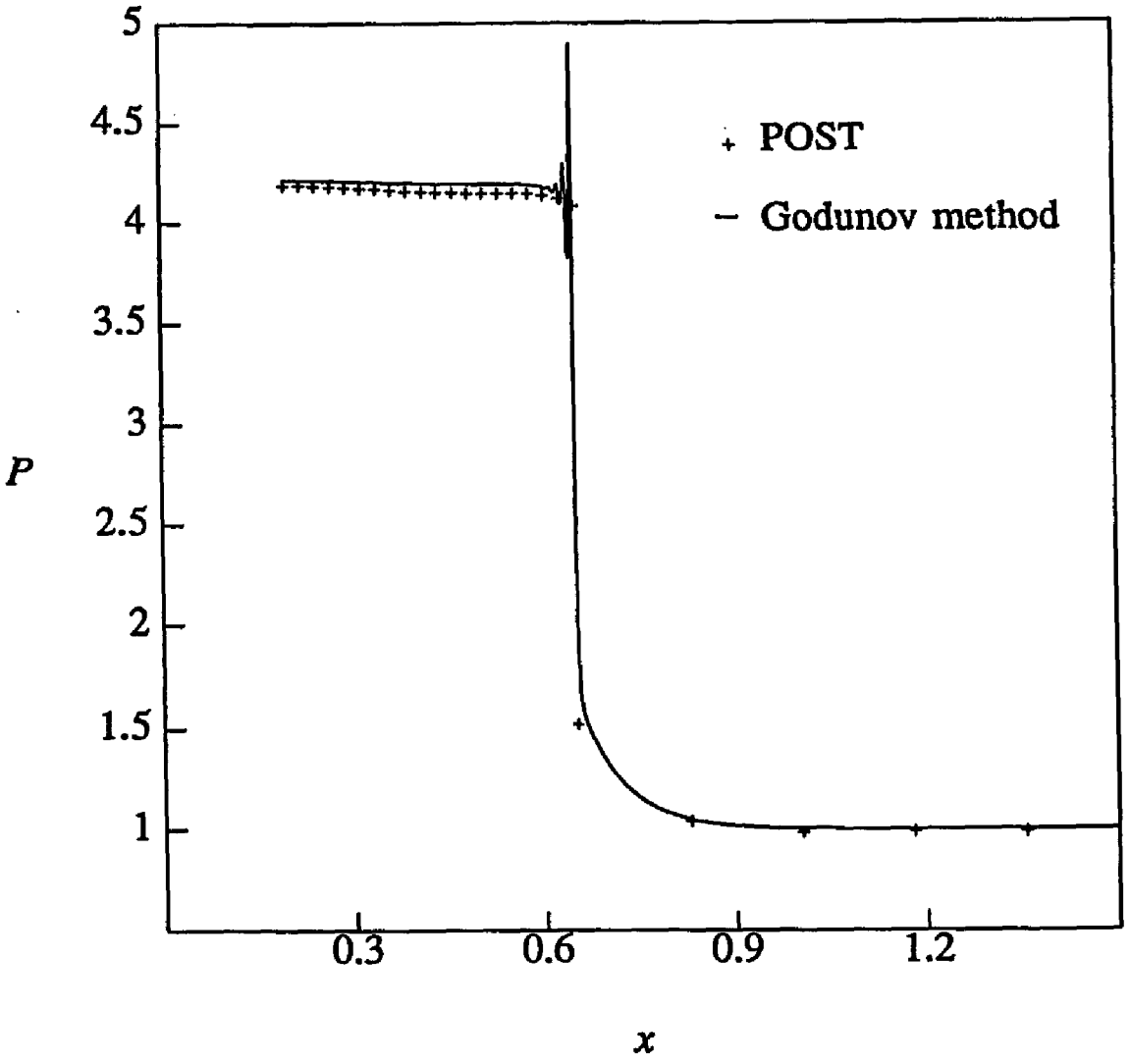

FIG. I.10. The numerical solution for pressure in the same problem as in Fig.(I.9). The spikes in the solution via Godunov's scheme are due to the first order algorithm and a relatively small number of mesh points (1000).

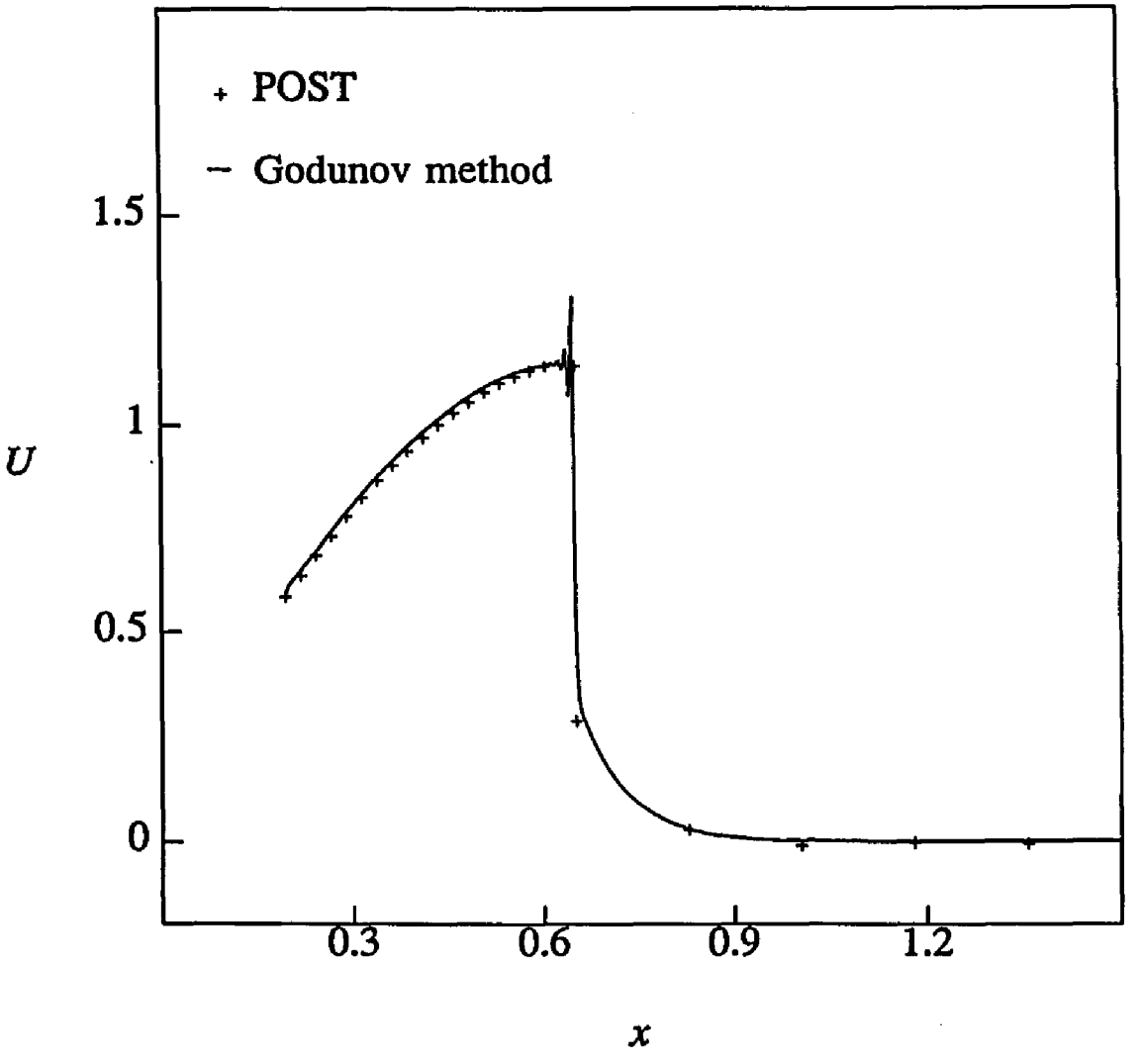

FIG. I.11. The numerical solution for velocity in the same problem as in Fig.(I.9).

Part II.

Electron Transport Through Parabolic Quantum Wells.

General Description of Electron Transport in Heterostructures.

1. Introduction.

A large amount of theoretical and experimental data has been obtained recently on the subject of the resonant tunneling through double barriers. The studies were motivated by the structures proposed by Tsu and Esaki[1]. Most of these studies have so far involved rectangular quantum wells. In the past few years a series of experiments were made by F. Capasso and collaborators[2-4] on tunneling through double barrier with a parabolic quantum well.

The parabolic well was fabricated by MBE on *GaAs* substrates. The 300 Å well was sandwiched between two 20 Å undoped barriers. The parabolic portion of the well was achieved by means of an $Al_{0.50}Ga_{0.50}As$–*GaAs* 15 Å period superlattice. In the experiments the authors measured the differential conductance for a representative diode from the sample described above. In Fig.(II.1) we have presented the results for the differential conductance of the parabolic quantum well. This graph was copied from Fig.(3) of Ref.(3). The results can be interpreted physically by means of the band diagrams which are depicted in Fig.(II.2) (Fig.(1) of Ref.(3)). When the bias is increased from 0 to 0.3V, the lower energy levels remain confined by the parabolic

well. The spacing of the levels is practically independent of the bias. The actual spacing in the material is about 35 meV. This equal spacing has been observed in Capasso's experiment[3].

It should be interesting to study theoretically the relaxation of electrons in such parabolic wells. Specifically, equally spaced energy levels in the parabolic wells may produce a pronounced feature in the electron relaxation (see the peaks in the Fig.(II.1)). In the systems, when a quantum well is sandwiched between semiconductor barriers, all carriers are dynamically two-dimensional (2D) since they have quantized energy levels in the direction normal to the junction plane, while they are essentially free in the other two directions. After the carriers are displaced from equilibrium either ohmically or optically, they relax via inelastic scattering with lattice excitations. Photoluminescence experiments in the steady state and the time dependent distribution of hot electrons in $GaAs$–$Ga_xAl_{1-x}As$ devices show that the distribution function of the hot electrons is well described by the single electron temperature T_e. Also, for $T_e > 50\ K$ the dominant energy-loss mechanism from the electrons to the lattice is the emission of longitudinal-optical (LO) phonons.

In this part of the thesis, recently developed techniques for coupling 2D carriers with phonons will be applied to the system of electrons in $GaAs$–$Ga_{1-x}Al_xAs$ heterojunctions. Specialization to the parabolic well will also be taken. The electrons inside the well are coupled to the LO phonons via the Frolich interaction. In the following part we will assume the electron-electron interaction relaxation time to be much smaller than the time scales present in our calculations. Therefore we will be able to use a temperature model for the distribution function of the electrons with given temperature T_e.

First we will write the equation which describes transport of the 2D electrons in the presence of the electron-phonon interaction. Then we will specialize to the case of the multilayered system that creates a parabolic confining potential for the electrons. And finally we will consider the effect of a magnetic field applied to the system.

2. Theoretical Background.

We start our theoretical investigation by writing the Hamiltonian of the system of electrons in the presence of the electron-phonon interaction:

$$\hat{H} = \hat{H}_e + \hat{H}_p + \hat{V}_{ep} \qquad \text{(II.1.1)}$$

where $\hat{H}_e$ and $\hat{H}_p$ are the electron and the phonon Hamiltonians, respectively, and $\hat{V}_{ep}$ denotes the electron - phonon interaction. We are mainly interested in the effects at $\approx 77^o$ temperature. At such temperatures the main contribution to the electron-phonon interaction comes from the interaction with LO phonons.

In the occupation number representation of 3D plane-wave phonon states, the longitudinal optical phonon Hamiltonian is given by

$$\hat{H}_p = \sum_{\mathbf{Q}} \hbar\omega_L \hat{b}_{\mathbf{Q}}^{\dagger} \hat{b}_{\mathbf{Q}} \qquad \text{(II.1.2)}$$

where $\mathbf{Q} = (\mathbf{q}, q_z)$ is the 3D phonon quasimomentum, and $\hat{b}_{\mathbf{Q}}^{\dagger}$ and $\hat{b}_{\mathbf{Q}}$ are the phonon creation and annihilation operators, respectively.

The states of the quasi-2D electrons at the interface of semiconductor hetero-junctions have been studied extensively[5]. Due to the confining potential in the direc-

tion normal to the interface, the 3D conduction band is split into 2D subbands. The wave function of a single electron in the n-th subband with 2D wave vector k is

$$\Psi_{n,\mathbf{k}}(\mathbf{r},z) = A^{-1}\,\zeta_n(z)\,\phi(\mathbf{k},\mathbf{r}) \tag{II.1.3}$$

where A is the layer area, and $\zeta_n(z)$ is the envelope function in the z direction. The explicit form of the envelope function depends on the confining potential[6].

In the second quantized form the electronic Hamiltonian is

$$\hat{H}_e = \sum_{n,\mathbf{k}} E_{n,\mathbf{k}}\,\hat{a}^{\dagger}_{n,\mathbf{k}}\,\hat{a}_{n,\mathbf{k}} + \hat{V}_{ee} \tag{II.1.4}$$

where $E_{n,\mathbf{k}} = E_n + E(\mathbf{k})$, and $\hat{a}_{n,\mathbf{k}}^{\dagger}$ and $\hat{a}_{n,\mathbf{k}}$ are the creation and annihilation operators of the electrons at the n-th 2D subband with k wave vector. The spin indices have been omitted. V_{ee} represents the Coulomb interaction between electrons, and is not specified here. We simply assume a temperature model with the temperature T_e for the electrons.

The electron - phonon interaction can be adequately described by the Frohlich continuum model

$$\hat{V}_{ep} = \frac{e}{4\pi}\int d\mathbf{R}\int d\mathbf{R}'\,\hat{\rho}(\mathbf{R})\frac{1}{|\mathbf{R}-\mathbf{R}'|}[-4\pi\nabla'\cdot\hat{\mathbf{P}}(\mathbf{R}')] \tag{II.1.5}$$

where $\hat{\rho}(\mathbf{R})$ is the electron density operator, and the divergence term is the charge density due to the polarization of the medium. The latter is related to the relative displacement of positive and negative ions

$$\hat{\mathbf{u}}(\mathbf{R}) = \hat{\mathbf{u}}_{+}(\mathbf{R}) - \hat{\mathbf{u}}_{-}(\mathbf{R}) \tag{II.1.6}$$

$$\hat{\mathbf{P}} = (\frac{e^*}{\upsilon_c})\,\hat{\mathbf{u}} \tag{II.1.7}$$

where e^* is an effective charge given by

$$e^* = [(\mu\upsilon_c / 4\pi)\omega^2_L(1/\varepsilon_\infty - 1/\varepsilon_o)]^{1/2} \tag{II.1.8}$$

with μ being the atomic reduced mass, υ_c - the volume of the unit cell, and ε_∞ and ε_o - the high frequency and the static dielectric constants, respectively.

In the second quantized form for the phonon operators, the displacement operator associated with the longitudinal optical modes can be represented as

$$\hat{\mathbf{u}}(\mathbf{R}) = \left[\frac{\hbar}{2\omega_L\mu N}\right]^{1/2} \sum_{\mathbf{Q}} \frac{\mathbf{Q}}{Q}(\hat{b}_{\mathbf{Q}} e^{i\mathbf{Q}\cdot\mathbf{R}} + \hat{b}^{\dagger}_{\mathbf{Q}}\, e^{-i\mathbf{Q}\cdot\mathbf{R}}) \tag{II.1.9}$$

where N is the number of unit cells.

Later we will use two different representations of the many-body electron operators. First we will derive the transport equations for the electrons and phonons by using the second-quantized 2D plane wave representation for the many electron system. In the last Section, where the effects of the magnetic field will be considered, we will regard the electronic system as one electron and use the magnetic basis functions. The final result will be multiplied by the equilibrium electron distribution function to provide the many-body properties (ignoring the statistics of the spin).

In the second quantized representation $\hat{V}_{ep}(\mathbf{R})$ takes the form[7]:

$$\hat{V}_{ep}(\mathbf{R}) = \frac{i\alpha}{\sqrt{A}} \sum_{n,\mathbf{k}} \sum_{n',\mathbf{k}'} \sum_{\mathbf{Q}} [\hat{b}_{\mathbf{Q}}\delta_{\mathbf{k}',\mathbf{k}+\mathbf{q}} G_{n,n'}(q_z,\mathbf{q}) - \hat{b}^{\dagger}_{\mathbf{Q}}\,\delta_{\mathbf{k}',\mathbf{k}-\mathbf{q}} G_{n,n'}{}^*(q_z,\mathbf{q})]\hat{a}^{\dagger}_{n'\mathbf{k}}\,\hat{a}_{n\mathbf{k}} \tag{II.1.10}$$

where α is the Frohlich electron-LO-phonon coupling constant

$$\alpha = [2\pi e^2 \hbar\omega_L(1/\varepsilon_\infty - 1/\varepsilon_o)]^{1/2} \qquad \text{(II.1.11)}$$

and $G_{n',n}(q_z, \mathbf{q})$ is the matrix element of the operator $\exp(i\mathbf{Q}\cdot\hat{\mathbf{R}})$ between the electronic states $\Psi(\mathbf{R})$. For the case of the 3D electrons confined in the layer this matrix element is given by[7]

$$G_{n',n}(q_z,\mathbf{q}) = \frac{1}{Q\sqrt{L}} \int_{-\infty}^{+\infty} dz \xi^*_{n'}(z)\exp(iq_z z)\xi_n(z) \qquad \text{(II.1.12)}$$

where Q denotes the magnitude of the three-dimensional wave vector $\mathbf{Q}$ and L is the length of the layer.

It may be appropriate here to make some simplifications regarding the phonon-phonon interaction. This interaction in general leads to the decay of the LO phonons into acoustic phonons. These acoustic phonons then thermalize with the equilibrium lattice. In the following part we will use a single relaxation time approximation for the contribution of such process to the phonon kinetic equation. Moreover, we will assume the relaxation time to be constant (i.e., independent of the wave vector). It will be regarded as a parameter of the problem.

3. Derivation of the Phonon Kinetic Equation.

In our study we are interested in the transport of the electrons and phonons in the quantum well. To get transport properties of the system we have to start with a kinetic equation for the carriers. In deriving the kinetic equation we will follow closely the paper by W.Cai et al.[7] We start with the Liouville equation for the nonequilibrium density matrix of the electron-phonon system

$$i\hbar\frac{\partial\hat{\rho}(t)}{\partial t} = [\hat{H},\hat{\rho}(t)] \qquad \text{(II.1.13)}$$

From Eq.(1.13) for nonequilibrium system of electrons and phonons we can, using the method of Zubarev[8], get a simpler equation for the distribution functions of phonons and electrons separately. Zubarev's method is based on the Bogoliubov's idea that, after an initial transient, the nonequilibrium state of a classical system is well described in terms of the expectation values of a reduced number of macroscopical observables. The choice of the observables depends on the time scale of the processes, which we are interested in. The same method may be applied to quantum systems as well.

Being concerned with the description of the kinetic stage of the relaxation, we choose the observables of interest to be the one-body density matrices of the electron and the phonon gases, respectively. The one-body density matrix of the phonon gas is permitted to be spatially inhomogeneous in the z direction. Thus nondiagonal matrix elements in the z component of the momentum in the plane wave representation are retained:

$$n_{\mathbf{q}}(q_z, q_z', t) = \mathrm{Tr}[\hat{b}^{\dagger}_{\mathbf{q},q_z}\,\hat{b}_{\mathbf{q},q_z'},\hat{\rho}(t)] \qquad \text{(II.1.14)}$$

The average values of all phonon one-body observables can be expressed in terms of this density matrix. If we are not considering the "hot" phonon effects, the phonon occupation number is a Bose distribution. Therefore in following sections we will assume that $n_{\mathbf{q}}(q_z,q_z',t) = n_{\mathbf{q}}\,\delta(q_z,q_z')$ (see also Appendix D).

Similarly, the one-body electron density matrix is defined as

$$f_{nk}(t) = \mathrm{Tr}[\hat{a}^{\dagger}_{nk}\,\hat{a}_{nk},\hat{\rho}(t)] \tag{II.1.15}$$

This matrix can be and has been assumed diagonal in the chosen plane wave representation.

We define a "collective" object $\gamma(t) = [n_q(q_z, q'_z, t); f_{nk}(t)]$ as our macroscopic observable both electronic and phonon. Now, the Liouville equation may be rewritten in the form

$$i\hbar\frac{\partial F(\gamma(t))}{\partial t} = \mathrm{Tr}\left\{[F(\hat{\gamma}), \hat{H}]\hat{\rho}(t)\right\} \tag{II.1.16}$$

The essential assumption used in the derivation of the preceding equation is (following W.Cai et al.[7]) that for times longer than a microscopic collision time, t_0, the nonequilibrium density matrix depends on time only via the time dependence of the macroscopic observable, i.e.,

$$\hat{\rho}(t) = \hat{\rho}(\gamma(t)), \quad \text{for } t \gg t_0 \tag{II.1.17}$$

For times much larger than t_0 the time evolution of the nonequilibrium state is described by a set of coupled kinetic equations for the components of $\gamma(t)$. To second order in the interaction potential $\hat{V}$ one obtains:

$$\frac{\partial F(\gamma(t))}{\partial t} = \frac{i}{\hbar}\mathrm{Tr}[\hat{H}_p, F(\hat{\gamma})]\hat{\rho}_0(t) + \left[\frac{i}{\hbar}\right]^2 \lim_{\varepsilon\to 0^+}\int_{-\infty}^{0} d\tau e^{\varepsilon\tau}\mathrm{Tr}\left\{[\hat{V}(\tau), [\hat{V}, F(\hat{\gamma})]]\hat{\rho}_0(t)\right\} \tag{II.1.18}$$

In this equation the operators are in the interaction representation, e.g.:

$$\hat{V}(\tau) = \exp[i(\hat{H}_e + \hat{H}_p)\tau/\hbar]\,\hat{V}\exp[-i(\hat{H}_e + \hat{H}_p)\tau/\hbar] \tag{II.1.19}$$

In Eq.(1.18) the quasiequilibrium density matrix $\hat{\rho}_0(t)$ is the Gibbsian

$$\hat{\rho}_0(t) = \frac{1}{\Theta} \exp\left[-\sum_i B_i(\gamma(t))\hat{\gamma}_i\right] \tag{II.1.20}$$

with Θ - a normalization constant and the functions B_i to be determined by the requirement that each element γ_i of γ obeys

$$\gamma_i(t) = \mathrm{Tr}(\hat{\gamma}_i\hat{\rho}_0(t)) \tag{II.1.21}$$

Eq.(1.18) is the kinetic equation we are interested in, and our further investigation will be based on this equation.

4. Power, Radiated into the Phonons.

The kinetic quantity of interest for experiments is the total power, radiated into the phonons due to the electron-phonon interaction. This power is equal to the energy-loss rate of the electrons resulting from the inelastic collisions with the LO phonons. Per electron this power may be calculated from the equation:

$$P(t) = \frac{1}{N_e}\sum_{\mathbf{Q}} \hbar\omega_{LO}(\mathbf{Q}) \left[\frac{\partial n_{\mathbf{q}}(q_z,q_z,t)}{\partial t}\right]_{ep} \tag{II.1.22}$$

where N_e is the total number of electrons in the 2D layer. If we insert $\partial n_{\mathbf{q}}(q_z, q_z)/\partial t$ from our kinetic equation (see Eq.(1.18)), we obtain

$$P_e = \frac{\hbar\omega_L{}^2\, 2\pi\alpha^2}{N_e\hbar A}\sum_{n\mathbf{k}}\sum_{n'\mathbf{k}'} f_{n\mathbf{k}}(t)\left[1-f_{n'\mathbf{k}'}(t)\right]\sum_{\mathbf{q}}\sum_{q_z}\sum_{q_z'} G^*_{n'n}(\mathbf{q},q_z)G_{n'n}(\mathbf{q},q_z') \tag{II.1.23}$$

$$\times\left[\,\delta(\mathbf{k}',\mathbf{k}-\mathbf{q})\delta(E_{n,\mathbf{k}}-E_{n',\mathbf{k}'}-\hbar\omega L)\,\left[\delta(q_z,q_z')+n_{\mathbf{q}}(q_z,q_z',t)\right]\right.$$

$$- \delta(\mathbf{k}',\mathbf{k}+\mathbf{q})\,\delta(E_{n,\mathbf{k}} - E_{n',\mathbf{k}'} + \hbar\omega_L) n_{\mathbf{q}}(q_z, q_z', t)]]$$

In principle, the evaluation of the power P_e requires simultaneous solution of both phonon and electron kinetic equations. Even when the electron distribution function $f_{n\mathbf{k}}$ is given, the equation for the phonon distribution function $n_{\mathbf{q}}(q_z, q_z', t)$ is an integral equation. To simplify this integral equation, Cai, Marchetti and Lax[7] have introduced the envelope function

$$N_{n',n,m',m} = \frac{\sum_{q_z}\sum_{q_z'} G^*_{n',n}(\mathbf{q}, q_z) n_{\mathbf{q}}(q_z, q_z', t) G_{m',m}(\mathbf{q}, q_z)}{F_{nn',mm'}(\mathbf{q})/2q} \qquad \text{(II.1.24)}$$

as the new phonon state distribution function weighted with electronic subband wave functions. The function $F_{n',n,m',m}(\mathbf{q})$ is the electronic form factor

$$F_{n',n,m',m} = 2q \sum_{q_z} G^*_{n',n}(\mathbf{q}, q_z)\, G_{m',m}(\mathbf{q}, q_z) \qquad \text{(II.1.25)}$$

As shown in the cited paper[7], the equation for this phonon occupation number N is an algebraic equation in contrast to an integral equation for n.

We will not elaborate further on that matter but will turn to a simple case of known distributions for the electrons and phonons at specific temperatures (see the discussion below in this section). The purpose of our work is to apply kinetic equation (Eq.(1.18)) to the case of the parabolic confining potentials for the 2D electrons without the magnetic field and to the case where a magnetic field perpendicular to the layers (in the z - direction) is present.

Electron Transport in the Parabolic Quantum Well.

From this part, we will specialize to the parabolic quantum wells. The wave functions of the electrons in the 2D subbands in the parabolic potential are represented by:

$$\xi_n(z) = (2\pi)^{-1/4}(n!)^{-1/2}\left[\frac{2m\omega_0}{\hbar}\right]^{1/4} e^{-\frac{m\omega_0 z^2}{2\hbar}}\, \mathrm{He}_n\left[\sqrt{\frac{2m\omega_0}{\hbar}}\, z\right] \qquad \text{(II.2.1)}$$

where the Hermite polynomials $\mathrm{He}_n(y)$ have been weighted by a Gaussian.

The first step in the calculation of the power is the evaluation of the function $G_{n'n}(\mathbf{q}, q_z)$, which enters every equation for the kinetic quantities in the preceding sections (see Eqs.(1.16-1.25)). We are rewriting this function here: Eq.(1.12)

$$G_{n'n}(\mathbf{q}, q_z) = \frac{1}{\sqrt{L}\sqrt{\mathbf{q}^2 + q_z^2}} \int_{-\infty}^{\infty} dz\, \xi^*_{n'}(z)\xi_n(z)e^{iq_z z} \qquad \text{(II.2.2)}$$

We define the dimensionless variables x, k, p^2 via

$$x = \sqrt{\frac{2m\omega_0}{\hbar}}\, z\ ; \qquad k = \frac{q_z}{\sqrt{\frac{2m\omega_0}{\hbar}}}\ ; \qquad p^2 = \frac{\mathbf{q}^2}{\frac{2m\omega_0}{\hbar}}\ . \qquad \text{(II.2.3)}$$

In terms of these variables, after taking the integral in the Eq.(2.2), the G - function takes the form (see, for example, Ting et al.[9]):

$$G_{n'n}(\mathbf{q}, q_z) = \frac{(-1)^{\frac{n'-n}{2}}}{\sqrt{L}}\left[\frac{n!}{n'!}\right]^{1/2} \frac{1}{(p^2+k^2)^{1/2}(\frac{2m\omega_0}{\hbar})^{1/2}}\, k^{n'-n} e^{-\frac{k^2}{2}} L_n^{n'-n}(k^2) \qquad \text{(II.2.4)}$$

Here and elsewhere $n' > n$ is assumed. The functions $L_n^m(x)$ in the above equation are the associated Laguerre polynomials. They are given by

$$L_n^m(x) = \sum_{l=0}^{n}(-1)^l \frac{(n+m)!}{(m+l)!(n-l)!}\frac{x^l}{l!} \quad \text{for } m > 0 \tag{II.2.5}$$

$$L_n^m(x) = \sum_{l=-m}^{n}(-1)^l \frac{(n+m)!}{(m+l)!(n-l)!}\frac{x^l}{l!} \quad \text{for } m < 0 \tag{II.2.6}$$

With the help of the Eq.(2.4) the double sum in the Eq.(1.22) can be put into a form

$$A_{n'n}(\mathbf{q}) \equiv \sum_{q_z}\sum_{q_z'} \delta(q_z, q_z')\, G^*_{n'n}(\mathbf{q}, q_z)\, G_{n'n}(\mathbf{q}, q_z') =$$

$$\frac{n!}{n'!}\frac{1}{(\frac{2m\omega_0}{\hbar})^{1/2}}\int_{-\infty}^{\infty} dk \frac{k^{2(n-n')}e^{-k^2}\left[L_n^{n-n'}(k^2)\right]^2}{k^2+p^2} \tag{II.2.7}$$

again, with $n' \geq n$. Notice, that the function $A_{n'n}$ is symmetric with respect to the indices n, n' - a quality, which we will use later.

Collecting the terms in the equation for the energy dissipation (Eq.(1.22)) we obtain

$$P_e(t) = C\sum_{\mathbf{k}\mathbf{k}'}\sum_{n'n}\sum_{\mathbf{q}} f_{n\mathbf{k}}(1 - f_{n'\mathbf{k}'})\, A_{n'n}(\mathbf{q}) \tag{II.2.9}$$

$$\times [\, \delta(\mathbf{k}', \mathbf{k}-\mathbf{q})\, \delta(E_{n\mathbf{k}} - E_{n'\mathbf{k}'} - \hbar\omega_L)\, (1 + n_p(t, \mathbf{q})) - \delta(\mathbf{k}', \mathbf{k}+\mathbf{q})\, \delta(E_{n\mathbf{k}} - E_{n'\mathbf{k}'} + \hbar\omega_L)\, n_p(t, \mathbf{q})\,]$$

$$= C\sum_{n'n}\sum_{\mathbf{q}} A_{n'n}(\mathbf{q})\, [(1 + n_p(t, \mathbf{q}))\, \Gamma^-_{n'n}(\mathbf{q}) - n_p(t, \mathbf{q})\, \Gamma^+_{n'n}(\mathbf{q})]$$

Here we define

$$I^{\pm}_{n'n}(q) = \sum_{k} f_{nk}(1 - f_{n'k'\pm q})\delta(E_{nk} - E_{n'k\pm q} \pm \hbar\omega_L) \qquad \text{(II.2.10)}$$

and the constant C represents all the multiplicative constants which appear in front of the sums in the equation for $P_e(t)$ (see Eq.(1.22)).

$$C = \frac{\hbar\omega^2{}_L 2\pi\alpha^2}{N_e \hbar A} \qquad \text{(II.2.11)}$$

The calculations can be greatly simplified if we will make an assumption that for the temperatures at which the experiments were performed (over $77K^0$) the electron distribution function f_{nk} can be approximated by a Maxwellian

$$f_{nk} \approx M\exp\left(\frac{-E_n(k)}{k_B T_e}\right) \qquad \text{(II.2.12)}$$

and, correspondingly,

$$1 - f_{nk} \approx 1 \qquad \text{(II.2.13)}$$

For the parabolic wells the energy of the electron in the n-th level and with k wave vector, E_{nk} is given by

$$E_{nk} = \hbar\omega_0\left(\frac{1}{2} + n\right) + \frac{\hbar^2 k_x{}^2}{2m} + \frac{\hbar^2 k_y{}^2}{2m} \qquad \text{(II.2.14)}$$

Making use of the previous assumptions (see Eqs.(2.12),(2.13)) we can get, after some algebraic transformations, an expression for $I^{\pm}$:

$$I^{\pm}_{n'n}(q) \approx \mp \frac{\mu^{3/2}(2\pi k_b T_e)^{1/2} L^2}{\hbar^3} e^{\frac{\hbar}{2k_b T_e}[(n+n'+1)\omega_0 \mp \omega_L]} \frac{e^{-aq^2 - \frac{b^{\pm}}{q^2}}}{q} \qquad \text{(II.2.15)}$$

with the definition

$$a \equiv \frac{\hbar^2}{8mk_bT_e}; \qquad b^{\pm} \equiv \frac{[\omega_L \pm \omega_0(n-n')]^2}{2k_bT_e}m \tag{II.2.16}$$

A closer view at Eq.(1.22) for the power radiated into the phonons suggests that the double summation over the energy levels n can be performed. To do this summation we will use a formula, based on the simple rearrangement of the terms:

$$\sum_{n=0}^{\infty}\sum_{n'=0}^{\infty} C_{nn'} = \sum_{k=1}^{\infty}\left\{\sum_{n=0}^{\infty}\left[C_{n,n+k} + C_{n+k,n}\right]\right\} + \sum_{n=0}^{\infty} C_{nn} \tag{II.2.17}$$

with $C_{nn'}$ - any function of two indices. After this rearrangement the equation for the power will contain a factor

$$\sum_{n=0}^{\infty} e^{-\frac{\hbar\omega_0(n+\frac{1}{2})}{k_BT_e}} A_{n,n+k}(q) \tag{II.2.18}$$

with $A_{n,n'}(q)$ defined in Eq.(2.10). The summation over n can be performed using the sum formula (see Bateman[10]):

$$\sum_{n=0}^{\infty} \frac{L^l_n(x)L^l_n(y)z^n n!}{\Gamma(n+l+1)} = \frac{(xyz)^{\frac{l}{2}}}{1-z} e^{-z\frac{x+y}{1-z}} I_l\left[2\frac{\sqrt{xyz}}{1-z}\right] \tag{II.2.19}$$

where $I_l(x)$ are the modified Bessel functions. The result of the summation is:

$$\sum_{n=0}^{\infty} e^{-\frac{\hbar\omega_0(n+\frac{1}{2})}{k_BT_e}} A_{n,n+k}(q) = \left(\frac{2m\omega_0}{\hbar}\right)^{-\frac{1}{2}} \frac{1}{1-z_0} \int_0^{\infty} dx \frac{e^{-x}x^{-1/2}}{x + \frac{q^2}{\frac{2m\omega_0}{\hbar}}} e^{-2x\frac{z_0}{1-z_0}} I_k\left(2x\frac{z_0^{\frac{1}{2}}}{1-z_0}\right) \tag{II.2.20}$$

here, we used Eq.(2.7) and defined

$$z_0 \equiv \exp\left(-\frac{\hbar\omega_0}{k_B T}\right) \tag{II.2.21}$$

Next a simplification is possible if we assume that the equilibrium phonon distribution $n_q(t)$ is independent of **q** (the case when $n_q(t)$ is a Maxwellian in **q** can be handled similarly). Moreover, we recall that the main contribution to the interaction with the LO phonons comes from the electrons with the $q \approx 0$. At this point the ω_L can be approximated by a **q** - independent constant. With the help of these assumptions we can perform the two dimensional integration over **q** to obtain the final expression (Eq.(2.22)), from which the power can be calculated numerically:

$$P_e = P_0 \left[\frac{1}{\sinh(\Omega_0)}\right]^{1/2} \sum_{n=0}^{\infty} \int_0^{\infty} dx Q_{n-0.5} \left[\cosh(\Omega_0) + \frac{1}{2}\Omega_0 \sinh(\Omega_0) x\right] \tag{II.2.22}$$

$$\times \frac{\left\{e^{-\sqrt{1+x}\,|\Omega_L - n\Omega_0|} + e^{-\sqrt{1+x}\,|\Omega_L + n\Omega_0|}\right\}}{\sqrt{1+x}} \left[e^{-\Omega_L}(n_q + 1) - e^{\Omega_L} n_q\right]$$

where the constant factor P_0 is

$$P_0 \equiv \frac{8\pi^4 \mu^{3/2} e^2 L^2 (\hbar\omega_L)^2 (\hbar\omega_0)^{1/2}}{\hbar^4 N_e} \left[\frac{1}{\varepsilon_\infty} - \frac{1}{\varepsilon_0}\right] \tag{II.2.23}$$

In the above equation $Q_{k-0.5}(y)$ are the Legendre polynomials of half-integer order (see, for instance, Morse and Feshbach[11]), and Ω_L and Ω_0 are the dimensionless frequency of the LO phonons and the natural frequency of the electron in the parabolic well, defined as

$$\Omega_L = \frac{\hbar\omega_L}{2 k_b T_e}\ ; \qquad \Omega_0 = \frac{\hbar\omega_0}{2 k_b T_e}\ . \tag{II.2.24}$$

and n_q is the Planck function

$$n_q = \frac{1}{e^{2\Omega_L T_e/T_{ph}} - 1} \qquad \text{(II.2.25)}$$

As Eq.(2.22) shows, the presence of the absolute values in the exponents makes the energy rate have a kink at the values of the LO phonon frequency ω_L approximately equal to the integer number of the energy spacing in the parabolic well ω_0. This is an expected result, because the electron energy levels are discrete in one direction and free in the other two. Kinks are the remainder of the discrete part of the electronic energy levels. To obtain the actual quantitative result we have to perform computer calculations of Eq.(2.22). Numerical results for the power radiated into the phonons are plotted in Fig.(2.3). In Fig.(2.4) we have also plotted the relaxation of the electron temperature with time at the "resonance" and off the "resonance".

From the result of the calculations, presented in Fig.(2.3), we can see that the effect of the equally spaced energy levels of the electrons in the 1D parabolic well is greatly diminished by the continuum energy spectrum in the transverse direction. Kinks in the power radiated into phonons are of the order of a few parts of a percent. Therefore it may be impossible to observe them experimentally. In order to enhance the singularities, electrons should be confined in the transverse direction as well. This confinement can be achieved by means of an external magnetic field in the direction perpendicular to the layers. In the next section we will investigate a layout with the magnetic field in the z - direction present.

Effects of Magnetic Field on Electron Transport.

1. "Coherent" Representation of the Magnetic Field.

We present now the analytical solution of the problem of interaction of the 2D electrons with 3D LO phonons when an external magnetic field is present. The direction of the magnetic field is chosen to be perpendicular to the *GaAs* layers, which confines the electron gas in all directions: by the parabolic potential perpendicular to the layer and by the cyclotron orbit in the layer. The wave function of the electron in this case is a product of the sums of the Hermite polynomials in z and $\rho = \sqrt{x^2+y^2}$. The use of the standard energy representation will produce an intractable result with many sums and integrations to be performed. Therefore, we will instead use here a coherent representation for the electron operators. The same results could be obtained in the energy representation if one found all the sum formulas implicitly involved in the coherent representation.

To get a simple solution, we will assume a single electron instead of the many electron gas. At the end we will multiply the result by the electron distribution function, giving it the "flavor" of the many-body equilibrium features (the spin will obviously be neglected).

The total Hamiltonian for one electron interacting with the 3D phonons and confined by the parabolic potential in the z direction and by the magnetic field along z is

$$\hat{H} = \hat{H}_{el} + \hat{H}_{ph} + \hat{V}_{ep}$$

$$= \hbar\omega_z (\hat{a}^\dagger \hat{a} + \frac{1}{2}) + \hbar\omega_m (\hat{\Pi}_+ \hat{\Pi}_- + \frac{1}{2}) + \sum_{\mathbf{Q}} \hbar\omega \hat{b}_{\mathbf{Q}}^\dagger \hat{b}_{\mathbf{Q}} \qquad \text{(II.3.1)}$$

$$+ (-\frac{iee^*}{v_c})(\frac{\hbar}{2\omega mN})^{\frac{1}{2}} \sum_{\mathbf{Q}} \frac{1}{Q} \left[e^{i\mathbf{Q}\cdot\hat{\mathbf{R}}} \hat{b}_{\mathbf{Q}} - e^{-i\mathbf{Q}\cdot\hat{\mathbf{R}}} \hat{b}_{\mathbf{Q}}^\dagger \right]$$

where e the electron charge and all other parameters were defined in the first section.

In the above equation only the phonon operators are in the "second quantization" form. The electronic operators are assumed to be in the "first quantization". Therefore, $\hat{\mathbf{R}}$ is an operator. In writing the Hamiltonian of the electron in the magnetic field in Eq.(3.1), we used a representation of the electron position $\hat{\mathbf{R}}$ and momentum $\hat{\mathbf{P}}$ in terms of "boson - like" operators $\hat{X}_\pm$, $\hat{\Pi}_\pm$, $\hat{a}$ and $\hat{a}^\dagger$ (see, for example, Feldman and Kahn[12]):

$$\hat{z} = \left[\frac{\hbar}{2m\omega_z} \right]^{\frac{1}{2}} (\hat{a} + \hat{a}^\dagger) \qquad \text{(II.3.2)}$$

$$\hat{\Pi}_\pm = \hat{p}_x \pm i\hat{p}_y \pm \frac{im\omega_m}{2}(\hat{x} \pm i\hat{y}) \qquad \text{(II.3.3)}$$

$$\hat{X}_\pm = \frac{\hat{x}}{2} \pm i\frac{\hat{y}}{2} - \frac{\hat{p}_y}{m\omega_m} \pm i\frac{\hat{p}_x}{m\omega_m} \qquad \text{(II.3.4)}$$

where the $\omega_m = (eH)/(mc)$ is the cyclotron frequency. All operators in Eq.(3.1) obey the usual "boson" commutation relations:

$$[\hat{a}, \hat{a}^\dagger] = 1; \quad [\hat{b}_{\mathbf{Q}'}, \hat{b}_{\mathbf{Q}}^\dagger] = \delta_{\mathbf{Q}'\mathbf{Q}}; \quad [\hat{X}_+, \hat{X}_-] = 1; \quad [\hat{\Pi}_-, \hat{\Pi}_+] = 1; \qquad \text{(II.3.5)}$$

with all other commutators equal to zero. The representation of the magnetic field via

$\hat{X}_{\pm}$ and $\hat{\Pi}_{\pm}$ operators makes the unperturbed Hamiltonian look like a set of harmonic oscillators. A natural representation for the harmonic oscillator is the "coherent representation". In this representation all of the above operators are diagonal, and it may be possible to go from the algebra of the operators to the algebra of the "c - numbers". We introduce the "ket" vector of the "coherent" state

$$|\beta\rangle \equiv |\zeta\rangle\,|\alpha\xi\rangle \tag{II.3.6}$$

This state vector has the following properties:

$$\hat{a}\,|\zeta\rangle = \zeta\,|\zeta\rangle$$

$$\hat{X}_{+}\,|\alpha\xi\rangle = \xi\,|\alpha\xi\rangle \tag{II.3.7}$$

$$\hat{\Pi}_{-}\,|\alpha\xi\rangle = \frac{\alpha}{i}\,|\alpha\xi\rangle$$

and the corresponding complex conjugate relations for $\hat{a}^{\dagger}$, $\hat{X}_{-}$, $\hat{\Pi}_{+}$ with α^{*}, ζ^{*}, ξ^{*} in place of α, ζ, ξ.

It can be shown (see Klauder[13] and Louisell[14]) that the vectors $|\beta\rangle$ constitute an overcomplete nonorthogonal set:

$$\langle\beta\,|\,\beta\rangle = 1 \tag{II.3.8}$$

$$\langle\beta\,|\,\beta'\rangle = e^{-\frac{1}{2}|\beta|^2+\beta^{*}\beta'-\frac{1}{2}|\beta'|^2} \tag{II.3.9}$$

where

$$|\beta|^2 \equiv |\alpha|^2 + |\xi|^2 + |\zeta|^2\,; \qquad \beta^{*}\beta' \equiv \alpha^{*}\alpha' + \xi^{*}\xi' + \zeta^{*}\zeta' \tag{II.3.10}$$

For the purposes of subsequent calculations we will write down the time depen-

dences of the operators involved in the Hamiltonian (Eq.(3.1)). This can be simply done by using the Heisenberg equation of motion for the operators

$$\frac{d\hat{O}}{dt} = \frac{1}{i\hbar}[\hat{O}, \hat{H}] \tag{II.3.11}$$

which gives

$$\hat{b}_q^\dagger(t) = e^{i\omega t}\hat{b}_q^\dagger; \qquad \hat{b}_q(t) = e^{-i\omega t}\hat{b}_q \tag{II.3.12}$$

$$\hat{a}^\dagger(t) = e^{i\omega_s t}\hat{a}^\dagger; \qquad \hat{a}(t) = e^{-i\omega_s t}\hat{a} \tag{II.3.13}$$

$$\hat{\Pi}_-(t) = e^{-i\omega_m t}\hat{\Pi}_-; \qquad \hat{\Pi}_+(t) = e^{i\omega_m t}\hat{\Pi}_+ \tag{II.3.14}$$

$$\hat{X}_\pm(t) = \hat{X}_\pm \tag{II.3.15}$$

The main advantage of the "coherent" representation is that it allows us to represent a function of operators as a function of the "normal ordered" products of the complex numbers. The other usable feature is the simplicity of calculating the traces over Gaussian distribution functions. This will become apparent in the following section, where we will provide some intermediate steps in the calculation of the power radiated into the phonons, based on the kinetic equation (Eq.(1.18)).

2. Statistical and Quantum Mechanical Averaging.

The kinetic equation (Eq.(1.18)) and therefore, the equation for the power radiated into the phonons (Eq.(1.22)) involve statistical averaging. The average is obtained by taking the trace of the quantum mechanical operators against a density

matrix of the electron system which interacts with the phonons. The phonons are assumed to be in thermal equilibrium with an external bath. The electrons are at temperature T_e (in the following equations β represents $1/(k_B T_e)$) and can be described by a Maxwellian distribution. In Eq.(1.18) this average is denoted by Tr. The quasiequilibrium density matrix that enters Eq.(1.18) is equal to the product of the individual density matrices, i.e.

$$\hat{\rho}_0(t) = \hat{\rho}_0^{el}(t) \cdot \hat{\rho}_0^{ph}(t) \tag{II.3.16}$$

This permits us to split the operation of taking the trace into two separate traces over phonons and electrons, respectively. The averaging over the equilibrium phonon system gives the result (see also Appendix D):

$$\mathrm{Tr}(\hat{b}_q^{\dagger} \hat{b}_{q'} \hat{\rho}_0^{ph}) = n_q \, \delta(q, q') \tag{II.3.17}$$

The calculations of the electronic part require much more complicated algebra. First we use the theorem[14] from the "coherent" state representation technics concerning the evaluation of the trace of a product of an operator with the density matrix:

$$\mathrm{Tr}(\hat{O} \hat{\rho}_0) = \int\int \frac{d^2\mu'}{\pi} <\mu \mid \hat{O}^{(n)} \mid \mu'><\mu' \mid \hat{\rho}_0^{(a)} \mid \mu> \tag{II.3.18}$$

where superscripts (n) and (a) mean normal or antinormal ordering of the constituent operators in the $\hat{O}$ and $\hat{\rho}$. The density matrix of the electron system at the inverse temperature β may be expressed[14]:

$$\hat{\rho}_0^{el} = \frac{1}{Z} e^{-\beta\hbar\omega_z(\hat{a}^{\dagger}\hat{a}+1/2)} \, e^{-\beta\hbar\omega_m(\hat{\Pi}_+\hat{\Pi}_- +1/2)} = (1-e^{-\beta\hbar\omega_z})(1-e^{-\beta\hbar\omega_m}) e^{-\beta\hbar\omega_z\hat{a}^{\dagger}\hat{a}} \, e^{-\beta\hbar\omega_m\hat{\Pi}_+\hat{\Pi}_-} \tag{II.3.19}$$

The matrix element of the antinormal ordered density matrix in the "coherent represen-

tation" can be easily found:

$$<\alpha \mid \hat{\rho}_0^{(a),el} \mid \alpha> = (1-e^{-\beta\hbar\omega_z})(1-e^{-\beta\hbar\omega_m}) \exp\left[(1-e^{\beta\hbar\omega_z})\bar{\xi}\xi\right] \exp\left[(1-e^{\beta\hbar\omega_m})\frac{\bar{\alpha}\alpha}{2l^2}\right] \tag{II.3.20}$$

where $l^2 \equiv \hbar/(m\omega_m)$. In deriving the above expression we used the relation:

$$<\alpha \mid \left[e^{-x\hat{a}^\dagger\hat{a}}\right]^{(a)} \mid \alpha> = e^x \sum_{l=0}^{\infty} \frac{(1-e^x)^l}{l!} <\alpha \mid \hat{a}^l \hat{a}^{\dagger l} \mid \alpha> = e^x e^{(1-e^x)\bar{\alpha}\alpha} \tag{II.3.21}$$

After some algebraic transformations we arrive at the result for the trace in Eq.(1.18):

$$\mathrm{Tr}\left\{\hat{\rho}_0\left[\hat{V}(t),\left[\hat{V},\hat{b}_q^\dagger\hat{b}_{q'}\right]\right]\right\} = v^2 \sum_Q \frac{1}{Q} <\hat{b}_q^\dagger \hat{b}_Q> \frac{e^{-i\omega_{Q'}t}}{q'} \left(C_{Qq'} - C^*_{Qq'}\right) F_{Qq'} \tag{II.3.22}$$

$$- v^2 \sum_Q \frac{1}{Q} <\hat{b}_Q^\dagger \hat{b}_{q'}> \frac{e^{i\omega_Q t}}{q'} \left(C_{Qq} - C^*_{Qq}\right) F_{-Q,-q} + v^2 \frac{e^{-i\omega_q t}}{qq'} C_{qq'} F_{qq'} + v^2 \frac{e^{i\omega_{q'} t}}{qq'} C^*_{qq'} F_{-q,-q'}$$

Here the functions $C_{q,q'}$ and $F_{q,q'}$ are defined as:

$$C_{Q,Q'} \equiv \exp\left\{-\frac{Q_z^2 + Q_z^{2\prime} - 2Q_z Q_z' e^{-i\omega_z t}}{4m\omega_z/\hbar} - \frac{l^2}{2}\left(Q_x^2 + Q_y^2\right)\left(1 - e^{-i\omega_m t}\right)\right\} \tag{II.3.23}$$

$$F_{Q,Q'} \equiv 8\pi l^2 \delta\left(Q_x - Q_x'\right)\delta\left(Q_y - Q_y'\right) \tag{II.3.24}$$

$$\times \exp\left\{-\frac{Q_z^{2\prime} + Q_z^2 - 2Q_z Q_z' \cos(\omega_z t)}{2\hbar\omega_z(e^{\beta\hbar\omega_z} - 1)} - \frac{l^2}{(e^{\beta\hbar\omega_z} - 1)}\left(Q_x^2 + Q_y^2\right)\left(1 - \cos(\omega_m t)\right)\right\}$$

3. Calculation of the Power Radiated into Phonons.

We rewrite the equation for the power radiated into the phonons once again here, with an insertion that $n_q(q_z, q_z') = n_q \cdot \delta(q_z, q_z')$:

$$P_z = C \sum_{q} \sum_{q_z} \sum_{q'_z} \frac{\delta_{q_z, q'_z}}{(q^2 + q'^2_z)^{1/2} (q^2 + q_z^2)^{1/2}} \tag{II.3.25}$$

$$\times \left\{ n_q \left[I^+(-\omega_L, q_z) - I^-(-\omega_L, q_z) \right] - n_q \left[I^+(\omega_L, q_z) - I^-(\omega_L, q_z) \right] + \left[I^+(-\omega_L, q_z) + I^-(\omega_L, q_z) \right] \right\}$$

As before, the constant C in the above equation represents all multiplicative constants (see Eq.(2.11)). The quantity $I^{\pm}$ in Eq.(3.25) is defined as

$$I^{\pm} \equiv \exp\left\{ \frac{\hbar}{2m\omega_z} q_z^2 \coth\frac{\beta\hbar\omega_z}{2} + \frac{\hbar}{2m\omega_m} q^2 \coth\frac{\beta\hbar\omega_m}{2} \right\} \tag{II.3.26}$$

$$\times \int_{-\infty}^{0} dt\, e^{\varepsilon t} e^{i\omega_L t} \exp\left\{ \frac{\hbar q_z^2}{2m\omega_z \sinh\frac{\beta\hbar\omega_z}{2}} \cos\left[\omega_z t \mp i\frac{\beta\hbar\omega_z}{2} \right] + \frac{\hbar q^2}{2m\omega_m \sinh\frac{\beta\hbar\omega_m}{2}} \cos\left[\omega_m t \mp i\frac{\beta\hbar\omega_m}{2} \right] \right\}$$

The presence of the δ-function enables us to take the summation over q'_z in Eq.(3.25). However, there are still four summations (integrations) left in Eq.(3.25). Fortunately, further simplification of Eq.(3.25) is possible.

We will start with the time integration first. The exponential functions can be expanded in terms of the modified Bessel functions of the integer order, i.e.

$$e^{a\cos\phi} = \sum_{n=-\infty}^{\infty} e^{-in\phi} I_n(a) \tag{II.3.27}$$

Substituting this expansion into Eq.(3.25) and performing the integration over the time we will get a result proportional to the delta-function - $\delta(\omega_L + m\omega_m + n\omega_z)$. Note that in the "usual" energy (or occupation number) representation the time integration produces the energy conservation law for the transitions between two specific energy levels. The advantage of the "coherent" representation chosen by us is that it reflects not the definite energy states of the system, but rather changes in energy during the transition between levels m and n. Therefore we are getting the above delta-function with all m and n present.

After taking the integral over the time in Eq.(3.25) we arrive at the result:

$$P_s = C\left[(n_q + 1)F^+ - n_q F^-\right] \tag{II.3.28}$$

with the definition:

$$F^{\pm} \equiv \sum_m \sum_n e^{\pm\frac{\hbar\beta}{2}(n\omega_z + m\omega_m)} 2\pi \int_0^{\infty} dq^2 \int_{-\infty}^{\infty} dq_z\, \delta(\omega_L + n\omega_z + m\omega_m)$$

$$\times I_n\left[q_z^2 \frac{\hbar}{2m\omega_z \sinh\frac{\beta\hbar\omega_z}{2}}\right] I_m\left[q^2 \frac{\hbar}{2m\omega_m \sinh\frac{\beta\hbar\omega_m}{2}}\right] \frac{1}{q^2 + q_z^2} \tag{II.3.29}$$

$$\times \exp\left\{-q^2 \frac{\hbar \tanh\frac{\beta\hbar\omega_m}{2}}{2m\omega_m \sinh\frac{\beta\hbar\omega_m}{2}} - q_z^2 \frac{\hbar \tanh\frac{\beta\hbar\omega_z}{2}}{2m\omega_z \sinh\frac{\beta\hbar\omega_z}{2}}\right\}$$

Now, as in the preceding chapter, we make an approximation that ω_L is independent of the wave-vector. In this q-independent case the integrals over $\mathbf{q}$ will be easy to

perform with $x = q^2$, and $y = q_z^2$

$$F^{\pm} = \sum_m \sum_n \delta(m\omega_m + n\omega_z + \omega_L)\, e^{\pm\frac{\hbar\beta}{2}(m\omega_m + n\omega_z)} \int_0^{\infty} dx \int_0^{\infty} dy \frac{e^{-Cx} e^{-Dy} I_n(Ax) I_m(By)}{(x+y)\sqrt{y}} \qquad \text{(II.3.30)}$$

$$= \sum_m \sum_n \delta(m\omega_m + n\omega_z + \omega_L)\, e^{\pm\frac{\hbar\beta}{2}(m\omega_m + n\omega_z)} \int_0^{\infty} dt e^{-t(x+y)} \int_0^{\infty} dx \int_0^{\infty} dy \frac{e^{-Cx} e^{-Dy} I_n(Ax) I_m(By)}{\sqrt{y}}$$

$$= \sum_m \sum_n \delta(m\omega_m + n\omega_z + \omega_L)\, e^{\pm\frac{\hbar\beta}{2}(m\omega_m + n\omega_z)} \sqrt{\frac{2}{\pi}} \frac{1}{\sqrt{B\,A}}$$

$$\times \int_0^{\infty} dt\, Q_{m-1/2}\left[\frac{D+t}{B}\right] \left[\left[\frac{C+t}{A}\right]^2 - 1\right]^{-1/2} \left[\frac{C+t}{A} + \left[\left[\frac{C+t}{A}\right]^2 - 1\right]^{1/2}\right]^{-n}$$

where A, B, C, and D are defined as

$$A \equiv \frac{\hbar}{2\mu\omega_0 \sinh\frac{\hbar\omega_0}{2kT_e}}\,; \quad B \equiv \frac{\hbar}{2\mu\omega_z \sinh\frac{\hbar\omega_z}{2kT_e}} \qquad \text{(II.3.31)}$$

$$C \equiv \frac{\hbar\cosh\frac{\hbar\omega_0}{2kT_e}}{2\mu\omega_0 \sinh\frac{\hbar\omega_0}{2kT_e}}\,; \quad D \equiv \frac{\hbar\cosh\frac{\hbar\omega_z}{2kT_e}}{2\mu\omega_z \sinh\frac{\hbar\omega_z}{2kT_e}}\,; \qquad \text{(II.3.32)}$$

The presence of the δ-function in Eq.(3.30) makes the P_e exhibit a set of infinite peaks. In a real material such peaks are not present. They are broadened due to the dependence of the frequency of the LO-phonons on q. Another source of wide broadening in the real materials is the broadening of the Landau levels in the presence of the electron-phonon and electron-impurity interaction. In order to incorporate the latter in our calculations we are going to assume the density of states (DOS) of the electron on the Landau level to be Gaussian with a flat background. For simplicity the

DOS is assumed to be independent of the level number n. This type of DOS was proposed by Warmenbol[15]

$$D_n(E) = \left[\frac{\pi}{2\hbar\omega_m\Gamma_0}\right]^{1/2} e^{-\frac{\pi}{\hbar\omega_m\Gamma_0}(E-\hbar\omega_m(n+\frac{1}{2}))^2} + \text{const.} \qquad \text{(II.3.33)}$$

The width Γ_0 of the Gaussian depends on the strength of the electron-impurities and electron-phonons interactions. It will be regarded as an adjustable parameter.

The Gaussian part of the DOS (Eq.(3.33)) of the electron in the Landau levels broadens the sharp levels into a distribution of the cyclotron frequencies ω_m of the electron in the system. To show this we start with the δ function which enters Eq.(3.32)

$$\delta(m\omega_m + n\omega_z + \omega) = \frac{1}{\hbar}\,\delta(\hbar\omega_m(m_f+\frac{1}{2}) - \hbar\omega_m(m_i+\frac{1}{2}) + \hbar\omega n + \hbar\omega) \qquad \text{(II.3.34)}$$

$$= \int dE\,\delta(E - E_f^{\text{mag}})\,\delta(E - E_i^{\text{mag}} + \hbar\omega_z + \hbar\omega)$$

In the presence of the broadening each of the δ functions in the last expression should be replaced by the DOS from Eq.(3.32), producing the result:

$$\int dE D_f(E)\,D_i(E) \qquad \text{(II.3.35)}$$

$$= \left[\frac{\pi}{2\hbar\omega_m\Gamma_0}\right]^{1/2} \int dE \exp\left\{-\frac{\pi}{\hbar\omega_m\Gamma_0}\left[E - \hbar\omega_m(m_f+\frac{1}{2})^2 - (E - \hbar\omega_m(m_i+\frac{1}{2}) + \hbar n\omega_z + \hbar\omega)^2\right]\right\}$$

$$= \left[\frac{\pi}{2\hbar\omega_m\Gamma_0}\right]^{1/2} e^{-\frac{\pi}{\omega_m\Gamma_0}(m\omega_m + n\omega_z + \omega)^2}$$

The total density of states for the 2D electrons in the magnetic field in the presence of the scattering on the impurities also contains a long tail between the separate

Landau levels. In Eq.(3.33) those tails are approximated by a constant. We can incorporate this constant term in the DOS into our calculations with two simple observations: first, the term is additive, and, second, our previous result (see Eq.(2.22)) was obtained for the problem where there as no magnetic field present, e.g 2D electrons were free (constant density of states in the transverse direction). Therefore, the sum of Eq.(2.22) and Eq.(3.33) will constitute the solution for the more realistic DOS. This solution is represented in Fig.(II.5).

In conclusion to the above calculations we state that in the structures with parabolic quantum wells the relaxation time of the "hot" electrons is decreased (power rate is increased) in comparison with the relaxation in the rectangular wells. A much stronger effect may be seen in the experiments with a magnetic field in the direction perpendicular to the layers. A strong resonance will occur when the strength of the magnetic field is such, that the distance between Landau levels is equal integer times the energy of the LO phonons and energy spacing between the parabolic well levels. Even spread of the Landau levels due to the elastic collisions of the electrons with impurities will not diminish the resonance considerably.

The results were expected and we hope they will be substantiated by the upcoming experiments of F. Capasso and co-workers.

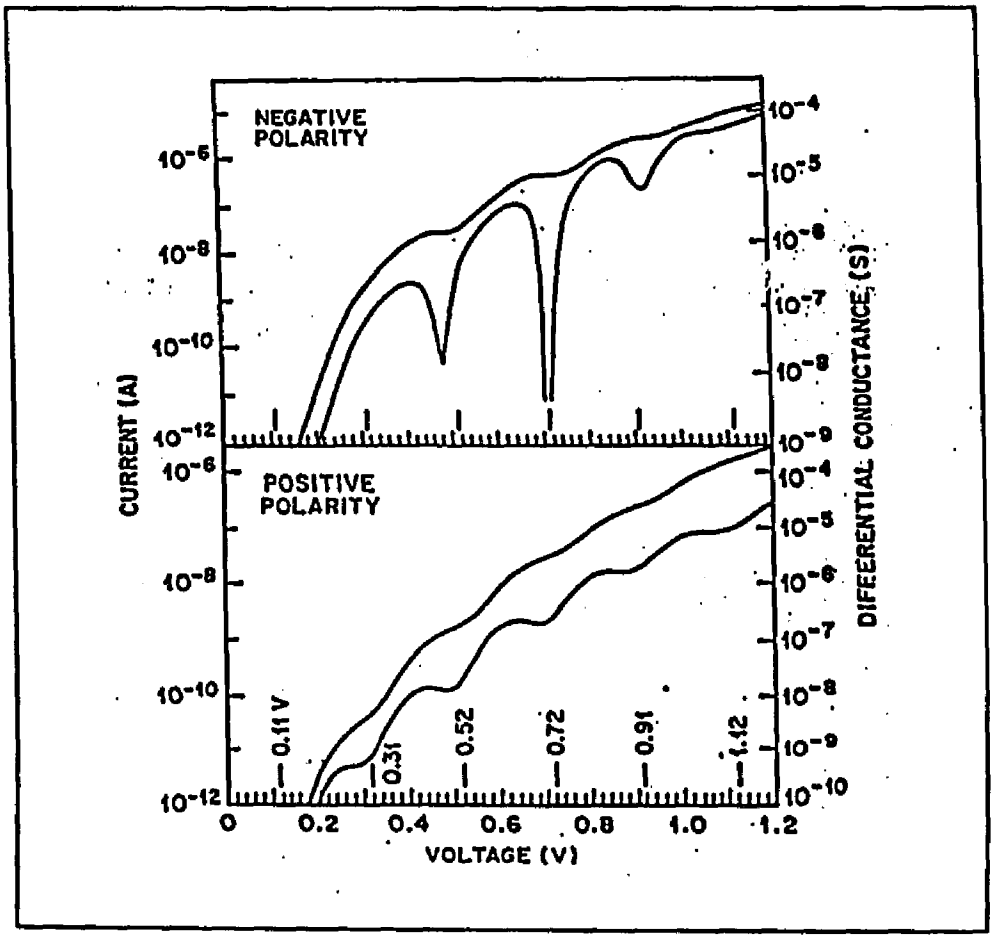

FIG. II.1. I-V characteristic and negative differential conductance for opposite bias polarities in the case of resonant tunneling through parabolic wells with width of 300Å.

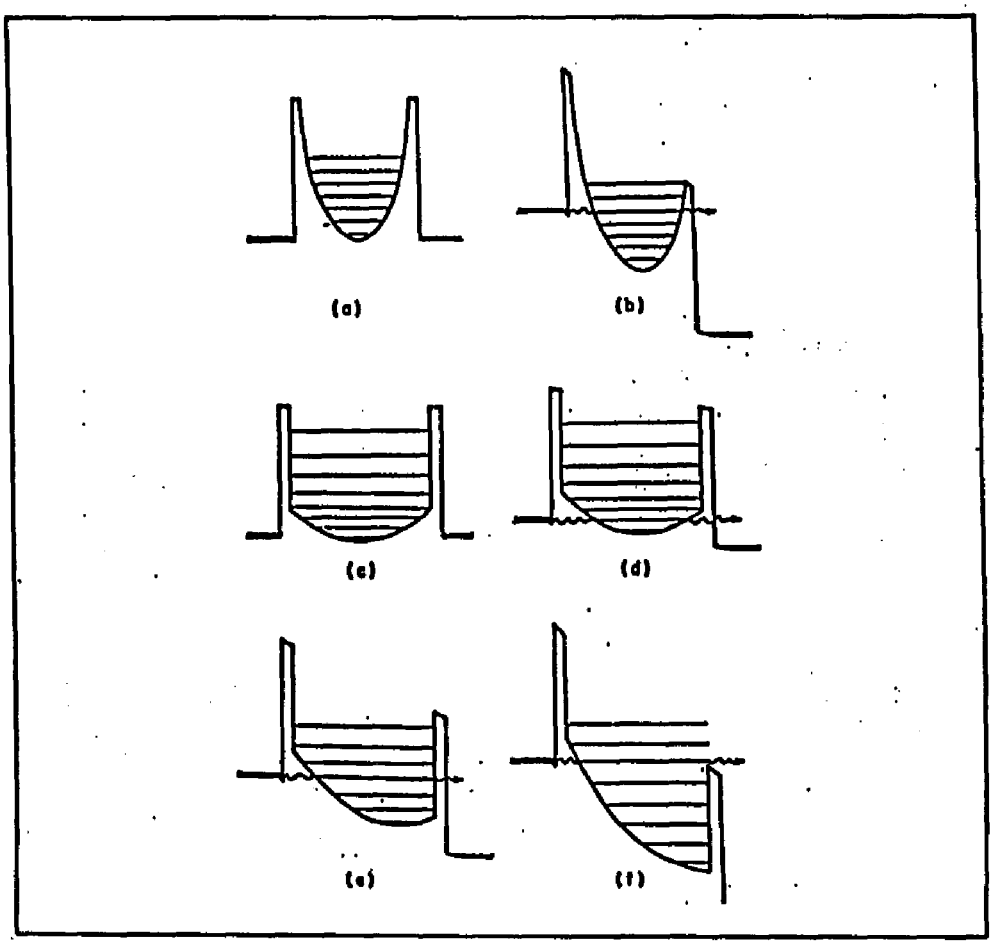

FIG. II.2. Conduction band diagram showing resonant tunneling through two different types of parabolic wells under different bias conditions.

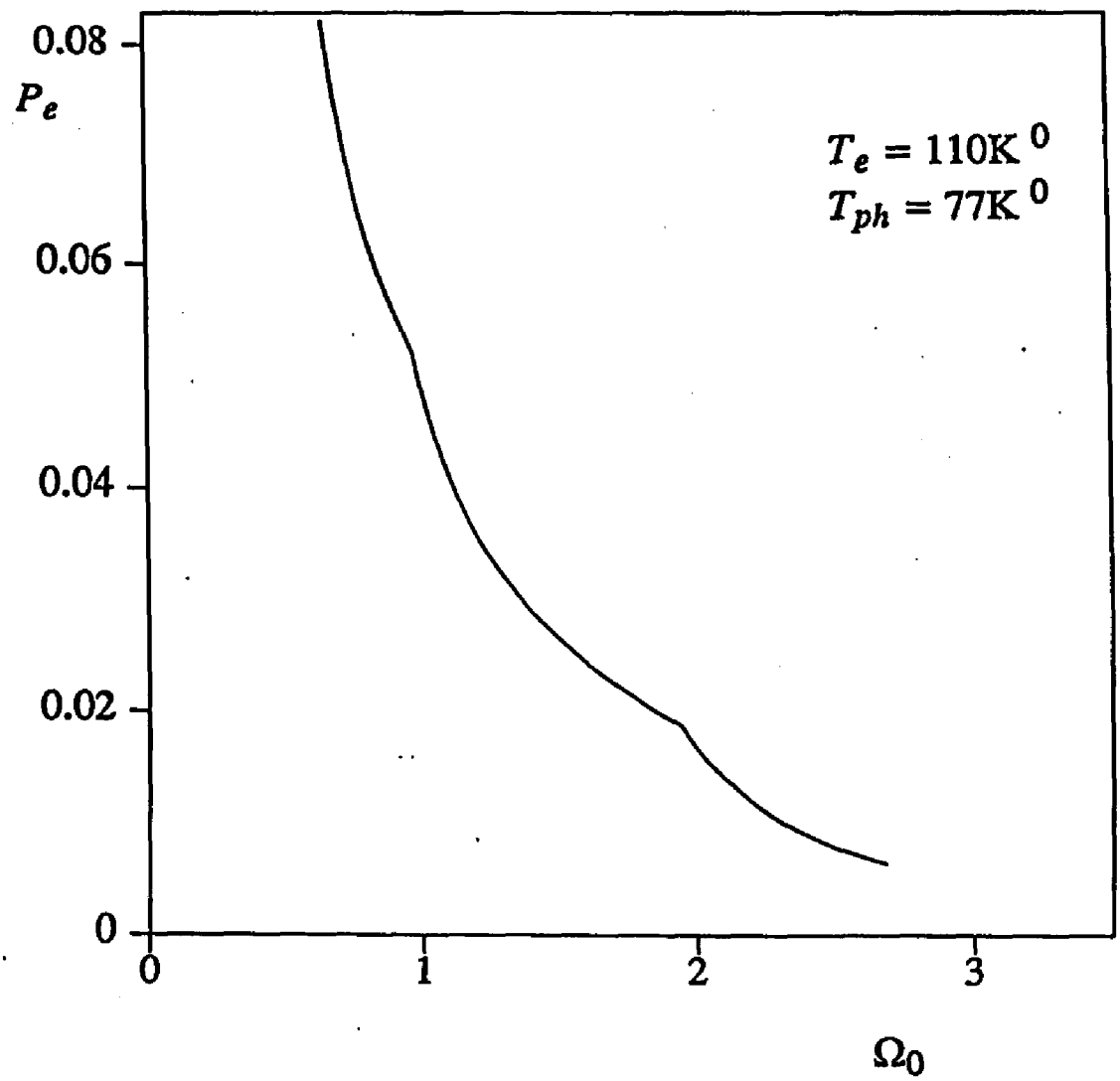

FIG. II.3. The energy loss rate of the electrons due to the interaction with the phonons as a function of the frequency of the LO phonons. The temperature of the electrons is $110K^0$ while the phonon temperature is $77K^0$. The kinks shown in the graph correspond to the frequency of the LO phonons equal to integer number of the electron energy spacing in the parabolic band.

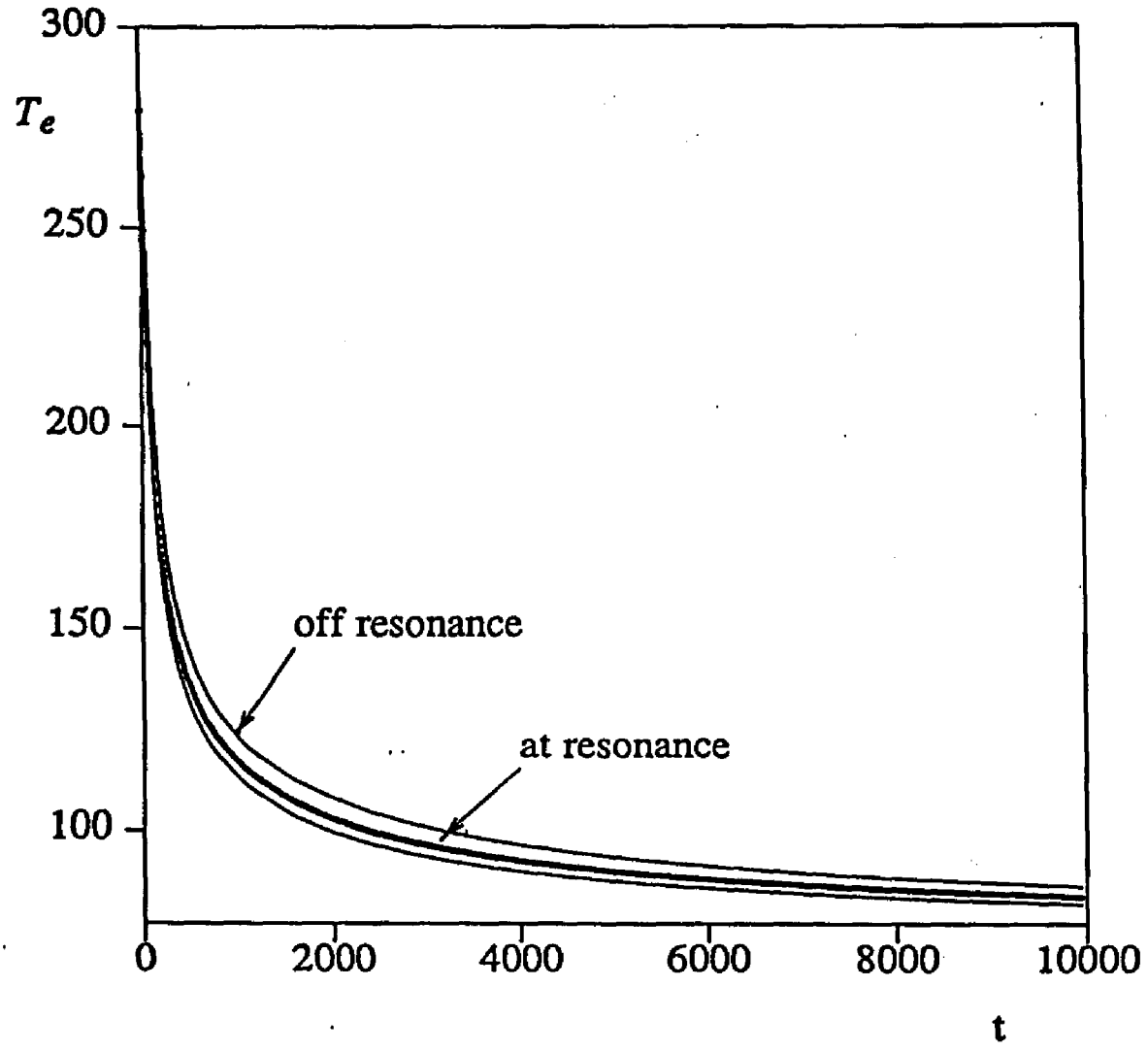

FIG. II.4. The electron cooling rate at the "resonance" and off the "resonance".

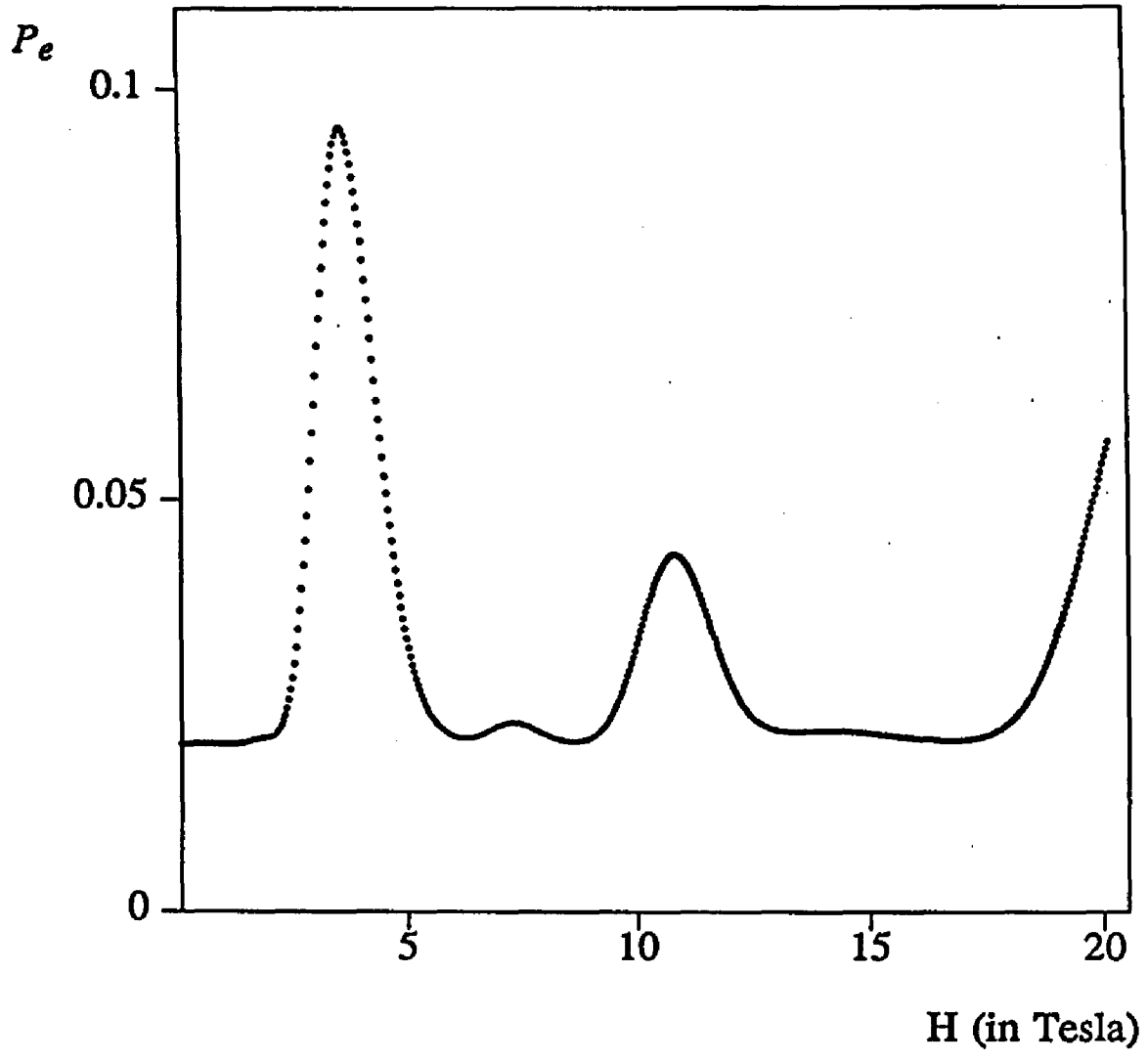

FIG. II.5. The energy loss rate of the electrons as a function of the magnetic field for the same conditions as on Fig.II.3. The "resonances" are highly pronounced even when the Landau levels are spread about 10% due to the electron-impurity and other interactions (the actual case in the calculations).

Appendix A. Basic Aspects of Fluid Dynamics.

The Eulerian Formulation of Fluid Dynamics.

The equations, that govern the fluid motion, can be derived from the conservation laws for the mass, momentum and energy of the fluid volume. Assuming continuity of the variables the integral form of the conservation equations can be transformed to the familiar partial differential equations:

$$\frac{\partial \rho}{\partial t} + \frac{\partial(\rho \upsilon)}{\partial x} = 0 \tag{A.1}$$

$$\frac{\partial(\rho \upsilon)}{\partial t} + \frac{\partial}{\partial x}(\rho \upsilon^2 + p) = 0 \tag{A.2}$$

$$\frac{\partial(\rho E)}{\partial t} + \frac{\partial}{\partial x}(\rho \upsilon E + p \upsilon) = W \tag{A.3}$$

The above equations are the simplified set for the case when no external sources of the momentum and mass are present and the flux is convective. Four unknown functions enter the equations: density - ρ, velocity - υ, pressure - p and the total energy per unit mass - E. It is possible to express the total energy E as a sum of the heat and kinetic energies:

$$E = I + (1/2)\upsilon^2 \tag{A.4}$$

In order to make the system complete we have to add a constituency relation - the equation which describes the fluid itself. It is an equation of state.

For many gases as well as liquids the equation of state can be approximated

by the Gruneisen equation:

$$p = p_H + \frac{\gamma_s}{V}(I - I_H) \tag{A.5}$$

where

$$p_H = \frac{c^2 (V_0 - V)}{\left[V_0 - s(V_0 - V)\right]^2} \tag{A.6}$$

$$I_H = \frac{1}{2}\left[\frac{c(V_0 - V)}{V_0 - s(V_0 - V)}\right]^2 \tag{A.7}$$

$$\gamma_s = 2s - 1, \quad V \equiv \frac{1}{\rho} \tag{A.8}$$

This is a three parameter expression, that describes well properties of a large number of gases and liquids. The parameters are ρ_0, the normal density of the material, c, the speed of sound in the unshocked material and γ_s, the Gruneisen ratio ($\gamma_s = \gamma - 1$).

If the departure from normal density is slight, then the Gruneisen equation can be simplified to the form

$$p = c^2(\rho - \rho_0) + (\gamma - 1)\rho I \tag{A.9}$$

This is "stiffened-gas" equation of state. For most analytical studies, this simple form is easier to manipulate, while still retaining the essential qualitative features of a large class of materials.

In many instances a much simpler equation is used - the perfect gas equation of state

$$p = (\gamma - 1)\rho I \tag{A.10}$$

This equation adequately describes most of the gases under normal conditions and it also applies to the liquids, if the γ is taken to be $\approx 3 - 7$.

At moderate pressure and normal temperatures most fluids cannot be compressed. This is expressed by the identity $\delta\rho = 0$. It seems to be an additional relation which overdetermines the system of the hydrodynamical equations. Actually, the "incompressibility" of the fluid means that pressure depends strongly upon the density. Therefore a small change in density produces a very large change in pressure. An acceptable form of the equation for this strong dependence may be:

$$p = A\left[\frac{\rho}{\rho_0}\right]^{\gamma} \tag{A.11}$$

for large γ and A.

The Eq.(11a) describes the water relatively correct (see Ref..) for the temperature range from 0 to 100 degree Celsius. On the other hand the above equation is similar to the adiabatic equation for the perfect gas

$$p = (\gamma - 1)\rho^{\gamma} K \tag{A.12}$$

with K - an initial constant.

One of the basic properties of the hydrodynamical equations (and hyperbolic equations in general) is the existence of the finite speed of propagation of the signals. This speed is called the sound speed. The formula for the sound speed is:

$$c^2 = \frac{\frac{p}{\rho^2} - \frac{\partial I}{\partial \rho}}{\frac{\partial I}{\partial \rho}} \tag{A.13}$$

where the partial derivatives are taken from the equation of state solved for I as a function of P and ρ. For the perfect gas the speed of sound is equal to

$$c = \sqrt{\frac{\gamma p}{\rho}} \tag{A.14}$$

The above equation (A.14) for the sound speed together with the equation of state (Eq. A.12) was used in the main text.

The Lagrangian Formulation of Fluid Dynamics.

The form of the Eqs.(A.1-3) suggests that the partial derivatives of the functions with respect to the time can be combined with the terms involving a product of the material velocity and the partial derivative with respect to the coordinate. This combination is a total time derivative of the function along the path of the fluid element It is called the Lagrangian time derivative, in term of which the Eqs.(1a-3a) can be rewritten as

$$\frac{d\rho}{dt} + \rho \frac{\partial \upsilon}{\partial x} = 0 \tag{A.15}$$

$$\frac{d\upsilon}{dt} + \frac{1}{\rho} \frac{\partial p}{\partial x} = 0 \tag{A.16}$$

$$\frac{dE}{dt} + \frac{1}{\rho} \frac{\partial (p\upsilon)}{\partial x} = 0 \tag{A.17}$$

Now, let x_0 be the coordinate of a particular fluid element at some reference time ($t = 0$). Then the value of x_0 will serve forever as a tag of that element and can be sought of as a coordinate (Lagrangian coordinate). The Lagrangian coordinate is constant in time in contrast to the Eulerian coordinate x which is time dependent.

We can make the transformation to the complete Lagrangian coordinates. First let $\rho_0(x_0)$ be the density at Lagrangian position x_0 and at time t_0. Then

$$\rho(x)\left[\frac{\partial x}{\partial x_0}\right]_t = \rho_0(x_0) \tag{A.18}$$

expresses the fact that the mass in any Lagrangian coordinate interval is equal to the mass in that interval as viewed from the Eulerian-coordinate point of view.

In general, the transformation to the Lagrangian coordinates is advantageous for the one dimensional case. The three-dimensional transformation will involve a complicated Jacobian. We should mention that Lagrangian coordinates nevertheless are frequently used in the numerical codes based on the Godunov's algorithm. An example of such a code is CAVEAT. We will need the Lagrangian description of the hydrodynamical equations, because we are making a test program for the CAVEAT as well as extending Godunov scheme for the case when external energy source is present.

In one dimension the Lagrangian equations are:

$$\frac{\partial \rho}{\partial t} + \frac{\rho^2}{\rho_0}\frac{\partial v}{\partial x_0} = 0 \tag{A.19}$$

$$\rho_0 \frac{\partial v}{\partial t} + \frac{\partial p}{\partial x_0} = 0 \tag{A.20}$$

$$\rho_0 \frac{\partial E}{\partial t} + \frac{\partial p\upsilon}{\partial x_0} = 0 \tag{A.21}$$

Characteristics.

Method of characteristics is a powerful tool in examining the properties of one dimensional flow (and a system of hyperbolic partial differential equations in general). It can be easily demonstrated on a particular example of an adiabatic flow, described by a set of Eqs.(A.1-3) with an ideal gas equation of state. After simple transformation these equations can be put into the form

$$\frac{\partial}{\partial t}(\upsilon + \sigma) + (\upsilon + c)\frac{\partial}{\partial x}(\upsilon + \sigma) = 0 \tag{A.22}$$

$$\frac{\partial}{\partial t}(\upsilon - \sigma) + (\upsilon - c)\frac{\partial}{\partial x}(\upsilon - \sigma) = 0 \tag{A.23}$$

$$\frac{\partial}{\partial t}S + \upsilon\frac{\partial}{\partial x}S = 0 \tag{A.24}$$

with S - the entropy and $\sigma = \int \frac{cd\rho}{\rho}$. The form of the above equations suggests that it is possible to interpret the derivatives as a total time derivatives along curves ($C^{\pm}$, C^0) in the $x - t$ plane defined by the equations:

$$\frac{dx}{dt} = \upsilon \pm c; \qquad \frac{dx}{dt} = \upsilon \tag{A.25}$$

Along these lines the corresponding quantities $\upsilon \pm \sigma$ and S are constant.

It is possible to prove[12], that a small perturbation in the solution propagates along one of the $C^{\pm}$ characteristics, and never crosses it unless there is a discontinu-

ous jump (shock etc.).

A set of equations (A.23-25) can be integrated over and a close form solution can be easily obtained (see Courant and Friedrichs[12]). A discussion of the role of characteristics in identifying the dependency regions and prescription of the boundary data is given in Appendix B.

Appendix B. Prescription of the Boundary Data.

In this appendix we discuss the number of boundary (and initial) conditions which should be specified in order to get a unique solution of a system of hydrodynamic equations. Our discussion is based on the corresponding analysis of Courant and Friedrichs[12], as well as Landau and Lifshitz[30]. Some extended discussion of the compatibility conditions can also be found in the paper by Shubin, Stephens and Glaz[31].

Without getting involved in the question of the existence and uniqueness of the solution of a system of hyperbolic partial differential equations (PDE) we can make a simple remark, concerning the prescription of the boundary data. The total number of boundary conditions (BC), that should be prescribed on both outer boundaries of the region where the solution exists and is continuous, must be equal to the number of PDE's (assuming they are of the first order in spatial and time derivatives). But the exact number of BC's which must be specified separately on each outer boundary depends on the motion of this boundary as well as the motion of the matter near the boundary. The difference between the total number of BC's and equations suggests that the solution inside the specified region exhibits discontinuities, or that some of PDE's are not independent. In this case (when the solution is not continuous in the entire spatial region) the spatial region should be split into a number of smaller regions separated by some surfaces such that the solution is continuous in each of them. Each of the separating surfaces must be treated as a boundary for the adjacent regions and the following discussion for the outer boundaries will apply as well.

According to the discussion in Landau and Lifshitz[30], to find the number of BC

on the given boundary, we have first to draw the line, that describes the motion of this boundary on the $r-t$ plane. Next we have to draw the characteristic lines, starting from this boundary (see Fig.(B.1)). The number of characteristics, that go into the region of interest (region II on Fig.(B.1)) specifies the number of independent quantities, that can be prescribed on the given boundary B. Note that the characteristics are in the positive t direction.

In the general case of non-isentropic flow there are three characteristics leaving each point in the $r-t$ plane. They are marked as C^+, C^- and C^0 and defined via equations: $\frac{dx}{dt} = \upsilon \pm c$ and $\frac{dx}{dt} = \upsilon$ with c - the local sound velocity and υ - the local matter velocity (here we assume $\upsilon > 0$). One special case arises when the boundary line coincides with the one of the characteristic lines. The number of independent quantities which should be specified on such boundary is smaller by one because there is a relation between variables on the characteristic - the integral of the characteristic equation. Different possibilities are presented in Figs.(B.2-B.4). An extended explanation of the figures is given in the figure captions.

In view of the stated mnemonic rule, we can justify the number of outer boundary conditions as well as the number of matching conditions on the inner boundaries (points of weak discontinuities) that are present in our problem. First let us recall that after the "folding transformation" we got six (instead of three) first order partial differential equations for six independent variables. At the same time after the folding, the space occupied by air became superimposed onto the space occupied by water. In each of these "subspaces" we still have three PDE, three BC, as well as three initial conditions (same as BC but defined along the x axis). We separately have depicted the water region in Fig.(B.5) and the air region in Fig.(B.6), although after the

transformation they occupy the same space. Note, that because of the "folding" the positive direction of the velocity in Fig.(B.6) is opposite to the direction of the velocity in Fig.(B.5) (where it goes to the right). The regions I, II, III, IV, V in the figures are defined as follows: I) from the left boundary at A to the head of the rarefaction wave (R.W.) at B, II) from the head to the tail of the R.W. at C, III) from the tail of the R.W to the interface boundary (I.B.) at D, IV) from the I.B. to the shock wave (S.W.) at E in the air and V) from the S.W. to infinity at F, which has folded into 0 ≡ A. The lines A, B, C, D in Fig.(B.5) and D, E, F in Fig.(B.6) represent the motion of the discontinuities, present in the solution.

There were two initially fixed boundaries at $r = \pm\infty$ for the 1D problem or $r = 0$, $r = \infty$ for the spherical problem. They were both mapped to the point $x = 0$ after the transformation. The velocity of the matter near this boundary is zero, therefore the line in the $r - t$ plane, that characterizes the motion of this boundary is vertical and coincides with the C^0 characteristic shown in Figs.(B.5,B.6). There are also C^- characteristics for the water variables and C^+ characteristic for the air variables starting on this boundary line which go into the regions I and V respectively (see Figs.(B.5,B.6). After the "folding" the right-most boundary for both water and air is the water - air interface (line xD). (Again, because the matter does not separate at the boundary, the latter propagates as a C^0 characteristic - the characteristic which describes the propagation of the matter).

Region I. Only one characteristic line goes into the region I from the left boundary - the C^+ characteristic. Therefore, we have to provide one BC on the boundary xA. This can be constancy of the pressure or constancy of the entropy (the latter is more general and does not depend on whether the wave has already hit the boun-

dary). Being itself a C^0 characteristic, the equation for the xA is: $\frac{dx}{dt} = \upsilon = 0$ (at this point the matter does not move). A corresponding initial condition will define completely the motion of this boundary. The other boundary is xB - the head of the rarefaction wave. It coincides with the C^- characteristic. The other two - C^0 and C^+ characteristics go into the region II, therefore no boundary data for the region I can be prescribed on the xB. On the other hand all three characteristics, starting from the x axis propagate into the region I, making it possible to prescribe three initial conditions. As can be seen, the state at any point in I is fully determined by either three initial conditions (Ia) or two initial and one boundary conditions (Ib).

Region II. Two conditions, prescribed on xB (constancy of pressure and density through interface) and one initial data at point R_0 will determine the state of the gas at any point in II. Constancy of the velocity across xB together with the characteristic equation $\frac{dx}{dt} = \upsilon - c$ and corresponding initial condition at the point R_0 determines the boundary motion itself.

Region III. Two conditions on xC and one condition on xD define the solution in region III. The latter condition can be chosen as constancy of the entrophy. The boundary xD - water - air interface moves together with the matter on both sides of it. Therefore the velocity is constant across this boundary. This condition together with the corresponding equation for the characteristic and initial data at R_0 will determine the motion of the interface xD.

For the air regions (IV and V) there is only one internal boundary - line xE at the shock (see Fig.(B.6)). The shock is supersonic for the flow behind it and subsonic for the flow in front of it. It is easier to understand the conditions on the shock front if

we split the line xE into two lines xE^- and xE^+. Three Hugoniot conditions relate the quantities on the xE^- to the quantities on the xE^+ line. One unknown parameter enters these conditions - the shock velocity. Therefore, one out of three conditions should be used as an equation (ODE) for this unknown a priori shock velocity. The remaining two relations will "transmit" boundary information across the shock.

Region IV. All three initial conditions must be specified on the x axis. One (C^+) characteristic starting on the water - air boundary xD propagates into the region IV - therefore one condition must be prescribed on xD. The natural choice for the case of negligible surface tension is continuity of the pressure across xD. On the shock tail (line xE^-) two characteristics propagate into the region IV (see Fig.(B.6)). Therefore two conditions must be prescribed on this boundary (two out of three Hugoniot conditions) for the region IV.

Region V. One condition can be specified at the far boundary (line xF). It can be a statement that the gas is nondisturbed ($\upsilon = 0$). At the same time, on the shock head (line xE^+) all three characteristics propagate out of the region V, therefore no boundary data is necessary on xE^+. Again, all three initial conditions must be specified on the x axis.

The conditions discussed in this appendix correspond to BC's and ODE's formulated in Section 2.

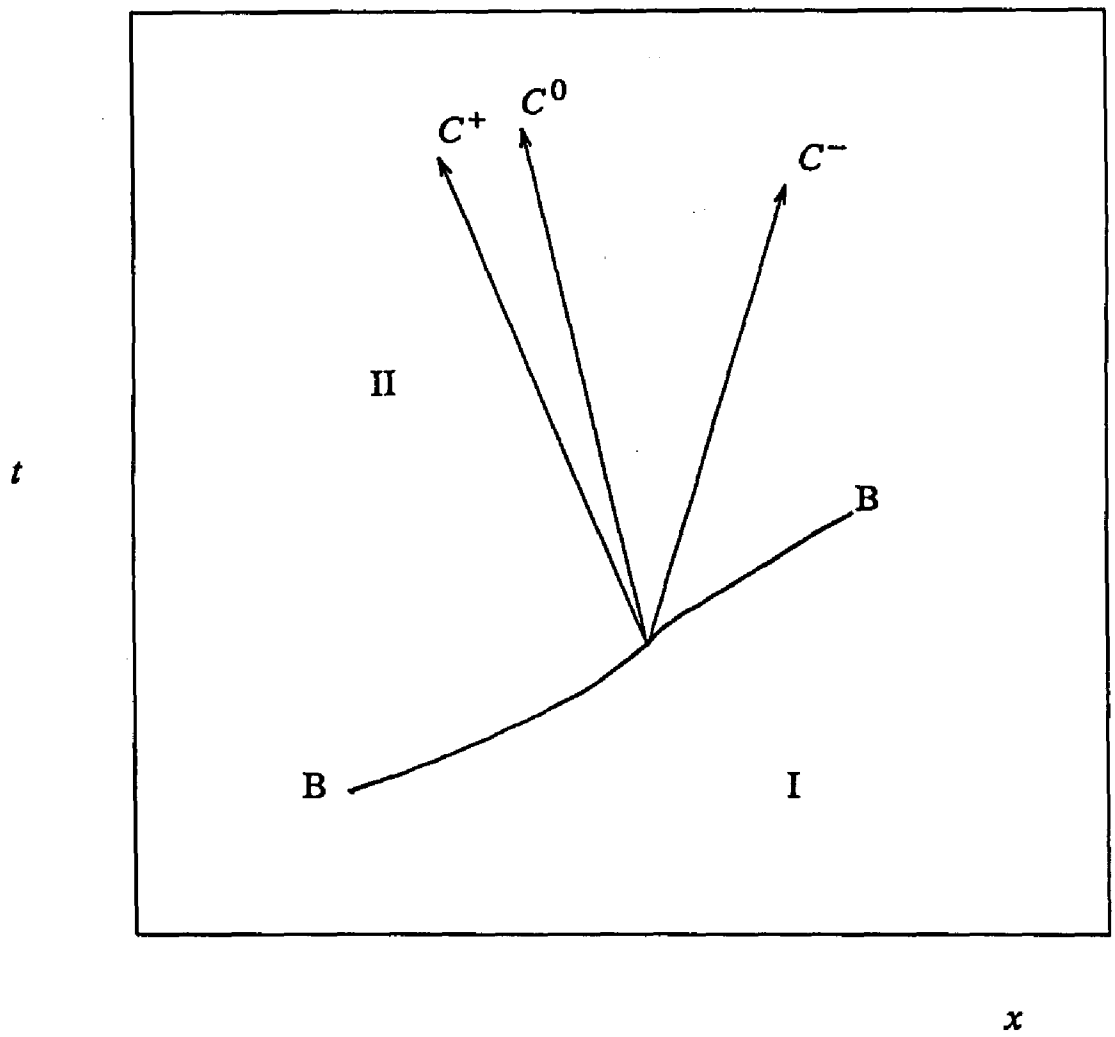

FIG. B.1. The three characteristics, which start at the line B-B (representing the boundary of the region of interest). The direction of the characteristic lines is assumed in the direction of increasing time.

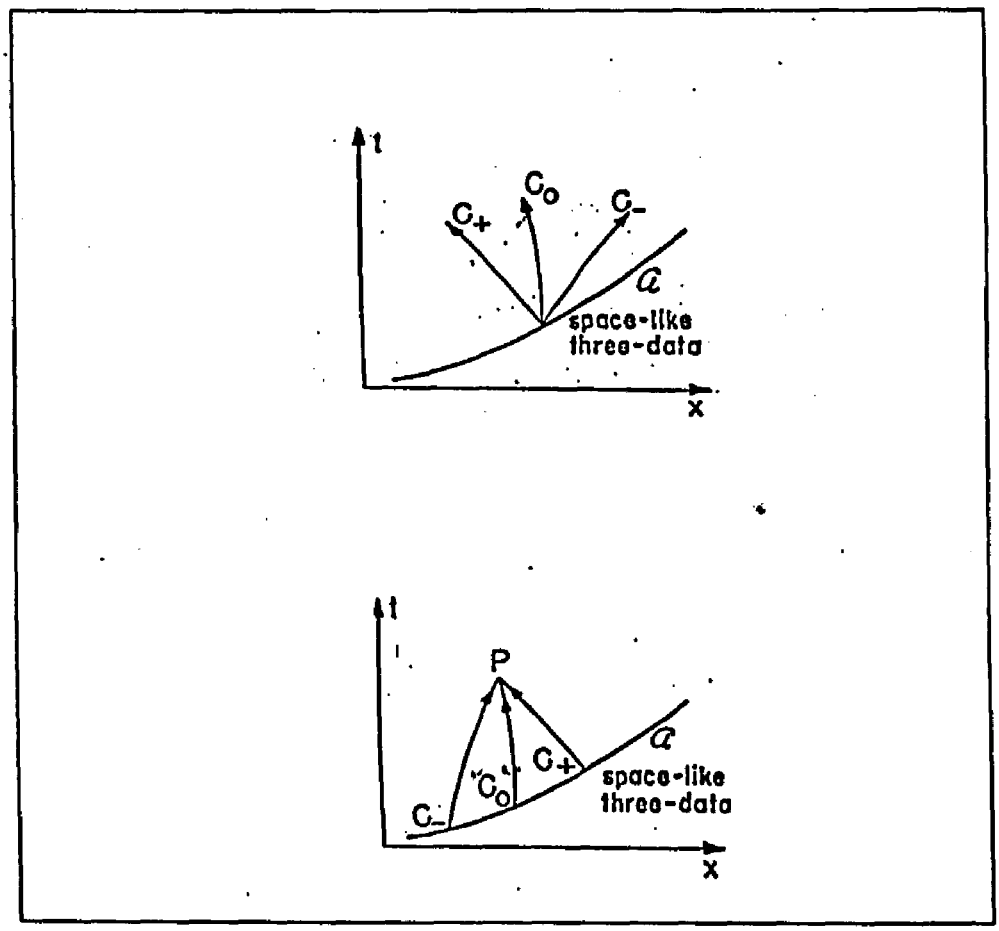

FIG. B.2. Space-like arc with three data for non-isentropic flow. A unique solution exists in the neighborhood of curve *A*, provided three quantities are prescribed on curve *A*. The domain of dependence of each point P is cut out of the initial curve by three characteristics through this point. Three data must be prescribed on such boundary.

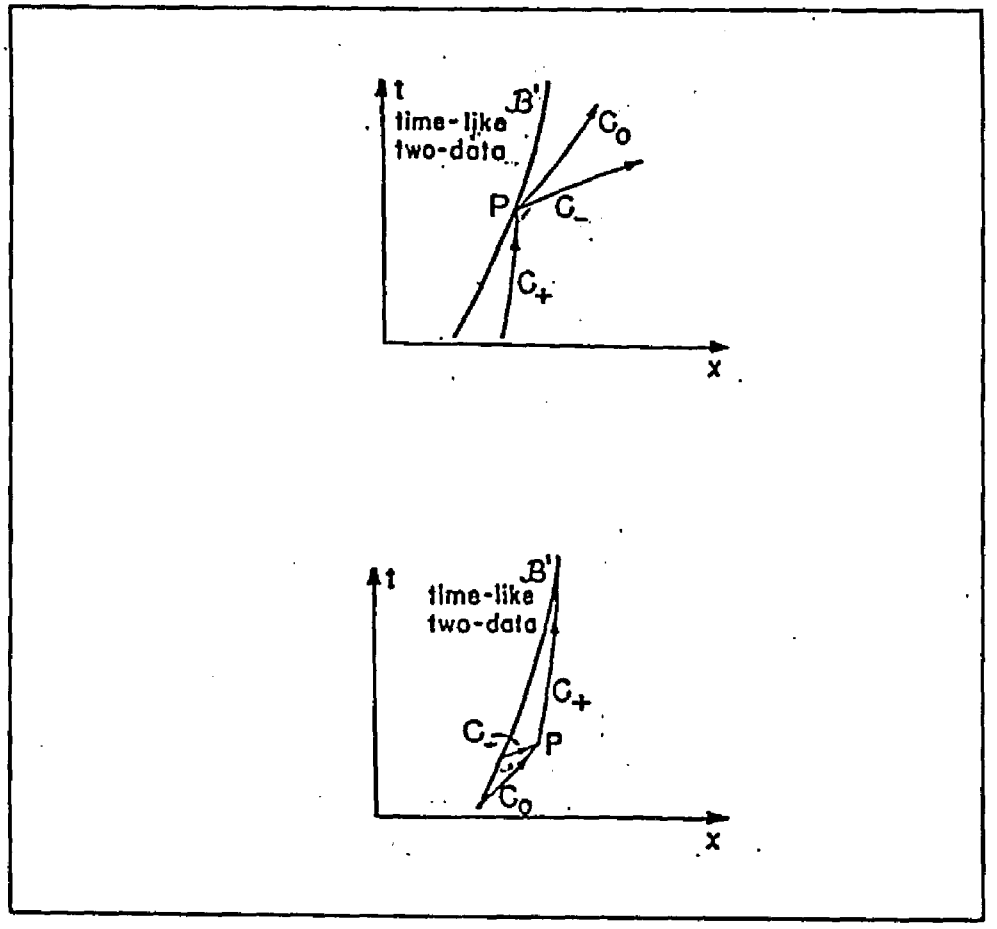

FIG. B.3. Time-like arc with two data for non-isentropic flow. The domain of dependence of point P is cut by only two characteristics (C^- and C^0), therefore only two quantities (two continuously differentiable data) must be prescribed on the curve B for a unique solution at P to exist. The remaining one boundary datum can be obtained from the conditions on the other boundary which may be present or from the initial conditions.

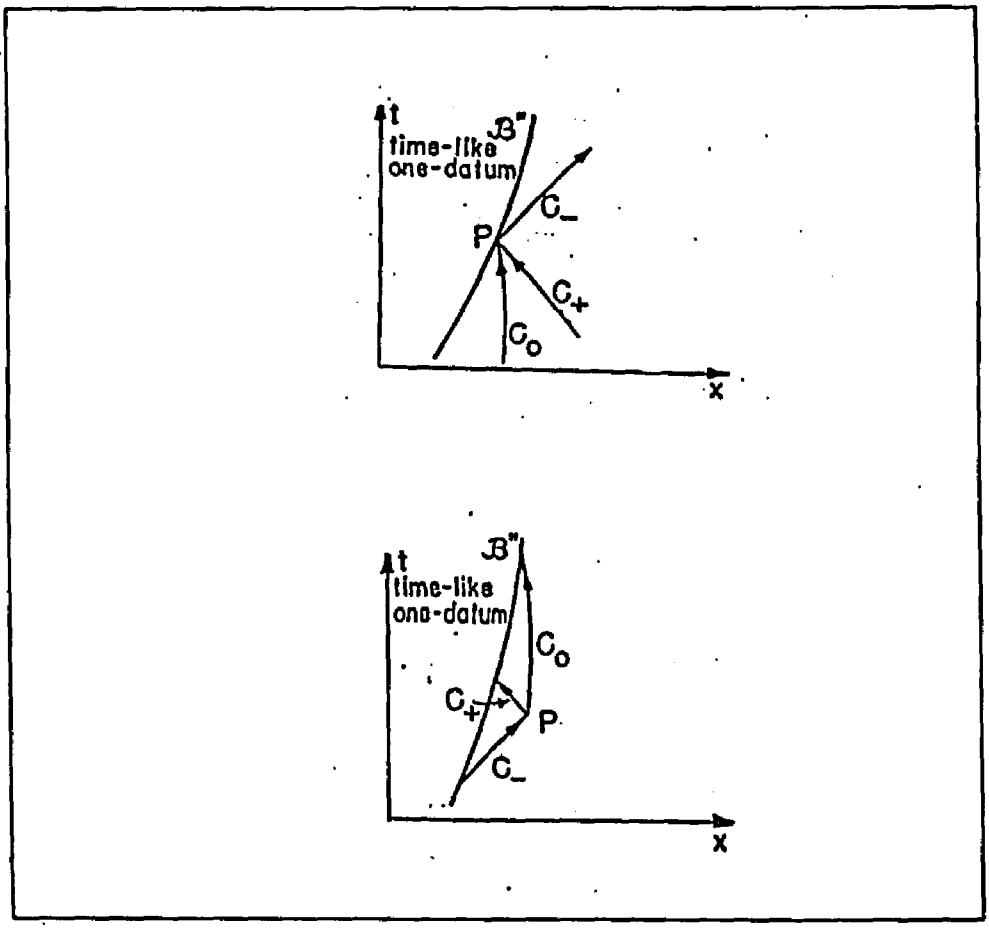

FIG. B.4. Time-like arc with one datum for non-isentropic flow. The two remaining data must come from the initial conditions or from the other boundary, that may be present in the problem.

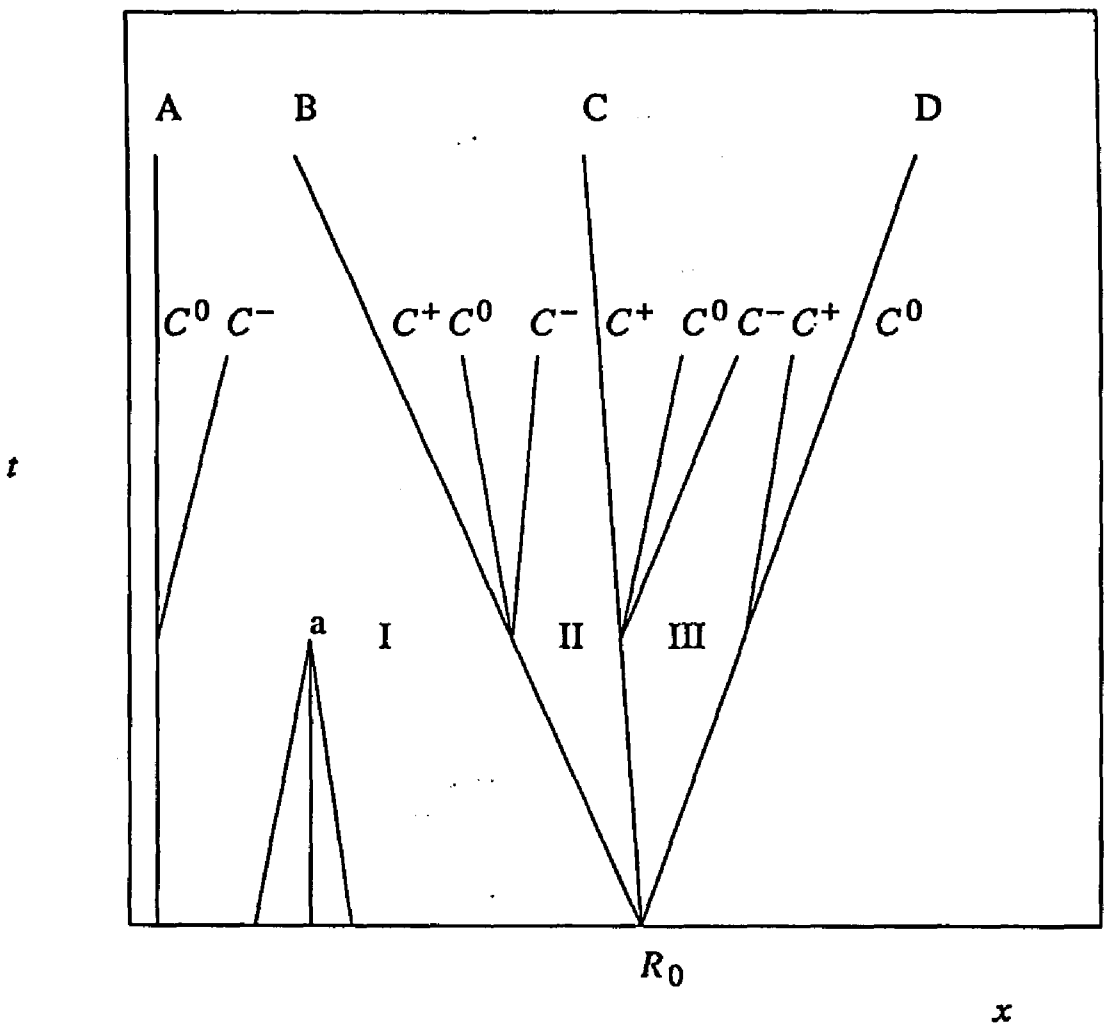

FIG. B.5. The boundary lines, that separate the regions of the continuous solution for the "water" part of the problem. Point R_0 corresponds to the initial position of the "water - air" boundary. Line A represents the center of the droplet, line B represents the head of the rarefaction wave, line C represents the tail of the rarefaction wave and line D represents the propagation of the "water - air" boundary. By counting the number of the characteristics, that start at the corresponding boundaries and propagate into the region of interest we can deduct the number of the boundary conditions, that must be prescribed on the corresponding boundary.

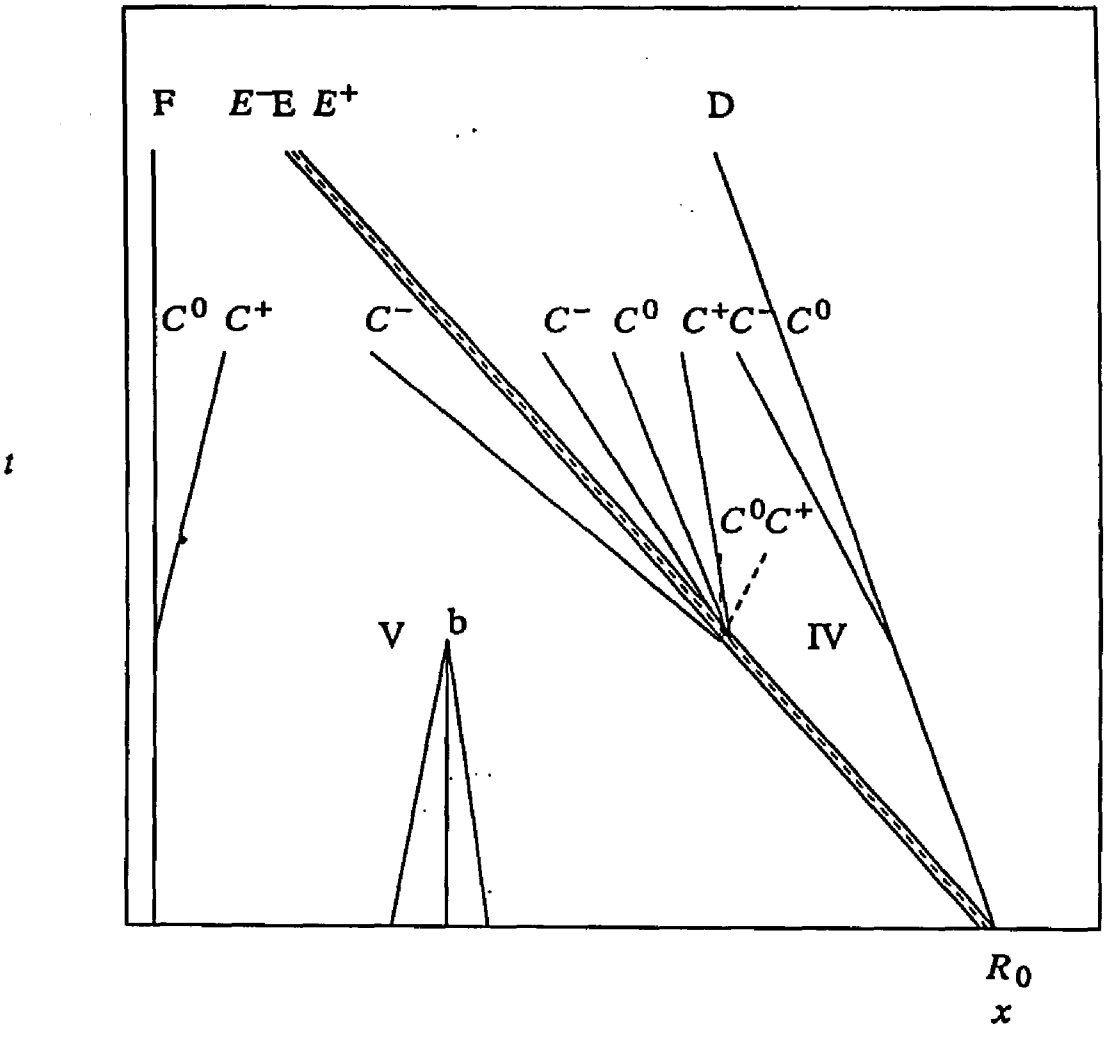

FIG. B.6. The boundary lines, that separate the regions of the continuous solution for the "air" part of the problem. Line F corresponds to the point at infinity, line E, together with lines $E^{\pm}$ corresponds to the propagation of the shock wave in the air and line D represents the "water - air" boundary. Because of the "folding" the positive x-direction is from the right to the left.

Appendix C. Some Computations with "Coherent" Representation.

The first step toward an expression from which the power radiated into the phonons, may be calculated numerically is to evaluate the term involving a product of two interaction potentials in Eq.(II.1.18). The algebra is straight forward and the result is:

$$\hat{A}_{q,q'} \equiv \left[\hat{V}(t),\left[\hat{V},\hat{b}_q^{\dagger}\hat{b}_{q'}\right]\right] = \upsilon^2\frac{f_{qq'}}{qq'}e^{-i\omega_q t}e^{i(q\cdot\hat{R}(t)-q'\cdot\hat{R})} + \upsilon^2\frac{f^{-1}_{qq'}}{qq'}e^{i\omega_{q'}t}e^{-i(q'\cdot\hat{R}(t)-q\cdot\hat{R})} \quad (C.1)$$

$$+\upsilon^2\sum_Q\frac{1}{Q}\left\{\frac{e^{-i\omega_Q t}}{q'}\hat{b}_q\hat{b}_Q^{\dagger}e^{i(Q\cdot\hat{R}(t)-q'\cdot\hat{R})}(f_{Qq'}-f^{-1}_{Qq'}) - \frac{e^{i\omega_Q t}}{q}\hat{b}_Q^{\dagger}\hat{b}_{q'}e^{-i(Q\cdot\hat{R}(t)-q\cdot\hat{R})}(f_{Qq}-f^{-1}_{Qq})\right\}$$

where we have defined

$$f_{qq'}(t) = e^{\frac{1}{2}[q\cdot\hat{R}(t),\,q'\cdot\hat{R}]} \quad (C.2)$$

and

$$\upsilon \equiv \frac{-iee^*}{\upsilon_c}\left[\frac{\hbar}{2\omega mN}\right]^{1/2} \quad (C.3)$$

In deriving Eq.(C.1) we used the following equality:

$$\mathrm{Tr}(\hat{\rho}_0\hat{b}\hat{b}) = \mathrm{Tr}(\hat{\rho}_0\hat{b}^{\dagger}\hat{b}^{\dagger}) = 0 \quad (C.4)$$

We have also used the relation which can be proved for the operators which obey Bose commutation relations[13]

$$e^{x\hat{a}^{\dagger}\hat{a}}f(\hat{a},\hat{a}^{\dagger})e^{-x\hat{a}^{\dagger}\hat{a}} = f(\hat{a}e^{-x},\hat{a}^{\dagger}e^{x}) \quad (C.5)$$

and a relation for the commutators of the exponential operators:

$$[e^{\hat{A}}, e^{\hat{B}}] = e^{\hat{A}} e^{\hat{B}} (1 - e^{-[\hat{A},\hat{B}]}) \quad \text{if } [A,[A,B]] = [B,[A,B]] = 0 \tag{C.6}$$

The last two equations can be easily derived using the "coherent" representation[13].

Notice that the operators in Eq.(C.1) are in the interaction representation. Therefore, they are time dependent. It will be more convenient to have the time dependence shifted into the nonoperator quantities, such as Q, leaving the operator $\hat{\mathbf{R}}$ time independent (i.e. at the initial time). We can achieve this by using Eqs.(C.1)-(C.4) as follows:

$$\mathbf{Q}\cdot\hat{\mathbf{R}}(t) = Q_x \left[\frac{\hat{X}_+(t) + \hat{X}_-(t)}{2} - i(\hat{\Pi}_+(t) - \hat{\Pi}_-(t)) \right] \tag{C.7}$$

$$+ Q_y \left[\frac{-i}{2}(\hat{X}_+(t) - \hat{X}_-(t)) - (\hat{\Pi}_+(t) + \hat{\Pi}_-(t)) \right] + Q_z \frac{\hat{a}^\dagger(t) + \hat{a}(t)}{\sqrt{\frac{2m\omega_z}{\hbar}}} = \mathbf{Q}(t)\cdot\hat{\mathbf{R}}$$

where

$$\hat{\mathbf{R}} = (\hat{a}^\dagger, \hat{a}, \hat{X}_-, \hat{X}_+, \hat{\Pi}_+, \hat{\Pi}_-) \tag{C.8}$$

$$\mathbf{Q}(t) = (Q_x \frac{e^{i\omega_z t}}{\sqrt{2m\omega_z/\hbar}}, Q_z \frac{e^{-i\omega_z t}}{\sqrt{2m\omega_z/\hbar}}, \tag{C.9}$$

$$\frac{l}{\sqrt{2}}(Q_x + iQ_y), \frac{l}{\sqrt{2}}(Q_x - iQ_y), \frac{-il}{\sqrt{2}}(Q_x - iQ_y)e^{i\omega_m t}, \frac{il}{\sqrt{2}}(Q_x + iQ_y)e^{-i\omega_m t})$$

Now we are in a position to calculate the $f_{qq'}$ (from Eq.(C.1)) with the result

$$f_{qq'} = \exp\left[\frac{i}{2} \left[\frac{-qq'}{m\omega_z/\hbar} \sin(\omega_z t) - l^2(q_x q'_x + q_y q'_y)\sin(\omega_m t) \right] \right. \tag{C.10}$$

$$+ l^2(q_x q'_y - q_y q'_x)(1 - \cos(\omega_m t))\Big]\Big]$$

The calculations for the exponential terms in the Eq.(C.1). are a little more involved. To use the simplicity of the "coherent" representation we start with transforming the factors into the normal order with destruction operators to the left of the creation operators. We also note that the time dependence is no longer in the operators but rather in the Q(t). This makes the transformation easier. Only the main steps in the calculations are presented here. First we do the transformation:

$$e^{i(\mathbf{Q}\cdot\hat{\mathbf{R}}(t)-\mathbf{Q}'\cdot\hat{\mathbf{R}})} = e^{i(\mathbf{Q}(t)\cdot\hat{\mathbf{R}}-\mathbf{Q}'\cdot\hat{\mathbf{R}})} = \prod_{i=1}^{6} e^{i(Q(t)-Q')_i\hat{R}_i} B_{QQ'} \tag{C.11}$$

where we defined

$$B_{QQ'} \equiv \exp\left\{-\frac{1}{2}i^2\sum_{j>i}(Q(t)-Q')_i(Q(t)-Q')_j[\hat{R}_i,\hat{R}_j]\right\} \tag{C.12}$$

After some tedious manipulations, $B_{QQ'}$ can be reduced to

$$B_{QQ'} = \exp\left\{-Q_z^2 + \frac{Q_z'^2 - 2Q_zQ_z'\cos(\omega_z t)}{4m\omega_z/\hbar}\right.$$

$$\left. - l^2\left[Q_x^2 + Q_y^2 + Q_x'^2 + Q_y'^2 - Q_xQ_x' - Q_yQ_y'\right]\right\} \tag{C.13}$$

$$\times\exp\left\{l^2\left[\cos(\omega_m t)\,(Q_xQ_x' + Q_yQ_y')\right] + l^2\left[\sin(\omega_m t)(Q_yQ_x' - Q_xQ_y'\right]\right\}$$

with the obvious relation

$$B_{QQ'} = B_{-Q-Q'} \tag{C.14}$$

Using the above formulas we arrive at the "final" result for the double

commutator $\hat{A}_{q,q'}$ in Eq.(II.1.18) defined in Eq.(C.1):

$$\hat{A}_{q,q'}(t) = + \frac{v^2}{qq'} \left[\hat{P}_{q,q'} C_{qq'} e^{-i\omega_q t} + \hat{P}_{-q,-q'} C^*_{qq'} e^{i\omega_q t} \right] \tag{C.15}$$

$$v^2 \sum_Q \frac{1}{Q} \frac{e^{-i\omega_Q t}}{q'} b^\dagger_q b_Q \hat{P}_{Q,q'} (C_{Qq'} - C_{Qq'})^* - v^2 \sum_Q \frac{1}{Q} \frac{e^{i\omega_Q t}}{q} b^\dagger_Q b_q \hat{P}_{-Q,-q} (C_{Qq'} - C^*_{Qq'})$$

where we defined

$$\hat{P}_{q,q'} \equiv \prod_i e^{i(q(i)-q')_i \hat{R}_i} \tag{C.16}$$

and

$$C_{qq'} \equiv B_{qq'} f_{qq'} \tag{C.17}$$

(see also Eqs.(C.10),(C.11)).

Appendix D. Comments on Nonequilibrium Phonon Distribution Function.

For heterostructures the plane wave formulation of the phonon system is inadequate, because the nonequilibrium phonon gas is inhomogeneous in the z direction. Therefore it is necessary to retain all the elements of the phonon density matrix in q_z, both diagonal and off-diagonal. But in a case of dispersionless LO phonons, i.e., $\hbar\omega_L(\mathbf{q}, q_z) = \hbar\omega_L$ (the case we are investigating in our thesis), an important simplification can be made in the kinetic equation for the phonons, namely an introduction of the phonon wave packet representation (see Eq.(II.1.23)). With this ansatz the phonon kinetic equation reduces to a set of coupled ordinary differential equations. The number of such equations is determined by the number of subbands occupied by electrons. For the purposes of our investigation only first few electronic subbands (in the z direction) are occupied. It was shown numerically by Marchetti and Cai[16] that a good approximation (less than 10% error) is obtained if only the diagonal terms in the phonon distribution function in the wave packet representation are retained in the phonon kinetic equation. Only these diagonal elements of the phonon distribution function are needed to evaluate the electronic macroscopic quantities such as electron cooling rate (or the power radiated into phonons due to the electron-phonon interaction). If, furthermore, the phonon wave packet occupation number is independent of $\mathbf{q}$ it implies that the plane wave phonon occupation number n is also diagonal in q_z. This is because the transformation from the plane wave representation to the wave packet representation is unitary.

References to Part I.

[1] R. L. Armstrong, Appl. Opt. **23** , 148 (1984).

[2] R. L. Armstrong, S. A. W. Gerstl and A. Zardecki, J. Opt. Soc. Am. A **2** , 1739 (1985).

[3] R. L. Armstrong, P. J. O'Rourke and A. Zardecki, Phys. Fluids **29** , 3573 (1986).

[4] A. Biswas et al., Opt. Lett. **12** , 313 (1987).

[5] S. I. Anisimov, Sov. Phys. JETP **27** , 182 (1968).

[6] F. G. Gebhardt, Appl. Opt. **15** , 1479 (1976).

[7] V. E. Zuev, "Laser Beams in the Atmosphere", Consultants Bureau, New York, (1982).

[8] R. L. Armstrong, J. Appl. Phys. **56** , 2142, (1984).

[9] F. L. Addessio, D. E. Carroll, J. K. Dukowicz, F. H. Harlow, J. N. Johnson, B. A. Kashiwa, M. E. Maltrud and H. M. Ruppel, "CAVEAT: A Computer Code for Fluid Dynamics Problems with Large Distortion and Internal Slip", (1985)

[10] S. K. Godunov, Matematicheskii Sbornik, **47** , 271, (1959).

[11] J. K. Dukowicz, J. of Computational Physics, **61** , 119, (1985).

[12] R. Courant and K. O. Friedrichs, "Supersonic Flow and Shock Waves", Interscience Publishers, Inc., New York, (1948).

[13] P. L. Roache, Comp. Fluid Dynamics, Hermosa, Albuquerque, (1982).

[14] Eli Turkel, Computers and Fluids, **11** , 121, (1982).

[15] P. Woodward, P. Colella, J. Comput. Phys., **54** , 115, (1985).

[16] G. Sod, J. Comput. Phys., **27** , 1, (1978).

[17] G. H. Meyer, "Numerical Methods for Free Boundary Problems: 1981 Survey" in "Free Boundary Problems: Theory and Applications", ed. A. Fasano and M. Primicerio, Pitman Advanced Publishing Program, (1981).

[18] R. D. Richtmyer, K. W. Morton, "Difference Methods for Initial Value Problems", Interscience, New York, (1967).

[19] D. L. Book, J. P. Boris, M. A. Fry, R. H. Guirguis, A. L. Kuhl, in "Eighth International Conference on Numerical Methods in Fluid Dynamics", Springer-Verlag, Berlin, Vol. 170, (1982).

[20] J. C. Carls, J. R. Brock, Aerosol Science and Technology, **7** , 79, (1987).

[21] S. K. Henshaw, J. Comput. Phys., **25** , (1986).

[22] N. L. Schryer, "Partial Differential Equations in One Space Variable," in Computing Science technical Report No. 115.

[23] N. L. Schryer, "Numerical Solution of Coupled Systems of Partial Differential Equations in One Spatial Variable and Time", in "Elliptic Problem Solvers", M. H. Schultz, editor, Academic Press, (1981).

[24] G. B. Whitham, "Linear and Nonlinear Waves", Willey & Sons, New York, (1974).

[25] A. Fasano, M. Primicerio, "Free boundary problems: theory and applications", Pitman Advanced Publishing Program, Boston, (1982).

[26] L. I. Sedov, "Similarity and Dimensional Methods in Mechanics", Academic Press, N.Y., (1959).

[27] G. I. Taylor, "The air wave surrounding an expanding sphere", Proc. R. Soc. London, A 186 , (1946).

[28] Y. B. Zeldovich and Y. P. Raizer, "Physics of Shock Waves and High-Temperature Hydrodynamics Phenomena", Academic Press, New-York, (1966).

[29] B. Van Leer, J. of Computational Physics, 32 , 137, (1979).

[30] L. D. Landau and E. M. Lifshitz, "Fluid Mechanics", Pergamon Press, Reading, Massachusetts, (1959).

[31] G. R. Shubin, A. B. Stephens and H. M. Glaz, J. Comput. Phys., 39 , 364-374 (1981).

References to Part II.

[1] R. Tsu and L. Esaki, "Tunneling in a finite superlattice", Appl. Phys. Lett., 22 , (1973).

[2] S. Sen, F. Capasso, A. C. Gossard, R. A. Spah, A. L. Hutchinson, S. N. G. Chu, "Observation of resonant tunneling through a compositionally graded parabolic quantum well", Appl. Phys. Lett., 51 , (1987).

[3] F. Capasso, K. Mohammed, A. Y. Cho, "Resonant tunneling through double barriers", IEEE J. Quantum Electronics, QE-22 , (1986).

[4] F. Capasso, R. A. Kiehl, J. Appl. Phys., 58 , (1985).

[5] see review paper: T. Ando, A. B. Fowler, F. Stern, Rev. Mod. Phys., 54 , (1983).

[6] S. Mori, T. Ando, Phys. Rev. B, 19 , (1979).

[7] W. Cai, M. C. Marchetti, M. Lax, Phys. Rev. B, 34 , 12, (1986)

[8] D. N. Zubarev, "Nonequilibrium Statistical Thermodynamics", Consultants Bureau, New York, (1974).

[9] C. S. Ting, S. C. Ying, J. J. Quinn, Phys. Rev., 16 , (1977).

[10] H. Bateman, "Higher Transtendental Functions", Vol.2, A. Erdelyi editor, McGraw-Hill Book Company, New York, (1953).

[11] P. M. Morse and H. Feshbach, (1958), "Methods of Theoretical Physics", McGraw-Hill, (1958).

[12] A. Feldman and A. Kahn, Phys. Rev. B 1 , 582, (1970).

[13] J. R. Klauder, Ann. Phys., 11 , 123, (1960).

[14] W. H. Louisell, "Quantum Statistical Properties of Radiation", John Wiley and Sons, New York, (1973).

[15] P. Warmenbol, F. M. Peeters and J. T. Devreese, Solid-State Electronics, 31 , (1988).

[16] M. C. Marchetti and W. Cai, Phys. Rev., B, 35 , 14, (1987).